Toward an Integrated, Physiologically Relevant

Microfluidic Model of the Human Body

by

Joseph M. Labuz

A dissertation submitted in partial fulfillment
of the requirements for the degree of
Doctor of Philosophy
(Biomedical Engineering)
in The University of Michigan
2016

Doctoral Committee:

Professor Shuichi Takyama, Chair
Assistant Professor Allen Liu
Professor Duxin Sun
Assistant Professor Sarah Veatch

Dedication

To Mom, Dad, Danny, and Stevie.
And to Cinder.

Acknowledgements

"Call me sentimental
I love things that are old
I'm just young and grateful
that I've had hands to hold" – The Donkeys

At every step of my education, I have been fortunate to enjoy teachers who were passionate, patient, and smart. Although at times faced with more resistance than necessary, they have unfailingly and without exception pushed the limits of my thought. Whatever flaws appear in this work are wholly my own and remain in spite of their best efforts.

My advisor, Shuichi Takayama, has given me the freedom to explore biomedical engineering, and indeed graduate student life. From discussing details of a specific assay in lab to considering broader trends in the way research and scholarship are conducted globally, Shu has encouraged me think critically about my work and how it fits into the world. The rest of my committee has also provided exemplary support: Duxin Sun patiently helped me grasp the finer points of pharmacokinetics and Michael Mayer, Allen Liu, and Sarah Veatch have each provided valuable insight and discussion.

Brendan Leung, Chris Moraes, and John Frampton were experienced post-docs were there to offer advice, give encouragement, and focus my work from the time I set foot on campus at UM until the time I graduated.

Cindy Chestek provided me with outstanding support during my time as a TA.

Several helpful collaborators have aided me where I lacked expertise, material, or equipment: Taehwa Chun, Masakuni Tokunaga, Mayumi Inoue, Chungmin Han, Jaesung Park, Remy Elbez, and Rose Ackerman.

Outside of engineering, Michigan provided me an exceptional opportunity to explore how science leaves the lab and makes its mark on the world, and how the world makes its mark on science. Shobita Parthasarathy, Jim Duderstadt, and Katherine Moynihan each provided invaluable guidance as I explored areas ancillary – but still important – to my degree.

As a 19-year old sophomore at Wisconsin, I had very little clue as to what biomedical engineering was or why I was majoring in it. Professor David Beebe and Dr. John Puccinelli generously took me into their lab and made the field real to me.

"Well we busted out of class
had to get away from those fools
we learned more from 3 minute record baby
than we ever learned in school" – Springsteen

Patrick, Erick, Tom, and Lance: you guys have been here long before this and will be here long after.

Having spent a considerable amount of time in lab, I am lucky to have been surrounded by a kind, intelligent, hard-working group such as this. Josh White and Sasha Cai Lesher-Perez were fellow Wisconsin alumni who particularly shaped my time in Ann Arbor. Beyond that, however, all Shu Lab members past and present deserve my gratitude for fostering a sustainable environment of inquiry, dissent, and comradery. I hope that my time has served to enhance – or at least sustain – that unique environment.

Having also spent a modest amount of time outside of lab, I would like to acknowledge those who made it worthwhile with trivia, pool, basketball, softball, MarioKart, grilling.

I have been fortunate (and occasionally a little surprised) that students have trusted me to mentor them. I can only hope that I helped them at least a little so as to repay the hard work and hard questions they have directed my way. Andrew Hartman, Christine Hathaway, Chang Che, and Michael Saunders have all taught me valuable lessons about science, people, and myself and all have invariable bright futures.

“I am gonna make it
through this year
if it kills me” – The Mountain Goats

I would like to acknowledge the benefactors who supported my studies at UM: Microfluidics in the Biomedical Sciences Training Program (NIH T32 EB005582), Graduate Assistance in Areas of National Need (US Department of Education), Tissue Engineering and Regenerative Medicine Training Program (NIH T32 HL007749), the EM-PACE collaborative, the Defense Threat Reduction Agency (N66001-13-C-2027 INteGrated Organoid Testing System), and the Rackham Travel Award.

“Can I graduate?” – Third Eye Blind

The administrators and support staff have kept me out of trouble, kept me on schedule, have always been a pleasure to interact with, and, when necessary, have held the bus for me: Maria Steele, Kathy McCrumb, Therese Kummer, Chuck Nicholas, Dana Jackson, Lorie Kochanek, Sarah Weiss, Sarah Ellerholz, and Kimberly Smith.

“Get right to the heart of matters
it’s the heart that matters more” – Counting Crows

AMDG: that this may, in some small sense, contribute thereto.

To Jessie, for your faith.

Finally, to my mom and dad, for showing me where to go. And to my brothers for pushing me to get there.

Table of Contents

List of Figures

List of Tables

List of Appendices

Abstract

New advances in the life sciences and engineering have enabled researchers to construct increasingly accurate experimental models of *in vivo* conditions. A logical next step would be to connect these discrete modules into increasingly complex networks forming an integrated, microphysiological model of the human body (a human on a chip or HOC). Such a system would be a powerful tool for probing myriad aspects of human health and disease. However, a generalizable HOC platform would require a rational, top-down design strategy and to date precious little time or energy have been spent examining such a problem. Here, we attempt to construct such an approach in three stages. First, we develop a cell-dense, 3-dimensional model of adipose tissue and demonstrate a functional response as measured by insulin-induced glucose uptake. We then use this microtissue construct to conduct a series of experiments that identify crucial parameters and potential problems for an HOC design strategy including control of cellular metabolism, circulating media or "blood" volume, and relative organ sizes. Finally, we address those issues using a variety of workarounds, compromises, and design criteria to induce *in vivo*-like system behavior, even in the face of apparently strange component values. We close by proposing design strategies for a physiologically relevant, 5-organ HOC that incorporates these lessons.

Chapter 1:

Introduction and Thesis Overview

1.1 The rising cost of biomedical research

As human health standards in the developed world have risen, so too have the costs of improving human health. This trend is starkly illustrated in the exponentially increasing cost of drug development (1, 2), but can also be seen in declining returns on biomedical research funding and the rising cost of domestic healthcare (3–5). In part, this growth is a natural consequence of progress: easy-to-discover drugs get discovered and regulatory standards tighten with an expanding knowledge base and drug library (2). As a result, scientists are faced with increasingly difficult problems and an increasingly constrained parameter space in which to solve them.

These trends, while challenging in their own right, are further exacerbated by a gap in knowledge that emerges between well-controlled, cost-effective experimental platforms (*e.g. in vitro* cell culture) and more complex, expensive approaches (*e.g.* clinical or animal studies). Conventional laboratory cell culture typically fails to capture the nuanced microenvironment of the body (6, 7). Animal studies, while offering the complexity of a genuine, living system, present their own challenges in throughput, translatability, and accuracy (8–11). Moreover, that complexity may frustrate

mechanistic studies necessary to explore specific hypotheses regarding drug action, disease progression, or toxin effect.

A well-controlled, cost-effective, and physiologically relevant experimental platform would address these concerns. Furthermore, such a system would allow a fundamental reworking of the paradigm under which biomedical knowledge is produced. New medical entity (NME) development, for example, can see as much as 90 percent attrition at the clinical stages – the most expensive steps of the process (12). Indeed, a sensitivity analysis of drug development identified Phase II and Phase III attrition as the top two drives of NME cost (13). Therefore, shifting NME attrition to *pre*-clinical stages by using improved *in vitro* models could eliminate "false positives" (*i.e.* drug candidates that appear promising but fail in clinical trials) and result in substantial gains for development efficiency. Those gains could be "reinvested" to keep other NME's in the pipeline for longer or more detailed periods of study, thereby reducing the number of "false negatives" as well. Surprisingly, that same analysis found that lead optimization was the third leading cost driver, indicating that the improved *in vitro* models could be drivers of substantial cost savings in and of themselves (13).

1.2 Microengineered models of biology

One way to address these issues is to build models that better represent the systems under study. Microfluidics and other microengineering techniques offer scientists many ways to control chemical, mechanical, and dimensional cues in the cellular microenvironment efficiently and with great precision (14, 15). In the late 1990's, a series of advances such a cleanroom batch processing and silicone micromoldling

rendered these advanced engineering techniques available to biomedical research labs across the word (16). By shrinking the scale of experiments, scientists reaped benefits associated with smaller material requirements, the potential for integrated sensing, actuation, and high-throughput processing. They were also able to take advantage of the unique properties of the microscale: fast mass and energy transport, large surface area to volume ratios, and laminar flow (17–19).

1.2.1 Organ on a chip

Coupled with more exquisite microfabrication techniques, microfluidics affords researchers the opportunity to construct complex, integrated systems capable of recapitulating key aspects of organ structure and function in a miniaturized platform – an “organ on a chip” or OOC (6, 7). Typically, these systems include chemical, mechanical and dimensional aspects that mimic the *in vivo* microenvironment and exhibit a greater range of function than conventional cell culture would allow. For example, lung function may be studied conventionally by plating lung epithelial cells in monolayer culture on a petri dish. Instead, a lung on a chip device allows for compartmentalized culture of both endothelial and epithelial cells on opposite sides of a permeable membrane. Furthermore, vacuum actuation provides cyclic, *in vivo*-like strain and fluid flow can be tuned to impart realistic shear stresses and introduce various cytokines, bacterial infections, or immune cells (20). Systems such as this provide a much richer degree of information and control compared to conventional *in vitro* experiments and scientists have developed on-chip models to study a variety of organ systems including the alveolus, heart, gut, kidney, and blood brain barrier (21–25).

1.2.2 Human on a chip

A natural extension of the concepts behind OOCs is the goal of developing a microphysiological model of the body or a “human on a chip” (HOC). In some ways, the problems confronting researchers in this field are akin to those faced by cartographers: just as mapmakers must determine the proper scale and amount of detail to include in a chart, so too must scientists and engineers determine the appropriate level of features for an HOC (26, 27). Too few details will result in a testing system that fails to provide relevant information or insights. Too many details yield a device that is unwieldy and indecipherable. Along with technical issues of how to best control the microenvironment and direct cell behavior, researchers must also struggle with establishing *how* to design these miniaturized systems.

Perhaps all present efforts to recapitulate interaction among organs within a microfluidic system can trace their ancestry to milk bottles. Although this pioneering arrangement was decidedly macro-fluidic, Michael Shuler and his colleagues at Cornell University broke important new ground when they published their first “cell culture analog” in 1995 by connecting compartmentalized “organs” contained in the aforementioned milk bottles. With motivations to improve on both *in vitro* and *in vivo* experiments that still echo today, the authors devised a microfluidic system to investigate naphthalene toxicity among three distinct organs (lung, liver, and “other tissue”) connected by tubing filled with cell culture media and driven by pumps to mimic the blood (28). Building on the milk bottle systems nearly a decade later, Viravaidya et al. successfully demonstrated interaction between lung, liver, fat, and “other tissue”

compartments in what was likely the first microfluidic HOC. This study again investigated naphthalene toxicity and observed that metabolites generated in the liver reduced glutathione production in the lungs and resulted in cell death (29). At the system level, Shuler and company design their HOC by reducing organ size linearly with system mass while compartment volumes and flow rates are selected to maintain residence times between humans and the HOC (30).

Later studies investigated the action of Tegafur, an anticancer prodrug, within an HOC comprising lung, liver, and bone marrow domains and realized on-chip 3D-hydrogel culture to support enhanced liver cell function and evaluated the results in light of a physiologically-based pharmacokinetic and pharmacodynamics (PB-PKPD) model (31, 32). When sufficient information such as drug behavior and metabolic rate constants are available, this combination of experimental and modeling approaches represents a powerful tool for designing and interpreting HOC-based experiments. Another effort investigated the effects of polystyrene nanoparticles on a two-circuit HOC: one course represented the gastrointestinal (GI) tract and was used to dose the nanoparticles by means of (simulated) oral exposure and a second mimicked the systemic circulation of the body. The two loops communicated via a two-layer co-culture intestinal compartment with the apical side (representing the lumen of the small intestine) being exposed to the GI/nanoparticle solution (33).

Rather than rely on linear scaling and residence time calculations to inform HOC design, John Wikswo of Vanderbilt University has proposed and HOC containing organ compartments designed according to empirical relationships between organ size and

animal mass (26, 34). While robust within the original dataset, extrapolating these relationships to HOC's of small total system mass remains a challenge. Arti Ahluwalia and her colleagues at the University of Pisa use quarter power scaling rules (QPSRs, see §1.3 for more information) to guide HOC design (35, 36). Coupled with these relationships, shear stress, principles of Euclidean geometry, and mass transport calculations govern the group's approach (37, 38). Microfluidic studies examined the effect of HOC culture on interactions between liver and endothelial cells. Although this study only contained two "organs," the ability to apply shear stress was a key consideration. Differences were not only observed between the dynamic, microfluidic system and monoculture, but also between the HOC system and traditional static co-culture (39, 40). More recently, Ahluwalia et al. have begun to advocate scaling by cell number, as it produces more consistent results *in vitro* and avoids challenging design requirements that may arise when metabolism and surface area are scaled by different exponents (41).

Other groups simply design their HOC according to organ mass. Yu and colleagues similarly attempted a proof of concept device examining the interaction of four organs (fat, kidney, liver, and lung). Each organ was represented by a cell-laden hydrogel and patterning of the system was controlled by microfabricated post arrays. Furthermore, the group incorporated Transforming Growth Factor Beta eluting gelatin microspheres and showed that varying levels of the cytokine can affect organ-specific behavior of each compartment (42). For their HOC device, Marx et al. scaled their organ compartments by mass. The two organ skin-liver system was capable of supporting a

variety of culture methods in each compartment. Despite the inclusion of only two organs, this device is an excellent example of microfluidic integration as the authors included an on-chip peristaltic pump to drive the recirculating fluid flow and reduce the device's footprint. Perhaps most notable about this work however is the inclusion of actual patient biopsies in the lung compartment of the HOC (43). While preliminary, these results highlight the potential of HOCs for applications in personalized medicine. A later report claimed the ability to examine absorption, distribution, metabolism, and excretion (ADME), key pharmacokinetic parameters (44).

Imura, Yoshimura, and Sato developed HOC for testing the anticancer drugs Tegafur and Cyclophosphamide that – in addition to an integrated two-circuit system – included stomach, liver, and tumor compartments. Cells in the stomach region were cultured on a porous membrane and served as the barrier between an acidic gastrointestinal circuit that was used to introduce the drugs to device and a blood circuit used to circulate the drugs and their metabolites among the organs. Importantly, this system allowed the researchers to carry out their experiments using only one-fifth the cells and one-tenth the reagents that would have been required by conventional cell culture techniques (45). These efforts are summarized in Table 1-1.

1.3 Relating animal size to biology

The complexities associated with changing animal mass have long been known and offer HOC designers some guidance when selecting various parameters for their systems. Galileo posited that size – be it biological or structural – possessed an upper limit (46). More recently, scientists have used scaling arguments to assess whether the

dinosaur *Tyrannosaurus Rex* was a capable runner (47). Although their findings indicated not, *T. Rex* was still theorized to be more capable of sprinting than a 6,000 kg chicken. In 1926, J.B.S. Haldane published an essay "On Being the Right Size" which provided a spirited and occasionally colorful argument that each animal carried a most convenient size and that for every change in size a change in form follows (48). Importantly, Haldane extended his treatment beyond mechanical scaling (*e.g.* bone cross section versus body mass or the implications of "getting wet" for animals of different sizes) and touched on issues of scaling in nutrition, sense, and metabolism.

"On Being the Right Size," however, still relied on geometric arguments to explore how different aspects of an organism change with mass, M. For example, Haldane assumed heat generation for warm-blooded mammals depended on mass and surface area – *i.e.* that it grew in proportion to $M^{2/3}$. A little over a decade later, Kleiber boldly suggested that energy expenditures grew commensurate with $M^{3/4}$ instead (36). At first met with skepticism, Klieber's quarter power scaling rule has gradually grown to be widely accepted (49). Remarkably, a host of other vital parameters follow a similar quarter-power pattern (50, 51).

The source of the three-quarter power exponent instead of the expected two-thirds – the source of that extra 1/12 – had long been debated until West, Brown, and Einquist, in 1997, demonstrated that it arose as a consequence of the evolutionarily optimized nutrient distribution system of animals (35, 52). Later Banavar et al. adjusted and confirmed the theory (53). In addition to validating Klieber's work over a half century after its publication, these studies demonstrated a clear mechanism of how not just

metabolism, but nearly every other vital parameter (lifespan, cardiac output, urination, etc.) depended on mass in a predictable way, generally mass raised to a quarter power or multiple thereof (50, 51, 54). Using this array of quarter power scaling rules, scientists can predict how animal life would look at many different sizes. QPSRs, then, provide designers of miniaturized physiologic models with powerful guidance for building relevant, scalable systems. However, there are no animals smaller than 1g that could confirm these predictions (52, 55). Beyond that, technical limitations (e.g. difficulties associated with small blood volumes) may force designers to deviate from the predictions of QPSRs (26, 44, 56). Whether and to what extent these changes may affect model fidelity remains an open question.

1.4 Dissertation overview

Table 1-1 provides a concise summary of notable HOC's to date and represents many outstanding efforts at engineering an integrated, physiologically relevant biomedical research platform. Nevertheless, most work in the field moves forward lacking a coherent, generalizable set of rules to guide design. Researchers may develop HOC's that work for a single stated purpose (*e.g.* observing the action of a specific anti-cancer drug), but have little hope of supporting any further exploration. Such cases, then, are of little use when applied to discovery. Unfortunately, that is exactly where the true power of an integrated, microphysiologic model of human health lies: the drug with an *unsuspected* metabolite, the disease with an *unknown* systemic effect, the adverse reaction with an *unanticipated* synergy (Figure 1-1) (56). Therefore, we endeavor to develop a set of design criteria for a generalized HOC capable of

providing relevant experimental results for a variety of inputs – regardless of *a priori* knowledge. If successful, this effort will help to bridge the gap between *in vitro* research and *in vivo* application (Figure 1-2, A).

To accomplish this, we work from the bottom up (Figure 1-2, B). In Chapter 2, we develop and characterize a cell-dense, 3-dimensional model of fat tissue using hanging drop culture. We then apply these adipospheroids to develop an explicit, experimentally supported set of HOC design rules in Chapter 3. Following those guidelines, Chapter 4 formulates a comprehensive, integrated strategy for a 5-organ, physiologically relevant and metabolically accurate model of human health. As necessary, we apply engineering controls to induce human-like cell behavior. Where design rules set challenging parameters, we examine potential workarounds and the implications thereof. Synthesizing conclusions from these experiments and from theoretical analyses, we conclude with a brief analysis of our HOC's suitability and leave the reader with a comprehensive set of design criteria for an integrated microfluidic model of the human body.

1.5 Works cited

1. Munos B (2009) Lessons from 60 years of pharmaceutical innovation. *Nat Rev Drug Discov* 8(12):959–968.

2. Scannell JW, Blanckley A, Boldon H, Warrington B (2012) Diagnosing the decline in pharmaceutical R&D efficiency. *Nat Rev Drug Discov* 11(3):191–200.

3. Bowen A, Casadevall A (2015) Increasing disparities between resource inputs and outcomes, as measured by certain health deliverables, in biomedical research. *Proc Natl Acad Sci* 112(36):11335–11340.

4. Catherine Rampell (2012) Why Tuition Has Skyrocketed at State Schools. *N Y Times*. Available at: http://economix.blogs.nytimes.com/2012/03/02/why-tuition-has-skyrocketed-at-state-schools/?_r=0 [Accessed February 1, 2015].

5. Healthcare CPI: All Urban Consumers (2015) Available at: http://www.bls.gov/data/ [Accessed March 7, 2015].

6. Moraes C, Mehta G, Lesher-Perez SC, Takayama S (2012) Organs-on-a-Chip: A Focus on Compartmentalized Microdevices. *Ann Biomed Eng* 40(6):1211–1227.

7. Bhatia SN, Ingber DE (2014) Microfluidic organs-on-chips. *Nat Biotechnol* 32(8):760–772.

8. Bracken MB (2009) Why animal studies are often poor predictors of human reactions to exposure. *JRSM* 102(3):120–122.

9. Sundstrom LE (2007) Thinking inside the box. *EMBO Rep* 8(1S):S40–S43.

10. Seok J, et al. (2013) Genomic responses in mouse models poorly mimic human inflammatory diseases. *Proc Natl Acad Sci* 110(9):3507–3512.

11. Greek R, Menache A (2013) Systematic Reviews of Animal Models: Methodology versus Epistemology. *Int J Med Sci* 10(3):206–221.

12. Kola I (2008) The State of Innovation in Drug Development. *Clin Pharmacol 38 Ther* 83(2):227–230.

13. Paul SM, et al. (2010) How to improve R&D productivity: the pharmaceutical industry's grand challenge. *Nat Rev Drug Discov*. doi:10.1038/nrd3078.

14. Christopher S. Chen, Milan Mrksich, Sui Huang, George M. Whitesides, Donald E. Ingber (1997) Geometric Control of Cell Life and Death. *Science* 276:1425–1428.

15. Takayama S, et al. (2003) Selective chemical treatment of cellular microdomains using multiple laminar streams. *Chem Biol* 10(2):123–130.

16. McDonald JC, et al. (2000) Fabrication of microfluidic systems in poly (dimethylsiloxane). *Electrophoresis* 21(1):27–40.

17. Beebe DJ, Mensing GA, Walker GM (2002) Physics and Applications of Microfluidics in Biology. *Annu Rev Biomed Eng* 4(1):261–286.

18. Walker GM, Zeringue HC, Beebe DJ (2004) Microenvironment design considerations for cellular scale studies. *Lab Chip* 4(2):91.

19. Paguirigan AL, Beebe DJ (2009) From the cellular perspective: exploring differences in the cellular baseline in macroscale and microfluidic cultures. *Integr Biol* 1(2):182.

20. Huh D, et al. (2010) Reconstituting Organ-Level Lung Functions on a Chip. *Science* 328(5986):1662–1668.

21. Douville NJ, et al. (2011) Combination of fluid and solid mechanical stresses contribute to cell death and detachment in a microfluidic alveolar model. *Lab Chip* 11(4):609–619.

22. Grosberg A, Alford PW, McCain ML, Parker KK (2011) Ensembles of engineered cardiac tissues for physiological and pharmacological study: Heart on a chip. *Lab Chip* 11(24):4165.

23. Kim HJ, Huh D, Hamilton G, Ingber DE (2012) Human gut-on-a-chip inhabited by microbial flora that experiences intestinal peristalsis-like motions and flow. *Lab Chip* 12(12):2165.

24. Jang K-J, Suh K-Y (2010) A multi-layer microfluidic device for efficient culture and analysis of renal tubular cells. *Lab Chip* 10(1):36–42.

25. Booth R, Kim H (2012) Characterization of a microfluidic in vitro model of the blood-brain barrier (μBBB). *Lab Chip* 12(10):1784.

26. Wikswo JP, et al. (2013) Engineering Challenges for Instrumenting and Controlling Integrated Organ-on-Chip Systems. *IEEE Trans Biomed Eng* 60(3):682–690.

27. Stokes C, Cirit M, Lauffenburger D (2015) Physiome-on-a-Chip: The Challenge of “Scaling” in Design, Operation, and Translation of Microphysiological Systems: Physiome-on-a-Chip. *CPT Pharmacomet Syst Pharmacol* 4(10):559–562.

28. L. M. Sweeney, M. L. Shuler, J. G. Babish, A. Ghanem (1995) A Cell Culture Analogue of Rodent PHysiology: Application to Naphthalene Toxicology. *Toxicol Vitro* 9(3):307–316.

29. Viravaidya K, Sin A, Shuler ML (2004) Development of a Microscale Cell Culture Analog To Probe Naphthalene Toxicity. *Biotechnol Prog* 20(1):316–323.

30. Abaci H, Shuler M (2015) Human on a chip Design Strategies and Principles for Physiologically Based Pharmocokinetics/Pharmacodynamics Modeling. *Integr Biol*. doi:10.1039/C4IB00292J.

31. Sung JH, Shuler ML (2009) A micro cell culture analog (*μ*CCA) with 3-D hydrogel culture of multiple cell lines to assess metabolism-dependent cytotoxicity of anti-cancer drugs. *Lab Chip* 9(10):1385.

32. Sung JH, Kam C, Shuler ML (2010) A microfluidic device for a pharmacokinetic–pharmacodynamic (PK–PD) model on a chip. *Lab Chip* 10(4):446.

33. Esch MB, Mahler GJ, Stokol T, Shuler ML (2014) Body-on-a-chip simulation with gastrointestinal tract and liver tissues suggests that ingested nanoparticles have the potential to cause liver injury. *Lab Chip* 14(16):3081.

34. Wikswo JP, et al. (2013) Scaling and systems biology for integrating multiple organs-on-a-chip. *Lab Chip* 13(18):3496.

35. West GB, Brown JH, Enquist BJ (1997) A General Model for the Origin of Allometric Scaling Laws in Biology. *Science* 276(5309):122–126.

36. Kleiber M (1947) Body size and metabolic rate. *Physiol Rev* 27(4):511–541.

37. Mattei G, Giusti S, Ahluwalia A (2014) Design Criteria for Generating Physiologically Relevant In Vitro Models in Bioreactors. *Processes* 2(3):548–569.

38. Sbrana T, Ahluwalia A (2012) Engineering Quasi-Vivo® in vitro organ models. *New Technologies for Toxicity Testing* (Springer), pp 138–153.

39. Guzzardi MA, Vozzi F, Ahluwalia AD (2009) Study of the crosstalk between hepatocytes and endothelial cells using a novel multicompartmental bioreactor: a comparison between connected cultures and cocultures. *Tissue Eng Part A* 15(11):3635–3644.

40. Vozzi F, Heinrich J-M, Bader A, Ahluwalia AD (2008) Connected culture of murine hepatocytes and human umbilical vein endothelial cells in a multicompartmental bioreactor. *Tissue Eng Part A* 15(6):1291–1299.

41. Ucciferri N, Sbrana T, Ahluwalia A (2014) Allometric Scaling and Cell Ratios in Multi-Organ in vitro Models of Human Metabolism. *Front Bioeng Biotechnol* 2. doi:10.3389/fbioe.2014.00074.

42. Zhang C, Zhao Z, Abdul Rahim NA, van Noort D, Yu H (2009) Towards a human-on-chip: Culturing multiple cell types on a chip with compartmentalized microenvironments. *Lab Chip* 9(22):3185.

43. Wagner I, et al. (2013) A dynamic multi-organ-chip for long-term cultivation and substance testing proven by 3D human liver and skin tissue co-culture. *Lab Chip* 13(18):3538.

44. Maschmeyer I, et al. (2015) A four-organ-chip for interconnected long-term co-culture of human intestine, liver, skin and kidney equivalents. *Lab Chip* 15(12):2688–2699.

45. Imura Y, Yoshimura E, Sato K (2012) Micro total bioassay system for oral drugs: evaluation of gastrointestinal degradation, intestinal absorption, hepatic metabolism, and bioactivity. *Anal Sci* 28(3):197–7.

46. Galileo Galilei (1952) *Dialogues concerning two new sciences (translated by H. Crew and A. De Salvio)* (Dover, New York).

47. John R. Hutchinson, Paul Segall (2002) Tyrannosaurus was not a fast runner. *Nature* 415:1018–1021.

48. Haldane JB (1926) On being the right size. *Harper's Mag* 152:424–427.

49. Stumpf MPH, Porter MA (2012) Critical Truths About Power Laws. *Science* 335(6069):665–666.

50. Peters RH (1983) *The Ecological Implications of Body Size* (Cambridge University Press, New York).

51. Schmidt-Nielsen K (1984) *Scaling: Why is Animal Size so Important?* (Cambridge University Press, New York).

52. West GB, Woodruff WH, Brown JH (2002) Allometric scaling of metabolic rate from molecules and mitochondria to cells and mammals. *Proc Natl Acad Sci U S A* 99(Suppl 1):2473–2478.

53. Banavar JR, et al. (2010) A general basis for quarter-power scaling in animals. *Proc Natl Acad Sci* 107(36):15816–15820.

54. Yang PJ, Pham J, Choo J, Hu DL (2014) Duration of urination does not change with body size. *Proc Natl Acad Sci* 111(33):11932–11937.

55. Rittmeyer EN, Allison A, Gründler MC, Thompson DK, Austin CC (2012) Ecological Guild Evolution and the Discovery of the World's Smallest Vertebrate. *PLoS ONE* 7(1):e29797.

56. Moraes C, et al. (2013) On being the right size: scaling effects in designing a human on a chip. *Integr Biol* 5(9):1149.

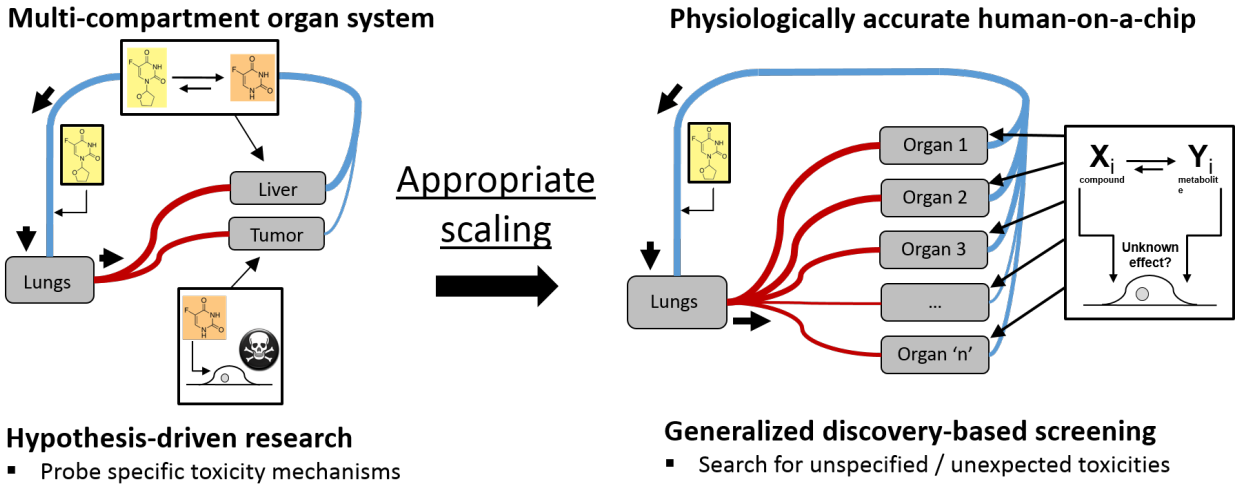

Figure 1-1. Detection of unknown or unsuspected toxicities with an HOC

Most current "HOC" efforts are merely multi-compartment organ systems designed to probe for specific and known toxicities or phenomena. A true, appropriately scaled HOC will be generalizable and therefore able to detect *unknown* or *unsuspected* effects.

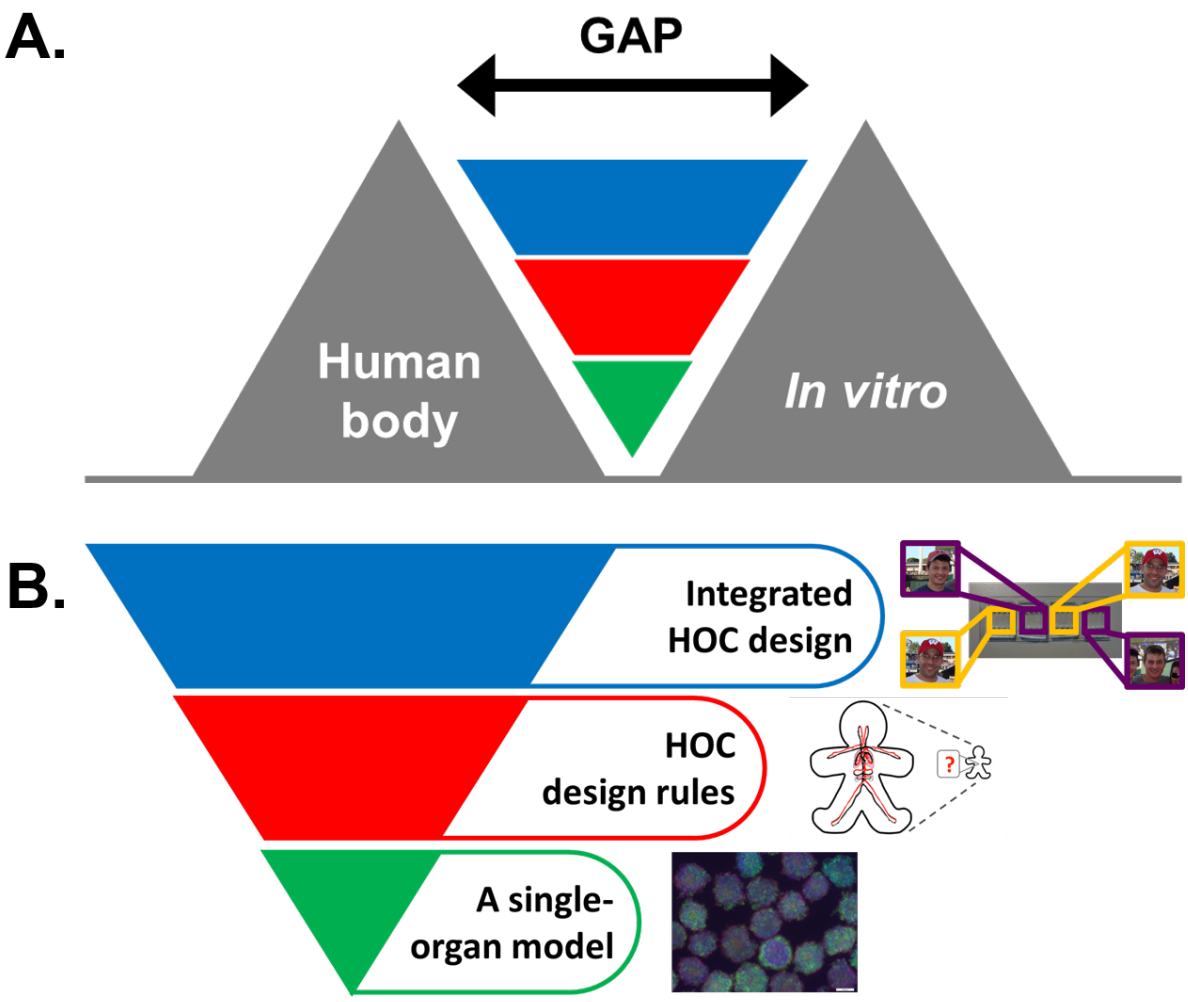

Figure 1-2. Bridging the gap: a thesis overview

(A) The gap between the way a drug or disease behaves in the body and cheap, fast, and easy *in vitro* experiments can be substantial and is a source of consternation for researchers in the biomedical sciences. Advances in microengineering represent an opportunity to engineer more realistic cell environments and interactions and thus generate actionable data about human health more quickly, accurately, and safely. (B) To bridge this gap, we develop a top-down design strategy for a microphysiological model of the human body (a "human on a chip" or HOC), ironically, from the bottom up. This thesis begins by developing and characterizing a cell-dense, 3-dimensional model of adipose tissue. Using that construct, we then conduct several experiments to formulate an explicit, experimentally-supported set of design rules. Finally, we apply those rules and examine the consequences of each and workarounds necessary to build a robust, physiologically relevant HOC platform.

Author	Year	Organs	Design approach	Application
Shuler et al. (29)	2004	Lung, liver, fat, “other tissue”	Mass and residence time scaling	Naphthalene toxicity
Yu et al. (42)	2009	Lung, liver, kidney, fat	Hydrogel culture; cytokine eluting microspheres	TGB-b efficacy, cell function
Ahluwalia et al. (40)	2009	Liver, endothelium	Alginate coating; WBE scaling; shear stress considerations	Cell function
Ahluwalia et al. (39)	2009	Liver, endothelium	Alginate coating; WBE scaling; shear stress considerations	Cell function
Shuler et al. (31, 32)	2009, 2010	Liver, tumor, bone marrow, “other tissue”	Mass and residence time scaling; hydrogel culture; PB-PKPD modeling	Tegafur metabolism/toxicity
Sato et al. (45)	2012	GI tract, liver, tumor	Two circuit fluid flow; carrier bead culture	Tegafur and cyclophosphamide metabolism/toxicity
Marx et al. (43)	2013	Skin, liver	Mass scaling; integrated pump; patient biopsies; transwell culture	Cell function
Shuler et al. (33)	2014	GI tract, liver, “other tissue”	Mass and residence time scaling; two circuit fluid flow	Nanoparticle uptake
Ahluwalia et al. (41)	2014	Liver, endothelium	Metabolic and surface scaling; cell number scaling	Liver function, glucose uptake
Marx et al. (44)	2015	Intestine, liver, skin, kidney	Patient biopsies, transwell culture, ADME, mass scaling	mRNA expression, glucose and LDH levels

Table 1-1. Summary of HOC efforts to date

A comprehensive list of human on a chip efforts to date. Clearly, researchers use a variety of disparate, often *ad hoc* design approaches that yield systems only valid for a narrow, specific set of experiments. A design strategy for a generalized model system would help unlock the true promise of these microphysiological model systems.

Chapter 2:

A Modular, 3-Dimensional Model of Fat Tissue

Since adipose tissue *in vivo* is lobular, we seek to create a cell-dense, 3-dimensional model of fat tissue. Using a previously established hanging drop culture platform, we demonstrate control over cell number/spheroid size and examine differences in size and morphology as "adipospheriods" of different cell numbers mature. Further, enzyme linked immunosorbent assay data shows that these microtissue secrete leptin and adiponectin, two important adipokines. Although conventional, 2D fat cultures also expressed these biomarkers, they do so at a much higher leptin to adiponectin ratio, clinically correlated with increased insulin resistance. Indeed, insulin-induced glucose uptake assay showed as much, with small, 3D spheroids proving most efficient at glucose uptake. Therefore, we conclude that these adipospheroids represent functional fat. Moreover, these modular microtissues can be manipulated easily: size is controlled by altering the number of spheroids included in any given assay and structure can be controlled by gentle dispersion.

2.1 Introduction

Adipose tissue is a critical regulator of homeostasis. Its canonical role is to respond to insulin signaling to remove glucose from the bloodstream. Not only can failure of this pathway be a sign of diabetes mellitus, but mounting evidence suggests implicates fat in the progession of other diseases as well (1). To be sure fat acts and an energy reservoir, storing triglycerides in times of plenty and mobilizing fatty acids during fasting. It is, however, also intimately involved in regulating its role in this process. Moreover, adipose-derived signaling molecules, or adipokines, play roles in many other important physiological pathways such as inflammation and vascular homeostastis. In a very real sense, fat acts as an endocrine organ unto itself (2). A common *in vitro* model of this critical organ is the 3T3-L1 murine cell line. Under appropriate conditions, these fibroblast-like progenitor cells undergo adipogenesis and, after about a week, emerge as mature fat (3, 4), capable of Glut4-mediated, insulin-induced glucose uptake (5–7).

Since adipocytes and adipose tissue are generally lobular, we investigate whether spheroid culture in a cell-rich, 3D-culture platform would enhance any aspect of fat "function." Previously, spheroid culture had been used to generate complex, '"Janus" tumor spheroids (8), had been found to induce *in vivo*-like morphology and function in liver cells (9), and had been used to grow fat spheroids as a model for inflammation (10, 11). These efforts do examine key adipose biomarkers and signaling molecules, and indicate that 3D culture may indeed improve L1 phenotype. The authors of the previous studies stop short, however, of any functional assessment (such as glucose uptake) and relied on a poorly controlled process of self assembly. Therefore, we aim to develop a

3-dimensional *in vitro* fat model that offers precise control over cell number and spheroid size. In this chapter, we assess the quality of this micro tissue by examining morphologic changes, biomarker expression, and Glut4-mediated glucose uptake in the presence of insulin.

2.2 Adipospheroid formation and differentiation

2.2.1 Formation and differentiation

Adipospheroids were grown in 384 well hanging drop (HD) plates developed previously to facilitate the formation of cell-laden microtissue for the study of cancer (12, 13). Using through-holes and a surface tension "collar," an array of 25 μL droplets can be maintained in place for weeks with minimal spreading or loss. Use of a liquid handling robot (CyBi Well; CyBio, Germany) for both cell seeding and media exchange greatly improves yield and throughput. 3T3-L1 murine preadipocyte cells (ATCC) were grown on tissue culture plastic in DMEM supplemented with 10 percent Newborn Calf Serum (NCS; Life Tech) and 1 percent antibiotic/antimycotic (anti/anti; LifeTech), passaged before 90 percent confluency, and used before passage 15. Adipospheroids were formed at Day -2 by seeding 40k cells/mL (1k cells/spheroid) or 320k cells/mL (8k cells/spheroid) in culture media supplemented with 0.24 percent Methylcellulose (A4M MethoCel, Dow Chemical), added to promote spheroid formation (14). Over two days, the cells self-assemble into 3D spheroids (Figure 2-1, A&B, top panels) and at Day 0, the media is changed to adipogenic induction media consisting of DMEM with 10 percent fetal bovine serum (FBS; Gemini Biosciences), 1 percent anti/anti, 1 μg/mL insulin (Sigma), 10 μM Troglitazone (Sigma), 0.25 μM Dexamethasone (Sigma), and 10

nM Triiodothyronine (T3; Sigma). This particular media formulation was chosen because it induces very little glycerol secretion by the fat cells. Other methods that resulted in high glycerol concentrations made the media too viscous to handle and were therefore not pursued further. At Day 3, the media is changed to DMEM with 10 percent FBS, 1 percent anti/anti, and 1 μg/mL Insulin. At Day 5, the media is changed to DMEM with 10 percent FBS and 1 percent anti/anti. Experiments were performed on "mature" adipospheroids at Day 7. Conventional, 2D differentiation was performed on confluent cells grown on tissue culture following the same schedule outlined above.

2.2.2 Adipospheroids increase in size and have altered morphology

Over the course of differentiation, the adipospheroids become larger and more disperse (Figure 2-1, A&B, bottom panels). To quantify this change in morphology, we measure the area and circumference of the spheroid cross section using ImageJ to follow the contours of the tissue (Figure 2-1, C and D). For the 1k spheroid size, cross sectional area (CSA) increases by 6.5x and perimeter by 4.6x. The fold increases for 8k spheroids were 3.9 and 4.0 respectively. This increase in size demonstrates that cells are getting larger – typical during adipogenesis as the fibroblast-like preadipocytes mature and accumulate lipids (15–17). Since the change in circumference is greater than the square root of the change in CSA, the data also indicate that the cells are becoming less adherent – another hallmark of adipogenesis. Nooks and crannies that appear in the mature adipospheroids result in a larger perimeter for the same cell volume. Importantly, these changes in CSA and perimeter are not uniform across spheroid sizes. Because 1k spheroids show a greater increase in size than 8k

spheroids, we hypothesis that smaller adiposhperoids experience a more efficient differentiation, possibly due to transport limitations and spatial constraints on cells at the core of the larger microtissue.

To examine the structure of our adipospheroids more closely, we fixed, embedded, and sectioned both 1k and 8k spheroids at Day 0 (before induction media was added) and at Day 7 (when spheroid differentiation was considered complete). Staining the samples with hematoxylin and eosin, we present a cross-sectional view of the microtissue (Figure 2-2). Despite some deformation from the embedding and sectioning process, the stained slices generally match microscope images. The post-differentiation slices show vacant, unstained regions within the cells which are the lipid vacuoles, the fat storage repositories of adipocytes. Comparing the presence and distribution of these vacuoles between the 1k and 8k spheroids, we observed an undifferentiated core at the center of the larger spheroid not present in the 1k condition, in agreement with our perimeter and area measurements of the microtissue.

2.3 Adipospheroids secrete adipokine biomarkers

We also examined the production of Leptin and Adiponectin (AdipoQ), two important adipokines involved in regulating homeostasis and metabolism. To further assess differentiation efficiency of our adipospheroids, we also assayed conventional, 2D fat cultures prepared using the same differentiation protocol as the microtissue. At day 7, mature fat was washed thoroughly with PBS. Adipopheroids were loaded into u-bottom, non-tissue culture treated well plates with 200 μL media and 2D fat was assayed in plate with 1 mL media. The conditions were placed in a cell culture incubator

for 24 hours at which point media samples were collected and frozen at -80 °C for later analysis with Quantikine ELISA kits (R&D Systems, Minnesota).

ELISA results showed that Leptin production varied considerably among tissue sizes and architecture (Figure 2-3, A). Perhaps unsurprisingly, 8k spheroids, with their non-differentiated core, produced the least Leptin over the 24-hour incubation with only two of five samples showing Leptin content above the limit of detection for the assay. Conventional 2D culture produced significantly more ($p<0.001$) Leptin than either 3D condition. AdipoQ was produced by all samples with adipospheroids producing more than 2D culture and 1k spheroids producing more than their larger counterparts (Figure 2-3, B). Clinically, Leptin to Adiponectin ratio (LAR) is a useful indicator of insulin resistance with higher LAR correlating with clinical measures of insulin resistance (18–20). Plotting this ratio, the data indicates that the 3D adipose tissue may be more sensitive to insulin signaling (Figure 2-3, C).

2.4 Functional assessment of adipospheroids

2.4.1 Characterization of insulin-induced glucose uptake

We sought to assess the functional characteristics of our adipospheroids by comparing the efficiency of insulin-induced glucose uptake between constructs of different size as well as conventional fat grown in 2D culture. To do this, mature fat was starved for 3 hours in Hank's Buffered Salt Solution supplemented with Ca^{2+}, Mg^{2+}, and 0.5 mM glucose (HBSS-g). Spheroids were collected manually using a cut-off 200 μL pipette tip to avoid shearing the cells since mature adipospheroids were quite delicate. Both adipospheroids and 2D fat were rinsed in HBSS-g. For the assay, adipospheroids

were placed in flat-bottom, glass vials and 2D was assayed in the 35 mm tissue culture dish it was grown in. At $t=0^-$, all conditions were suspended in a known volume of HBBS-g buffer and sampled by removing 2 μL of media with a pipette. Subsequently ($t=0^+$), HBSS-g with insulin was added to bring the total concentration of each experimental volume to 10 μg/mL insulin. A vehicle dose was added to bring the HCL concentration of each control (no insulin) condition to 0.05 mM HCl to account for acid in the insulin stock solution. Each volume was then placed in the incubator, gently agitated and sampled at t = 10, 30, 60, and 120 minutes.

To analyze the change glucose present in the media (and thus glucose consumed by the cells), we used AccuChek Aviva glucose test strips (Roche) and a PGStat 128N PotentioGalvanoStat (AutoLab/Metrohm) as described by others (21). Briefly, we applied a 150 mV potential across the test strip, introduced the sample using a pipette, and monitored the resulting current for 60 seconds. Amperometric data was converted to glucose levels by taking the average of current values in a 10-second window occurring 5 seconds after the maximum current value was reached and calibrating against solutions of known glucose values. Data is reported as cumulative glucose uptake per cell and analyzed for statistical significance using ANOVA and Tukey's post hoc test at confidence level $\alpha=0.05$ (Figure 2-4). In general, 1k spheroids uptook glucose more efficiently on a per cell basis than 8k spheroids, which were slightly (and not significantly) more efficient than 2D culture. This trend persisted throughout the experiment, but inter-sample variability decreased as time wore on.

2.4.2 Discussion of size-based differences in glucose uptake efficiency

The LAR data presented in §2.3 explains the variation between 3D and 2D fat – 3D fat is more sensitive to insulin. However, that same data would also suggest that 8k spheroids would uptake glucose more efficiently than 1k spheroids. Although the LAR is lower for the larger microtissue, each 8k adipospheroid likely contains less fat on a per cell basis than its 1k counterpart. This can perhaps be most clearly seen in the H&E stain of Figure 2-2, where a non-differentiated core was clearly visible in the large construct. Furthermore, the per cell production of both Leptin and AdipoQ was lower for 8k spheroids than for 1k; even if the adipocytes in the 8k spheroid are more sensitive to insulin, they are fewer in number (on a per cell basis) than both the 1k and 2D conditions.

To correct for this difference in *differentiation* efficiency, we discount the non-differentiated core and assume that only mature adipocytes are responsible for observed insulin induced glucose uptake. From our sectioned images, we can estimate the non-differentiated core to be about 170 μm in diameter for a 480 μm diameter spheroid (Figure 2-5, A). Then, assuming that mature adipocytes increase their diameter by 4x compared to preadiopcytes, we calculate the proportion of mature adipocytes in an 8k spheroid to be only ~25 percent. Applying this correction to observed per cell glucose uptake data gives us a corrected value of 73 pg/cell at 2 hours, larger than both 1k and 2D conditions and consistent with our LAR data (Figure 2-5, B). Note that since LAR is expressed as a dimensionless metric, it is unchanged by this analysis.

2.5 Conclusions

We successfully cultured spheroids composed of pre-adipocyte cells in hanging drop plates and differentiated them into mature fat *in situ*. Over the course of the 7-day differentiation, the adipospheroids increased in both cross sectional area and diameter. H&E staining of mature and undifferentiated microtissue revelaed the presence (or absence) of lipid vesicles and, in some cases, also showed patterns of heterogeneous differentiation across the radius of the spheroid. Adipospheroids were further characterized and compared to conventional 2D culture by examining Leptin and Adiponectin, two important adipose signaling molecules, secretion by ELISA. We also compared the function of these three different types of fat. In the presence of insulin, 1k spheroids uptook insulin more efficiently than both 2D and 8k conditions (though correcting for any non-differentiated core may be necessary to fully evaluate different-sized adipospheres against each other). This can be explained by its low leptin-adiponectin ratio (which indicates comparatively more insulin sensitivity) compared with 2D and by its greater differentiation efficiency compared to the larger, 8k adipospheroid.

2.6 Works cited

1. Poitout V, et al. (2010) Glucolipotoxicity of the pancreatic beta cell. *Biochim Biophys Acta BBA - Mol Cell Biol Lipids* 1801(3):289–298.

2. Trayhurn P, Beattie JH (2001) Physiological role of adipose tissue: white adipose tissue as an endocrine and secretory organ. *Proc Nutr Soc* 60(03):329–339.

3. Todaro GJ, Green H (1963) Quantitative studies of the growth of mouse embryo cells in culture and their development into established lines. *J Cell Biol* 17(2):299–313.

4. Scott MA, Nguyen VT, Levi B, James AW (2011) Current Methods of Adipogenic Differentiation of Mesenchymal Stem Cells. *Stem Cells Dev* 20(10):1793–1804.

5. Mayumi Inoue, Lisa J. Brunet, Joseph Hwang, Shian-Huey Chiang, Alan R. Saltiel (2003) The exocyst comlex is required for targeting of Glut4 to the plasma membrane by insulin. *Nature* 422(6932):629–633.

6. Zuber MX, Wang SM, Thammavaram KV, Reed DK, Reed BC (1985) Elevation of the number of cell-surface insulin receptors and the rate of 2-deoxyglucose uptake by exposure of 3T3-L1 adipocytes to tolbutamide. *J Biol Chem* 260(26):14045–14052.

7. Olefsky JM (1976) Effects of fasting on insulin binding, glucose transport, and glucose oxidation in isolated rat adipocytes: relationships between insulin receptors and insulin action. *J Clin Invest* 58(6):1450.

8. Hsiao AY, et al. (2012) 384 hanging drop arrays give excellent Z-factors and allow versatile formation of co-culture spheroids. *Biotechnol Bioeng* 109(5):1293–1304.

9. Ramaiahgari SC, et al. (2014) A 3D in vitro model of differentiated HepG2 cell spheroids with improved liver-like properties for repeated dose high-throughput toxicity studies. *Arch Toxicol*. doi:10.1007/s00204-014-1215-9.

10. Turner PA, Harris LM, Purser CA, Baker RC, Janorkar AV (2014) A surface-tethered spheroid model for functional evaluation of 3T3-L1 adipocytes. *Biotechnol Bioeng* 111(1):174–183.

11. Turner PA, Tang Y, Weiss SJ, Janorkar AV (2015) Three-Dimensional Spheroid Cell Model of *In Vitro* Adipocyte Inflammation. *Tissue Eng Part A* 21(11-12):1837–1847.

12. Tung Y-C, et al. (2011) High-throughput 3D spheroid culture and drug testing using a 384 hanging drop array. *The Analyst* 136(3):473–478.

13. Hsiao AY, et al. (2012) Micro-ring structures stabilize microdroplets to enable long term spheroid culture in 384 hanging drop array plates. *Biomed Microdevices* 14(2):313–323.

14. Leung BM, Lesher-Perez SC, Matsuoka T, Moraes C, Takayama S (2015) Media additives to promote spheroid circularity and compactness in hanging drop platform. *Biomater Sci* 3(2):336–344.

15. Howard Green, Olanlyi Khinde (1975) An Established Preadipose Cell Line and its Differentiation in Culture. *Cell* 5:19–27.

16. Gregoire FM (2001) Adipocyte differentiation: from fibroblast to endocrine cell. *Exp Biol Med* 226(11):997–1002.

17. Selvarajan S, Lund LR, Takeuchi T, Craik CS, Werb Z (2001) A plasma kallikrein-dependent plasminogen cascade required for adipocyte differentiation. *Nat Cell Biol* 3(3):267–275.

18. Inoue M, Maehata E, Yano M, Taniyama M, Suzuki S (2005) Correlation between the adiponectin-leptin ratio and parameters of insulin resistance in patients with type 2 diabetes. *Metabolism* 54(3):281–286.

19. Oda N, et al. (2008) The ratio of leptin to adiponectin can be used as an index of insulin resistance. *Metabolism* 57(2):268–273.

20. Zaletel J, Barlovic DP, Prezelj J (2010) Adiponectin-leptin ratio: a useful estimate of insulin resistance in patients with Type 2 diabetes. *J Endocrinol Invest* 33(8):514–518.

21. Cha KH, Jensen GC, Balijepalli AS, Cohan BE, Meyerhoff ME (2014) Evaluation of Commercial Glucometer Test Strips for Potential Measurement of Glucose in Tears. *Anal Chem* 86(3):1902–1908.

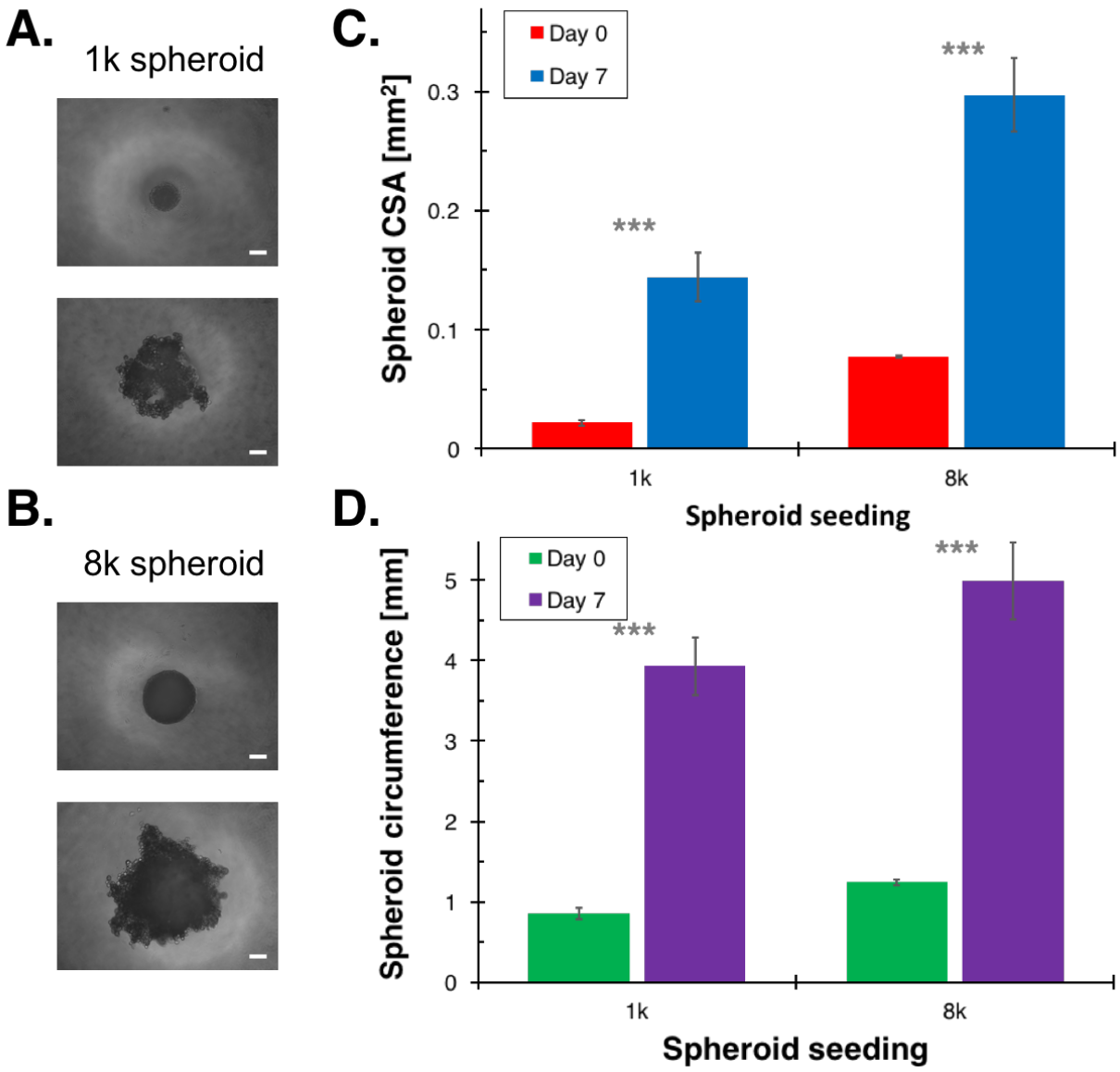

Figure 2-1. Adipospheroid size before and after differentiation protocol

Characterization of adipospheroid formation and differentiation. (A) 1k spheroid morphology goes from compact and small at Day 0 (top) to loose and large at Day 7 (bottom). (B) 8k spheroid morphology goes from compact and small at Day 0 (top) to loose and large at Day 7 (bottom). Quantitatively, spheroid size, as measured by (C) cross sectional area and (D) perimeter changes significantly over the course of the differentiation protocol. Scale bars = 100 μm; data as average ± standard deviation, n=3-5; *** indicates $p<0.001$ by Student's two-tailed t-test.

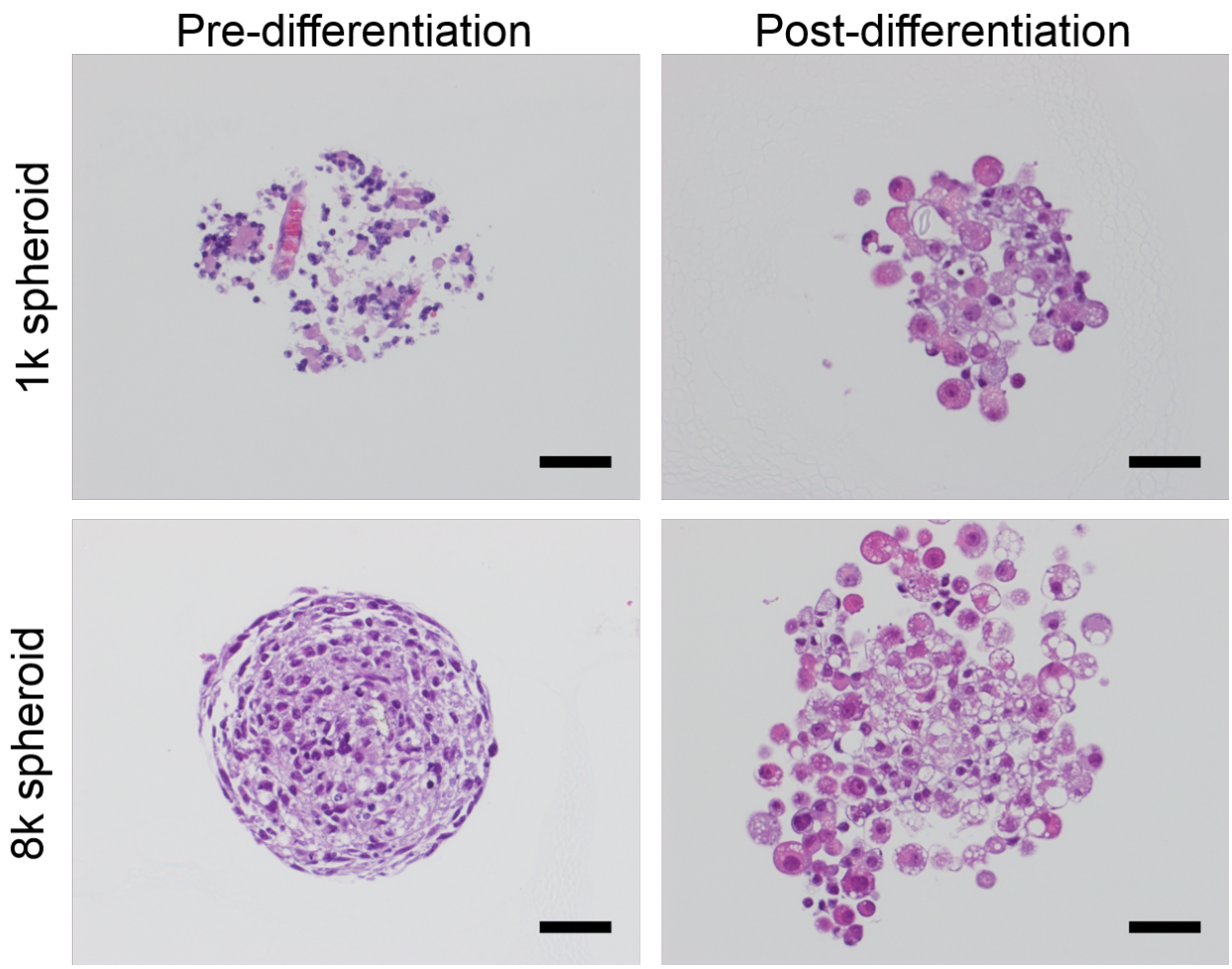

Figure 2-2. Adipospheroid cross section staining

Hematoxylin and eosin stain of sectioned adipospheroids at Day 0 (pre-differentiation) and Day 7 (mature, post-differentiation). The large vacuoles devoid of H&E staining and particularly prevalent in the post-differentiation images are lipid vacuoles. Note the change in cell morphology at the spheroid core between the 8k and 1k spheroids. Scale bars = 100 μm.

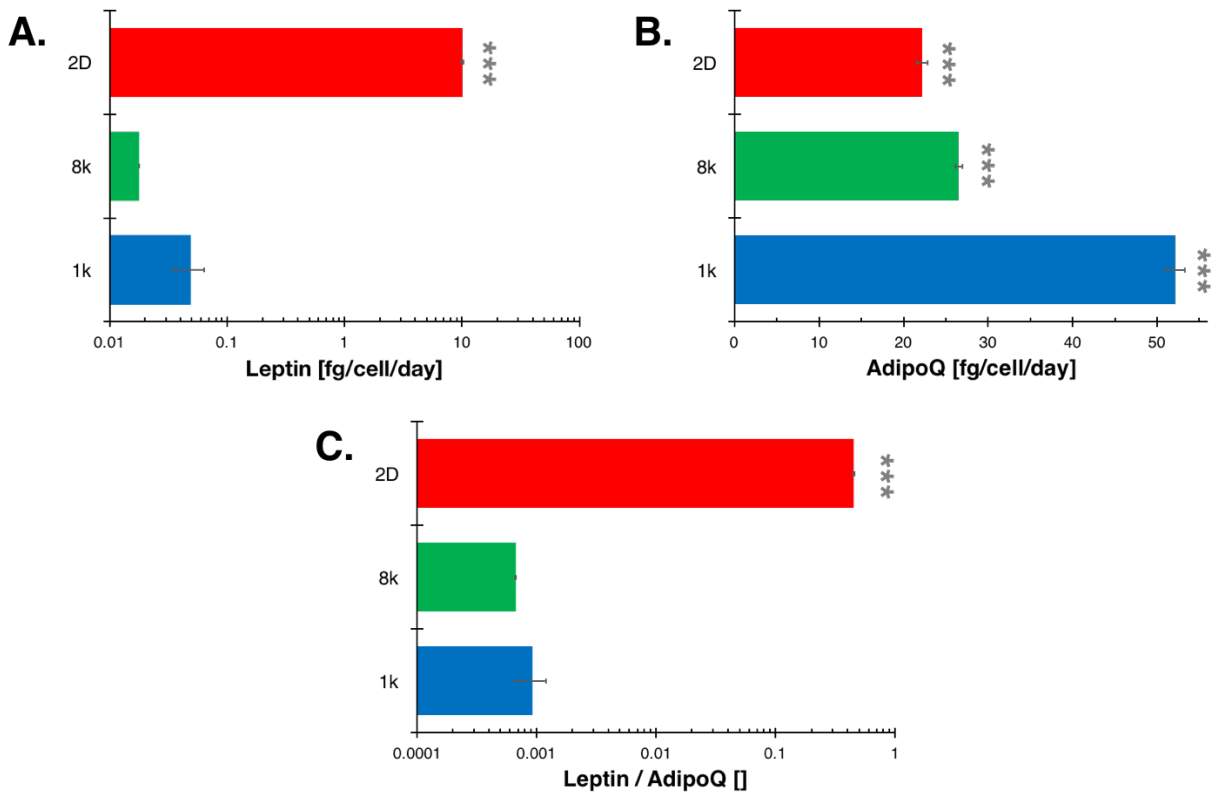

Figure 2-3. Comparison of Leptin and Adipoenctin expression of *in vitro* fat

(A) Conventional 2D culture secreted far more leptin than 3D adipospheroids over the 24-hour period starting on day 7 post-differentiation. Note that data is plotted on a $\log_{10}$ axis. (B) Adiponectin (AdipoQ) production was higher in spheroids compared to fat grown in a conventional 2D monolayer. (C) Leptin to AdipoQ ratio is plotted on a $\log_{10}$ axis. Data reported as average ± standard deviation, n=2-5; *** indicates $p<0.001$ versus all other conditions by ANOVA with Tukey post hoc test.

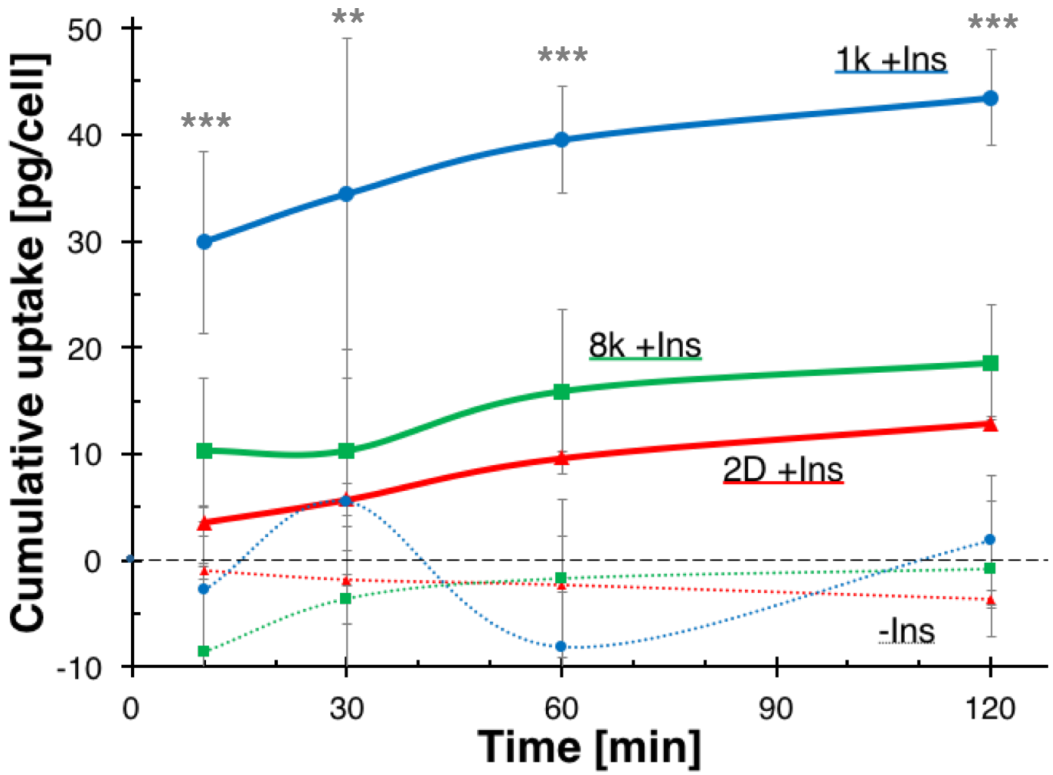

Figure 2-4. Insulin-induced glucose uptake by adipospheroids and conventional 2D culture

On a per-cell basis, 1k spheroids consumed significantly more glucose than larger (8k) spheroids or conventional 2D fat. In general, insulin-induced glucose consumption was marked by a rapid jump in the first 10 minutes and then a gradual increase in consumption over the remaining 110 minutes. This is consistent the general elevation of adipose biomarkers we observe in small, 3D culture. Data reported as average ± standard deviation, n=5; ** indicates $p<0.01$ and *** indicates $p<0.001$ for 1k (+Ins) versus all other conditions by ANOVA with Tukey post hoc test.

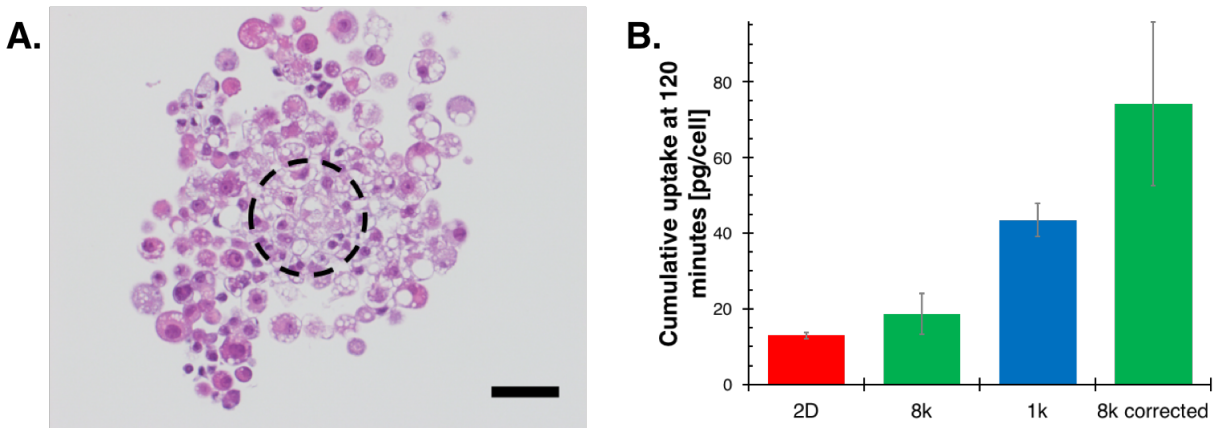

Figure 2-5. Correcting glucose uptake for undifferentiated core of 8k spheroid

(A) The larger 8k adipospheroid exhibits an undifferentiated core that does not contribute substantially to adipose function. Scale bar = 100 μm. (B) When correcting for this core, we find that adipocytes in the 8k spheroid uptake glucose most efficiently, in agreement with our LAR data. Data reported as average ± standard deviation, n=5, at time t=120 minutes.

Chapter 3:

Experiments to Inform the Design of a Human on a chip System Using a 3-Dimensional Fat Model

Top-down approaches to constructing a microphysiological model of the body must not only answer systems-level questions about how different components relate and interact, they must also set the terms on which those questions are considered. Conventionally, designers select parameters that seem (and likely are) important to guide their scaling strategies. Here, we seek explicit experimental support for each proposed constraint. Accordingly, we leverage our 3-dimensional, cell-dense model of fat tissue to identify key factors in scaling design and suggest how each may be important. These experiments identify four specific elements for further scrutiny: First, we examine oxygen tension and its effect on cell metabolic activity. Second, we probe how drug properties control distribution behavior and observable effects within an HOC. Third, we modulate tissue structure and explore its implications for mass transport and organ function. Finally, we examine how both relative size of each organ compartment and absolute size of the system as a whole are critical design parameters for a robust model. Moving forward, these conclusions offer both guidance and explicit support for top-down human on a chip design strategies.

3.1 Introduction

In building a microphysiological model of the body (a “human on a chip” or HOC), designers must choose or create guidelines to constrain their decisions as they scale down over several orders of magnitude. These strategies fall along a continuum between “bottom-up” and “top-down.” Bottom-up schemes concern themselves more with the disparate parts of the system, rather than the relationships therein, and closely related to tissue engineering. Top-down approaches first consider the system-level relationship between components of the whole and move forward to fill in the details at increasingly finer granularity. We focus on critical questions of size, form, and function that arise for top-down designers as they scale over approximately six orders of magnitude (1).

As detailed in §1.2.2, the oldest of these top-down strategies is mass-residence time scaling pioneered by Michael Shuler and his research group Cornell University (2–4). Shuler et al maintain the ratio between compartment (*i.e.* organ) and system (*i.e.* body) mass and also ensure that tissue resident times – how long the media remains in contact with each organ compartment – match those found in the body. Importantly, this approach lends itself well to physiologically based pharmacokinetic and pharmacodynamic modeling and the researchers demonstrate how such models may be used to interpret experimental results – so long as the relevant drug properties are known (5–7). Arti Ahluwalia and her research group at the University of Pisa similarly focus on organ mass but guide their design using quarter power scaling rules (QPSRs), a form of allometric scaling that has been analytically derived and experimentally

supported (8–10). QPSRs are examined in further detail in §4.1 and §4.2. Briefly, various parameters, like metabolism scale with animal mass, M, raised to the power of ¾. (The term allometric comes from the Greek *αλλος* meaning "other" or "different" – *i.e.* an exponent not equal to unity.) Further, Ahluwalia and colleagues scale surface area as $M^{2/3}$, in accordance with the principles of Euclidean geometry (11, 12). Recently, however, they have begun to place a greater emphasis on cell number (13). John Wikswo of Vanderbilt University relies on a different, entirely empirical form of allometric scaling: by inferring relationships between critical organ parameters (*e.g.* heart: volume pumped, lung: gas exchanged) from existing data, his research group proposes to design a HOC by extrapolating those relationships over several orders of magnitude (14, 15). Finally, Uwe Marx of Technische University in Berlin generally advocates scaling by mass, but also with some consideration for organ "functional units" and pharmacokinetic parameters such as absorption, distribution, metabolism, and excretion (16, 17).

To be sure, these approaches are all rooted in logic. The way in which each strategy identifies key parameters, however, can be more difficult to see. By intuition, most, if not all, of these factors appear significant. Nevertheless, we seek to provide *experimental* support for considering and controlling certain aspects of an HOC. To that end, we use our adipospheroids to demonstrate how four parameters – oxygen level, drug distribution, tissue size, and tissue structure – that seem important actually are important. From these data, we formulate several rules to aid in the design of a feasible, physiologically-relevant HOC.

3.2 Oxygen level impacts insulin response

Molecular oxygen is fundamental to animal life. Its most important role is perhaps as an oxidizing agent in the electron transport chain that lies at the heart of respiration and drives both cellular and systemic metabolism in aerobic organisms (18, 19). Thus, a rational consideration of oxygen level is fundamental to a physiologically relevant HOC. To investigate how varying oxygen tension may affect tissue *in vitro*, we again examine insulin-mediated glucose uptake of 3D multicellular fat spheroids. Conveniently, adipospheriods grown in hanging drop plates represent an excellent opportunity to test whether oxygen tension is an important consideration in designing an HOC. Because of the high droplet surface area and low volume, hanging drop (HD) culture offers superior gas exchange properties (unpublished data). Adipospheroids containing 8k cells/spheroid were cultured to maturity as described in §2.2. At day 7 post differentiation, half of the spheroids were transferred to an oxygen-controlled incubator and cultured in a 2 percent oxygen atmosphere, typical of the body, for another four days (Lo O_2). The remaining spheroids were cultured in 20 percent oxygen (Hi O_2), typical of laboratory incubator cell culture. Media for both sets of spheroids was changed at day 9 post-differentiation.

On the day of the experiment (day 11 post-differentiation), all spheroids were insulin starved for 3 hours in HBSS with 0.5 mM glucose and divalent cations (HBSS-g). Over the four extra days of culture, lipid accumulation continued in both lo and hi O_2 adipospheroids. As a result, many of these “fatter” tissue constructs floated, making retrieval by conventional means difficult once the spheroids were harvested from the HD

plates. To address this, we pipetted the adipospheroid-containing solution directly onto discs of filter paper (Fisher Scientific) cut to 10 mm in diameter. The filter paper allowed excess media to wick through to a paper towel placed below specifically for this purpose. Adipospheroids, however, remained on the filter paper so long as care was taken to pipette gently. To conduct the glucose uptake assay, filter paper discs containing 50 spheroids each were added to glass vials filled with 272 μL HBSS-g. At $t=0^-$, all conditions were sampled by removing 2 μL of media with a pipette. Subsequently ($t=0^+$), HBSS-g with insulin was added to bring the total volume of each experiment to 300 μL at a concentration of 10 μg/mL insulin. A vehicle dose was added to bring the HCL concentration of each control (no insulin) condition to 0.05 mM HCl to account for acid in the insulin stock solution. All samples were then placed in an incubator at 20 percent oxygen, gently agitated, and sampled at t = 10, 30, 60, and 120 minutes. Supernatant glucose levels were determined as described in §2.4.1 and are reported as cumulative glucose uptake per cell. Data was analyzed for statistical significance using ANOVA and Tukey's post hoc test at confidence level α=0.05 (Figure 2-1).

Although no conditions achieved significance by this metric, two timepoints (t=60 and t=120) did show p-values < 0.1 when comparing hi and lo O_2 insulin-containing conditions. A more aggressive analysis of the data, however, may apply Fisher's Least Significant Difference test. Typically, staticians avoid this test because it fails to correct for multiple comparisons (resulting in a higher rate of false positives). Like Tukey, it pools variances to increase power – especially important in this case where we have

few replicates (in some cases as low as n=3). Using Fisher's post hoc test, we report p-values of <0.05 for both t=60 and t=120 and denote them with a "+" sign.

Surprisingly, the data indicate that low oxygen actually increased fat activity (here measured by Glut4-mediated glucose uptake). Typically, low oxygen tends to suppress cellular basal metabolic rate (20). By extension, we would assume glucose uptake activity of adipocytes would similarly decrease. However, Glut4 is a passive transporter of glucose and therefore unlikely to be affected by subtle changes in cell metabolism, at least over short time periods (21). Furthermore, other researchers have demonstrated that oxidative stress has a similar effect on 3T3-L1 cells *in vitro* (22, 23). Recently, a clinical study observed and explored this same phenomenon *in vivo*, concluding that oxidative stress was capable of interfering with Glut4 glucose uptake and was chiefly responsible for the early onset of insulin resistance in patients placed on a high calorie diet (24). Although these results are unexpected, they are explained by the literature. More importantly – as the oxygen tension *in vitro* can differ from the body by a factor of up to ten (25) – they further highlight the need for careful consideration of the oxygen tension in any HOC.

3.3 Volume of distribution is an important consideration for drug toxicity studies

The way a drug spreads throughout the body and which tissues it partitions to at equilibrium are key considerations for pharmacologists. Collectively, these properties are called distribution and quantified by a "volume of distribution" measurement describing how much liquid the drug appears to be dissolved in, given the initial dose and the concentration in the blood according to Equation 3-1:

$$V_D = {}^{Dose}/_{C_B}$$

Equation 3-1

where V_D is the volume distribution, *Dose* is the total amount of drug administered, and C_B is the concentration of drug in the blood. V_D has units of volume and, at its most basic level, describes whether a drug prefers body water (and thus is more hydrophilic) or body tissue (and thus is more hydrophobic). Accordingly, V_D provides valuable information about how a drug behaves as it is administered, while in the body, and as it leaves (26, 27).

To assess how the inclusion of different tissues might affect drug distribution in an HOC, we constructed a simple distribution experiment to study how fat (or any other tissue) might modulate liver cell toxicity in the presence of amiodarone. An extremely hydrophobic drug, amiodarone is a WHO essential medicine commonly used to treat arrhythmias, but is also known to cause a variety of organ toxicities *in vivo* (28–30). HepG2-C3A cells (ATCC) were grown in DMEM with 10 percent FBS and 1 percent anti/anti and plated at 35k cells/well in a 96-well plated night before the experiment. Fat spheroids (8k cells/spheroid) were prepared as described in §2.2 so that they reached maturity (culture day 7) on the day of the experiment. The day of the experiment, adipospheriods were counted, harvested, and placed in wells containing a liver cell monolayer as 0, 1, 10, or 30 spheroids. Amiodarone (carried in DMSO) was added to designated wells at 0, 1, 10, and 100 μM and DMSO levels were kept constant at 1/1,000 (v/v) across all conditions. After 24 hours, the spheroids were rinsed away and cell metabolic activity was assayed by incubating cells with AlamarBlue (LifeTech) over

2 hours. In the presence of cellular respiration, non-fluorescent AlamarBlue is reduced to a fluorescent molecule and measured using a plate reader (BioTek Synergy Neo) at excitation and emission wavelengths of 560 nm and 590 nm, respectively. Subsequently, cell viability was measured using a CellTiterGlo (Promega) kit to assess cellular ATP levels. In both cases, values are normalized to the 0 μM amiodarone dose condition. Critical to the success of this experiment, differentiated fat is non-adherent – meaning there was no observable migration of cells from the spheroid to the plate. Experiments conducted with other spheroids types were frustrated by heavy cell migration or, in some cases, entire spheroids anchoring onto the monolayer, hopelessly confounding viability and metabolic activity measurements (data not shown).

These experiments show that, at sufficiently lethal doses of amiodarone, adipospheriods protected liver cell viability and metabolism, likely by sequestering the hydrophobic drug themselves. Measurements of both metabolic activity (Figure 3-2, A) and cell viability (Figure 3-2, B) indicated that the presence of adipospheriods significantly shielded liver cells from amiodarone toxicity (* $p<0.05$, ** $p<0.01$, *** $p<0.001$ by ANOVA with Tukey post hoc test). Although expected, these results highlight the importance of taking pharmacokinetic concepts (such as volume distribution) into consideration when designing an HOC. For example, the liver cells in each well have a mass of ~70 μg and a surface area of 32 mm^2 , both corresponding to the liver of a ~$4x10^{-8}$ scale human. Applying this same scaling factor to the drug concentration reveals that the 100 μM amiodarone condition from our experiment falls within an order of magnitude of the range of clinical amiodarone doses as well (up to

~10 mmol). Without considering volume distribution effects, we would advise doctors to never administer this drug as substantial toxicity appears to result from clinical doses administered to the liver cells alone. However, the 10 and 30 adipospheroid conditions (which have 1/6 and 1/2 the fat we would expect for a ~$4x10^{-8}$ human, respectively) shows substantially reduced toxicity and indicates that patient toxicity is likely to differ from our observations *in vitro*. Indeed, including even more tissue mass (*e.g.* the full amount of adipose tissue or a separate muscle tissue construct) would likely further restore liver metabolic function and viability. Accordingly, we conclude that our HOC must consider the impact of drug distribution behavior on relevant parameters such media concentration level of a given drug or metabolite.

3.4 Tissue geometry affects compartment function

Within the body, fat is anything but passive. Adipose tissue is a critical regulator of metabolism and nutrient supply as well as an important source of regulatory hormones such as Adiponectin and Leptin (31). In states of hyper- or hypoglycemia, fat is also charged with sequestering or mobilizing energy. In the case of the former, adipose cells respond to insulin by uptaking glucose from the blood via the Glut4 transporter (32). In any HOC, fat would play a crucial role in system homeostasis and should therefore be scaled appropriately. Accordingly, we leverage our adipospheriod cell constructs as a proxy to test whether size and structure are indeed important considerations for designing an HOC system. Intuitively, both considerations should be important, but we seek explicit confirmation.

3.4.1 Probing organ size and structure

In order to carry out experiments with a reasonable number of cells and maintain relevant cell-media volume ratios, we choose to use a simple microfluidic device to probe insulin-mediated glucose uptake by mature adipospheroids. The microfluidic chips used for all experiments consisted of 0.1 mm tall by 1 mm wide inlet and outlet channels connected to an open 3mm-diameter chamber (Figure 3-3, A&B). Microfluidic channels were fabricated using conventional soft lithography. Briefly, a mold was produced using SU-8 (Microchem) photolithography on silicon wafers, using protocols described by the manufacturers. Poly(dimethylsiloxane) (PDMS) base and curing agent (Sylgard 184, Dow Corning) were mixed in a 10:1 ratio by weight, degassed, and poured over the SU-8 mold. After curing at 60 °C overnight, the PDMS channels were cut, and a 3mm biopsy punch was used to core out the central chamber. The PDMS device was then bonded to glass slides using a plasma cleaner (Covance MP-1, Femto Science), and placed in a 120 °C oven to increase bonding strength and decrease hydrophilicity of the treated device.

To run an insulin-mediated glucose uptake assay, the central chamber was filled with a collagen gel containing either intact or dispersed adipogenically differentiated spheroids. 64k spheroids (Figure 3-4, A) were dispersed by incubating in a solution of 10 μg/mL collagenase IV (Worthington Biochemical) in phenol red-free DMEM (Life Technologies) at 37 °C for 5-10 minutes and manually repeat pipetted. A Live/Dead Cell Viability Kit (LifeTech) showed minimal cell death resulting from the dispersion protocol (Figure 3-4, B). Dispersed or whole spheroids were resuspended in 20 μL collagen gel

precursor solution, loaded into the central chamber with a pipette, and allowed to gel for 15 minutes at 37 °C. An array of 100 μm side-length posts similar to those described by Jeon and colleagues was designed to keep the cell-laden hydrogel precursors from flowing into either the inlet or outlet channels (33). To form the collagen gel precursor solution, 500 μL type I bovine collagen (BD Biosciences) was mixed with 60 μL 10x phosphate buffered saline, and 50 μL 0.8 M $NaHCO_3$ and kept on ice until ready for use. A PDMS slab was then used to seal the chamber for flow experiments. The chip was perfused with high glucose phenol red-free DMEM containing 10 μg/mL insulin at a constant flow rate of 1 μL/min. After 15 minutes of flow, 10 μL of perfusate was collected and stored on ice for later analysis. In order to improve sample collection, device dead volume was minimized. Before loading the central chamber, the device was primed by bringing the insulin/DMEM solution to the edge of the chamber. Moreover, the outlet channel only had a volume of 0.5 μL (1x0.1x5 mm). Although there remained ~4 μL of dead space in the collagen gel matrix, there was sufficient volume of perfusate available for collection at the end of the experiment. Glucose levels in perfusate were measured using an Amplex Red Glucose Oxidase Assay Kit (LifeTech). Outliers were identified and discarded according to Pierce's test (34) and data was analyzed for statistical significance using two-way ANOVA with Tukey's post hoc test.

To test the hypothesis that relative organ size is a critical consideration for a high-fidelity microfluidic model of the body, we used this microfluidic setup to examine a 2-organ (blood, fat) HOC system. Mature, dispersed adiposheroids were seeded in the tissue chamber in either 10x (192k cells) or 1x (19.2k cells) cell concentrations while the

media perfusion (*i.e.* the “blood” volume) was held constant. The 10x condition is consistent with a ~x10^{-7} volumetrically-scaled fat compartment while the 1x condition represents a case where the scaling is off by an order of magnitude. In control experiments, without insulin, there is no discernable change in glucose levels of the perfusate between the two conditions. Upon the addition of insulin, however, the 10x fat compartment uptakes ~5x more glucose than the 1x compartment ($p<0.001$), which remained near control levels (Figure 3-5). The glucose uptake by cells in the 10x condition agreed with previous reports of insulin-induced glucose uptake by adipocytes (35, 36). Glucose levels leaving the adipose chamber were substantially different depending on the scaling approach. As part of an integrated, multi-organ system, any imbalance in media glucose levels could have significant effects for other aspects of the HOC. We not only demonstrate this important design criterion for fat, but also argue that it holds across other organs as well. Therefore, this data highlights the importance of choosing HOC organ sizes that are correctly scaled relative to each other and relative to the system as a whole (37). Since these experiments, others have arrived at similar conclusions, albeit by different approaches (13).

The unique structure of our adipospheroids also provided us a convenient platform to test the hypothesis that the structure of a tissue, in addition to its size, is a critical consideration when designing an HOC. For this experiment, three 64k spheroids (192k cells, same as 10x condition above) were placed in the microfluidic chamber in either a dispersed configuration as before or wholly intact. Again, control (no insulin) experiments failed to demonstrate any meaningful difference between tissue structures,

but upon insulin stimulation, the dispersed condition consumed significantly more glucose ($p<0.01$, Figure 3-6). The difference is likely due at least in part to transportation limitations, but this data nevertheless emphasizes that HOC designers must consider in vivo organ structure when designing *in vitro* mimics, especially as part of an integrative system. We propose that identifying whether the critical function of each organ is associated with surface area or volume and scaling accordingly is one strategy that can address these concerns. This "functional" scaling will be discussed in greater detail in §4.5.1.

3.4.2 Selecting an appropriate HOC scale

In addition to considering the *relative* sizes of an HOC, we must also consider size in an *absolute* sense. To do this, we conduct a brief parameter sweep across several different miniaturization factors, examining implications for the lung, a primarily 2-dimensional organ, and fat, a primarily 3-dimensional organ (Table 3-1). In accordance with QPSRs, blood volume is scaled linearly with mass (9). In scaling the lung, we seek to maintain surface area and physiologic shear stress while accounting for the $M^{3/4}$ change in cardiac output (9, 37–40). Accordingly, 2D organ compartment dimensions are chosen to provide the most realistic culture space and shear stress is calculated according to Equation 3-2:

$$\tau = \frac{6\mu Q}{wh^2}$$

Equation 3-2

where τ = shear stress, μ = viscosity, Q = flow rate, w = chamber width, and h = chamber height (37). Fat mass is simply scaled linearly with body mass and cell number calculated by assuming an cell mass of ~1 ng (39, 41, 42).

Table 3-1 reveals key insights about what scale of HOC is most feasible. The $x10^{-7}$ size boasts attractive compartment dimensions for the lung that are easily obtained with conventional microfluidic fabrication techniques, but has a blood volume of 600 nL, quite small for an entire HOC system, even using microfluidic tools. For example, assuming a channel height of 40 μm and channel width of 100 μm, we would have only 150 mm of length along which to fit all relevant organs! Meanwhile a $x10^{-4}$ scale offers an attractive blood volume, but requires a lung compartment with 70 cm^2 of surface area – well outside the capabilities of conventional fabrication tools. Moreover, the $x10^{-4}$ fat compartment requires billions of cells which again strains current capabilities. At a $x10^{-6}$ miniaturization factor, surface areas, blood volumes, and cell numbers all appears somewhat manageable. Thus we proceed with the design of our HOC at a scale of $x10^{-6}$ compared to a full-sized human.

3.5 Conclusions

In this chapter, we attempt use the adipospheroids developed previously to establish a framework for key details to consider when designing a microphysiological model system of the human body (an HOC). By culturing fat spheroids in different oxygen environments, we showed that oxygen plays a vital role in cell metabolism. A brief study of amiodarone toxicity to liver showed that a realistic distribution space, in addition to appropriate inter-organ relationships, is a key scaling consideration. Lastly,

we explored both relative and absolute sizing. The unique, 3D structure of these spheroids allowed us to interrogate how size and structure may affect inter-organ crosstalk and a parameter sweep of lung, blood, and fat compartments indicated that a $x10^{-6}$ scale would be an appropriate miniaturization factor. These exercises all demonstrated key functional properties of these adipospheriods, but more importantly identified oxygen tension, drug distribution, and tissue size/structure as key design considerations warranting further scrutiny. Moving forward, we build on the principles established in this chapter to move towards a physiologically relevant HOC.

3.6 Works cited

1. Haldane JB (1926) On being the right size. *Harper's Mag* 152:424–427.

2. L. M. Sweeney, M. L. Shuler, J. G. Babish, A. Ghanem (1995) A Cell Culture Analogue of Rodent PHysiology: Application to Naphthalene Toxicology. *Toxicol Vitro* 9(3):307–316.

3. Viravaidya K, Sin A, Shuler ML (2004) Development of a Microscale Cell Culture Analog To Probe Naphthalene Toxicity. *Biotechnol Prog* 20(1):316–323.

4. Esch MB, Mahler GJ, Stokol T, Shuler ML (2014) Body-on-a-chip simulation with gastrointestinal tract and liver tissues suggests that ingested nanoparticles have the potential to cause liver injury. *Lab Chip* 14(16):3081.

5. Sung JH, Kam C, Shuler ML (2010) A microfluidic device for a pharmacokinetic–pharmacodynamic (PK–PD) model on a chip. *Lab Chip* 10(4):446.

6. Sung JH, et al. (2013) Microfabricated mammalian organ systems and their integration into models of whole animals and humans. *Lab Chip* 13(7):1201.

7. Abaci H, Shuler M (2015) Human on a chip Design Strategies and Principles for Physiologically Based Pharmocokinetics/Pharmacodynamics Modeling. *Integr Biol*. doi:10.1039/C4IB00292J.

8. Kleiber M (1947) Body size and metabolic rate. *Physiol Rev* 27(4):511–541.

9. West GB, Brown JH, Enquist BJ (1997) A General Model for the Origin of Allometric Scaling Laws in Biology. *Science* 276(5309):122–126.

10. Banavar JR, et al. (2010) A general basis for quarter-power scaling in animals. *Proc Natl Acad Sci* 107(36):15816–15820.

11. Vozzi F, Heinrich J-M, Bader A, Ahluwalia AD (2008) Connected culture of murine hepatocytes and human umbilical vein endothelial cells in a multicompartmental bioreactor. *Tissue Eng Part A* 15(6):1291–1299.

12. Mazzei D, Guzzardi MA, Giusti S, Ahluwalia A (2010) A low shear stress modular bioreactor for connected cell culture under high flow rates. *Biotechnol Bioeng*:127–137.

13. Ucciferri N, Sbrana T, Ahluwalia A (2014) Allometric Scaling and Cell Ratios in Multi-Organ in vitro Models of Human Metabolism. *Front Bioeng Biotechnol* 2. doi:10.3389/fbioe.2014.00074.

14. Wikswo JP, et al. (2013) Engineering Challenges for Instrumenting and Controlling Integrated Organ-on-Chip Systems. *IEEE Trans Biomed Eng* 60(3):682–690.

15. Wikswo JP, et al. (2013) Scaling and systems biology for integrating multiple organs-on-a-chip. *Lab Chip* 13(18):3496.

16. Marx U, et al. (2012) “Human on a chip”developments: a translational cutting-edge alternative to systemic safety assessment and efficiency evaluation of substances in laboratory animals and man? *Altern Lab Anim-ATLA* 40(5):235.

17. Maschmeyer I, et al. (2015) A four-organ-chip for interconnected long-term co-culture of human intestine, liver, skin and kidney equivalents. *Lab Chip* 15(12):2688–2699.

18. Donald Voet, Judith G. Voet (2004) *Biochemistry* (John Wiley & Sons, USA). 3rd Ed.

19. Widmaier EP, Raff H, Strang KT (2006) *Vander’s Human Physiology* (McGraw-Hill, New York). 10th Edition.

20. Schumacker PT, Chandel N, Agusti AG (1993) Oxygen conformance of cellular respiration in hepatocytes. *Am J Physiol-Lung Cell Mol Physiol* 265(4):L395–L402.

21. Watson RT, Pessin JE (2006) Bridging the GAP between insulin signaling and GLUT4 translocation. *Trends Biochem Sci* 31(4):215–222.

22. Damien Demozay, Jean-Christophe Mas, Stephane Rocchi, Emmanuel Van Obberghen (2008) FALDH Reverses teh Deleterious Action of Oxidative Stress Induced by Lipid Peroxidation Product 4-Hydroxynonenal on Insulin Signaling in 3T3-L1 Adiopcytes. *Diabetes* 57(5):1216.

23. Frohnert BI, Bernlohr DA (2013) Protein Carbonylation, Mitochondrial Dysfunction, and Insulin Resistance. *Adv Nutr Int Rev J* 4(2):157–163.

24. Boden G, et al. (2015) Excessive caloric intake acutely causes oxidative stress, GLUT4 carbonylation, and insulin resistance in healthy men. *Sci Transl Med* 7(304):304re7–304re7.

25. Carreau A, Hafny-Rahbi BE, Matejuk A, Grillon C, Kieda C (2011) Why is the partial oxygen pressure of human tissues a crucial parameter? Small molecules and hypoxia. *J Cell Mol Med* 15(6):1239–1253.

26. Malcom Rowland, Thomas N. Tozer (1995) *Clinical Pharmacokinetics: Concepts and Applications* (Williams & Wilkins, Baltimore). Third Edition.

27. Leon Shargel, Andrew B.C. Yu (1993) *Applied Biopharmaceutics and Pharmacokinetics* (Appleton & Lange, Norwalk, CT). Third Edition.

28. David W. Holt, Geoffrey T. Tucker, Peter R. Jackson, Gerard C. A. Storey (1983) Amiodarone pharmacokinetics. *Am Heart J* 106(4):840–847.

29. Marchilinski FE, Gansler TS, Waxman HL, Josephson ME (1982) Amiodarone pulmonary toxicity. *Ann Intern Med* 97(6):839–845.

30. Morse RM, et al. (1988) Amiodarone-induced liver toxicity. *Ann Intern Med* 109(10):838–840.

31. Trayhurn P, Beattie JH (2001) Physiological role of adipose tissue: white adipose tissue as an endocrine and secretory organ. *Proc Nutr Soc* 60(03):329–339.

32. Mayumi Inoue, Lisa J. Brunet, Joseph Hwang, Shian-Huey Chiang, Alan R. Saltiel (2003) The exocyst comlex is required for targeting of Glut4 to the plasma membrane by insulin. *Nature* 422(6932):629–633.

33. Huang CP, et al. (2009) Engineering microscale cellular niches for three-dimensional multicellular co-cultures. *Lab Chip* 9(12):1740.

34. Stephen M Ross (2003) Pierce's Criterion for the Elimination of Suspect Experimental Data. *J Eng Tech* 20(2):38–41.

35. Olefsky JM (1976) Effects of fasting on insulin binding, glucose transport, and glucose oxidation in isolated rat adipocytes: relationships between insulin receptors and insulin action. *J Clin Invest* 58(6):1450.

36. Zuber MX, Wang SM, Thammavaram KV, Reed DK, Reed BC (1985) Elevation of the number of cell-surface insulin receptors and the rate of 2-deoxyglucose uptake by exposure of 3T3-L1 adipocytes to tolbutamide. *J Biol Chem* 260(26):14045–14052.

37. Moraes C, et al. (2013) On being the right size: scaling effects in designing a human on a chip. *Integr Biol* 5(9):1149.

38. Peters RH (1983) *The Ecological Implications of Body Size* (Cambridge University Press, New York).

39. Williams LR, Leggett RW (1989) Reference values for resting blood flow to organs of man. *Clin Phys Physiol Meas* 10(3):187.

40. John E. Hall (2010) *Guyton and Hall Textbook of Medical Physiology* (Elsevier). 12th Edition.

41. Bosy-Westphal A, et al. (2004) Effect of organ and tissue masses on resting energy expenditure in underweight, normal weight and obese adults. *Int J Obes* 28(1):72–79.

42. Park K, et al. (2008) "Living cantilever arrays" for characterization of mass of single live cells in fluids. *Lab Chip* 8(7):1034.

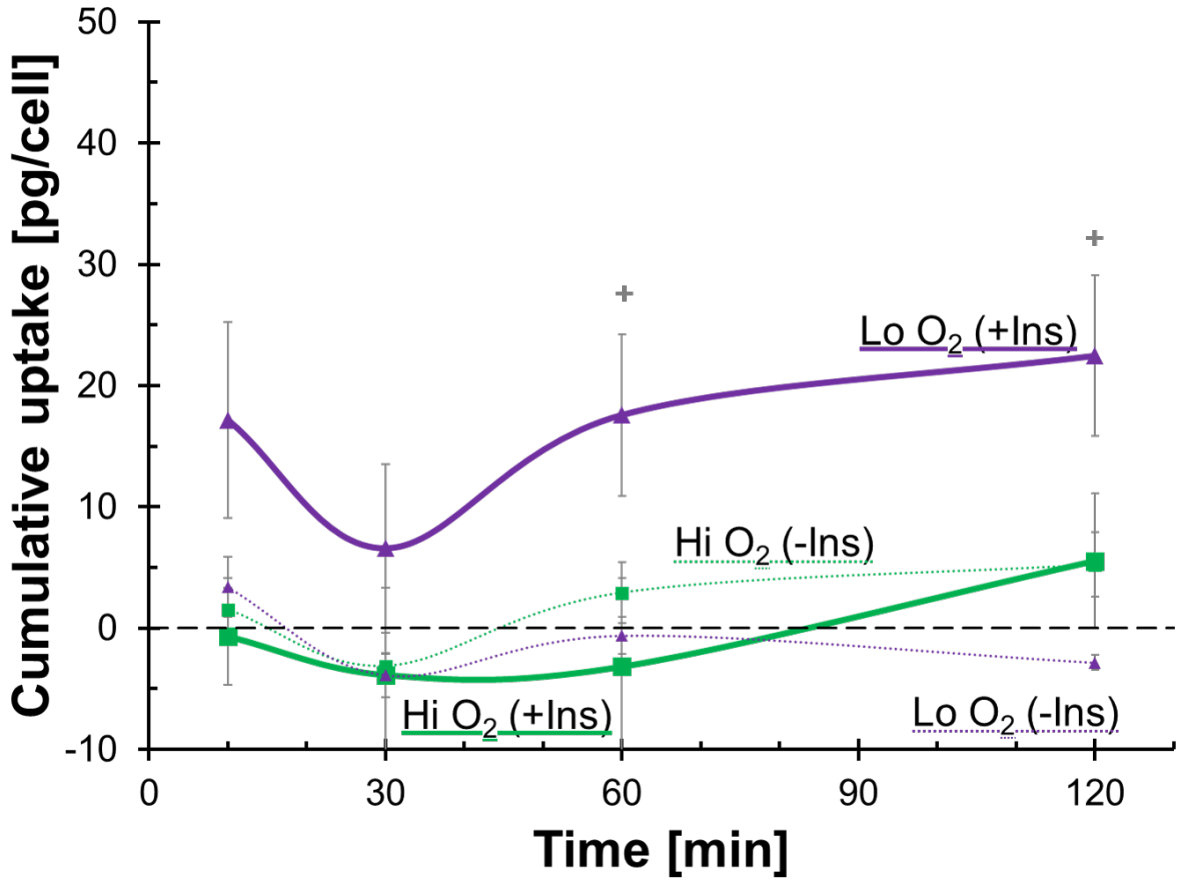

Figure 3-1: Culture oxygen level affects insulin-induced glucose uptake among 8k adipospheroids.

Mature adiposhperiods grown in either high (Hi; 20 percent, typical of laboratory incubator culture) or low (Lo; 2 percent, approximating oxygen tension in the body) oxygen conditions were stimulated with insulin and cumulative glucose uptake was measured over two hours. Under these conditions, adipospheroids grown at low oxygen levels demonstrated more efficient glucose uptake. Data reported as average ± standard deviation, n=3-5; $^{+}$ indicates $p<0.1$ by ANOVA with Tukey post hoc test.

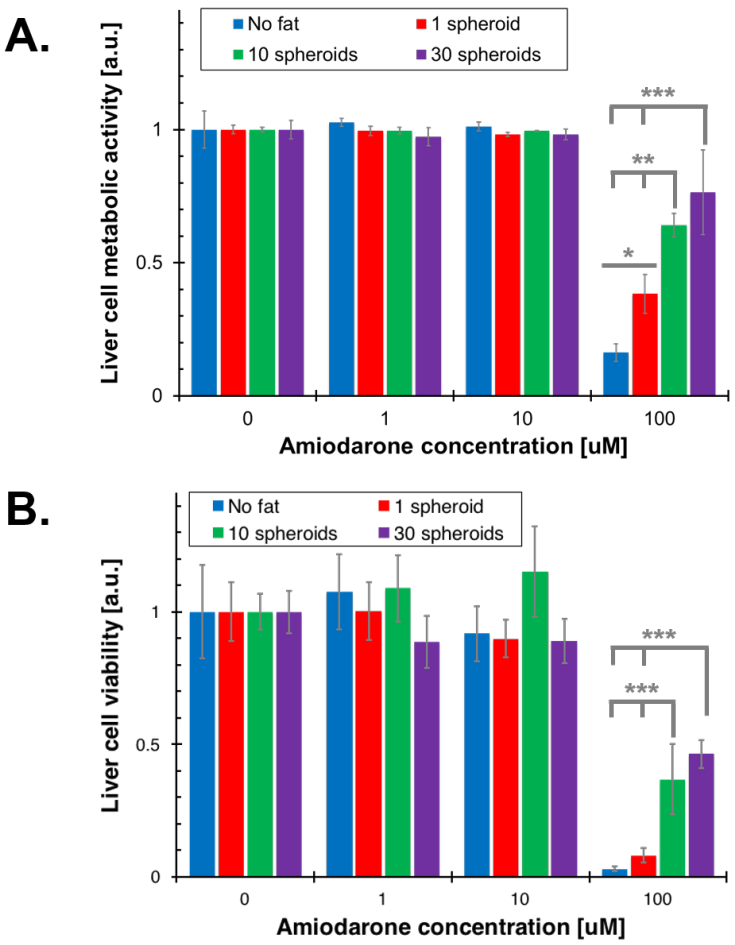

Figure 3-2. Adipose spheroids rescue liver cells from amiodarone toxicity

HepG2-C3A cells cultured in the presence of amiodarone showed a marked decreased in both (A) metabolic activity and (B) viability at high doses of the drug. Co-culture with mature adipospheroids abrogated these effects, especially culture with 10 or 30 fat spheroids (a number approximating the liver-adipose mass ratio in a healthy adult). Data reported as average ± standard deviation; n=3-4; * indicates $p<0.05$, ** indicates $p<0.01$, and *** indicates $p<0.001$ by ANOVA with Tukey post hoc test.

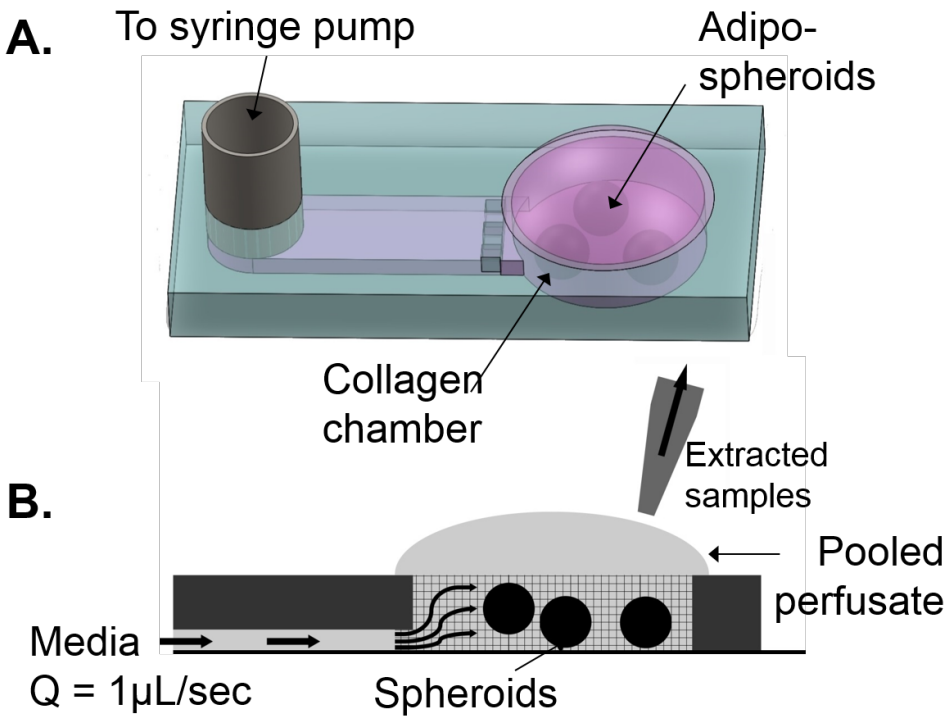

Figure 3-3. Experimental setup for insulin-mediated glucose uptake experiments

Two-compartment organ-on-a-chip devices. (A, B) Schematics demonstrating device structure and operation. Cell- or spheroid-laden collagen is gelled in the collagen chamber. The posts around the chamber prevent the collagen from travelling into the channels. A syringe pump forces media through the system at a volumetric flow rate Q of 1 μL/s, and the pooled perfusate is pipetted away at the end of the experiment.

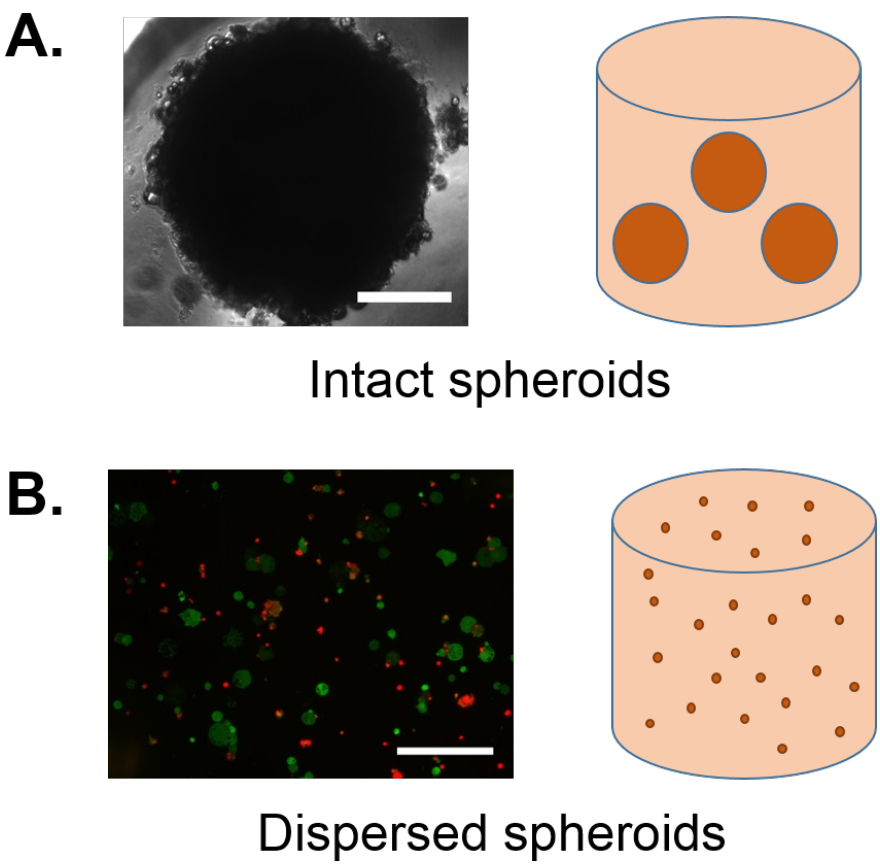

Figure 3-4. Adiposheroids containing 64k cells each were used to mimic fat

Tissue structure was manipulated by either (A) leaving the spheroid intact or (B) dispersing the spheroid with collagenase and gentle mechanical aspiration. After the dissociation process most cells remained viable as indicated by live/dead staining (green = calcein AM stained cells, live; red = ethidium homodimer stained cells, dead). Scale bars = 300 μm.

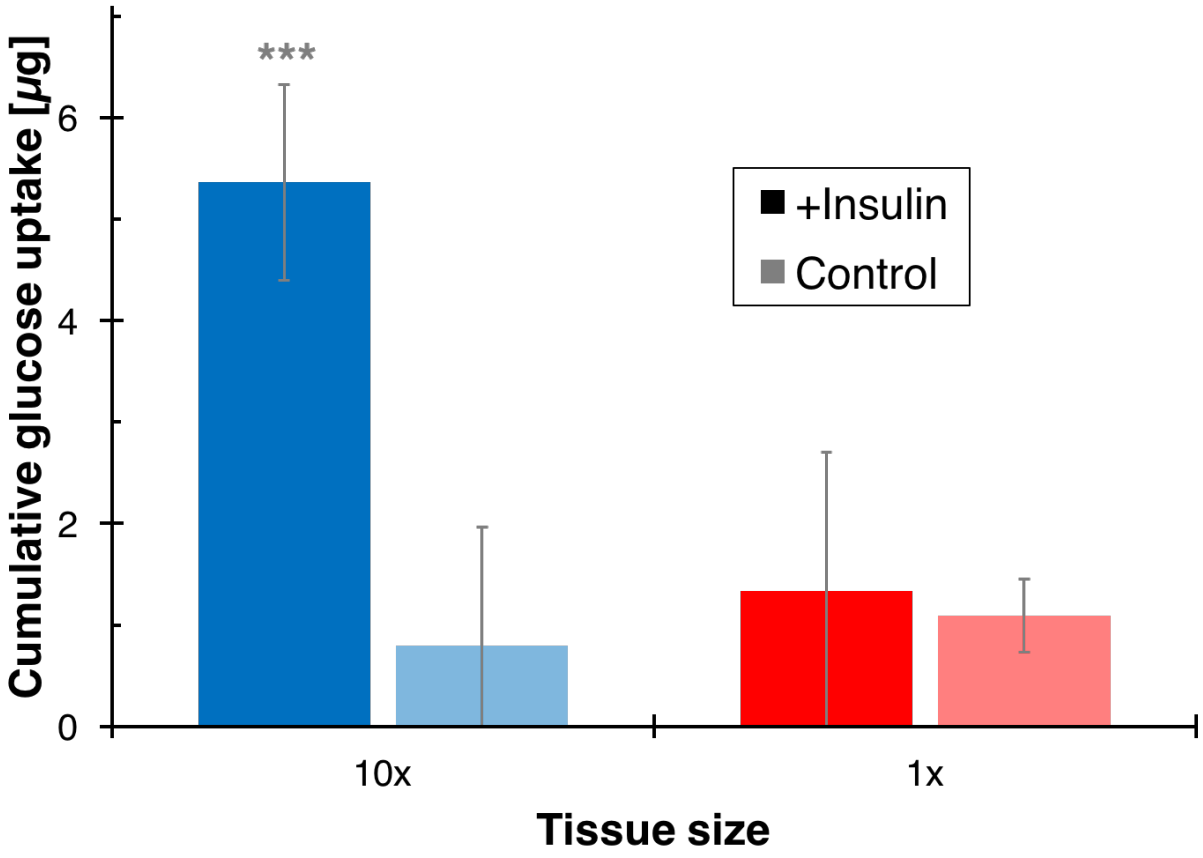

Figure 3-5. Effect of tissue size on glucose uptake

Tissue size (*i.e.* number of dispersed cells) significantly affects cumulative insulin-stimulated glucose uptake for a microfluidic model of fat. 10x condition corresponds to cells from 3 dispersed spheroids (approximately 192k cells) while 1x condition corresponds to approximately 19.2k cells. Data plotted as average ± standard deviation for n=7-8 with outliers identified and excluded by Pierce's test. *** indicates statistically significant against all other conditions by two-way ANOVA and Tukey post hoc test with $p<0.001$.

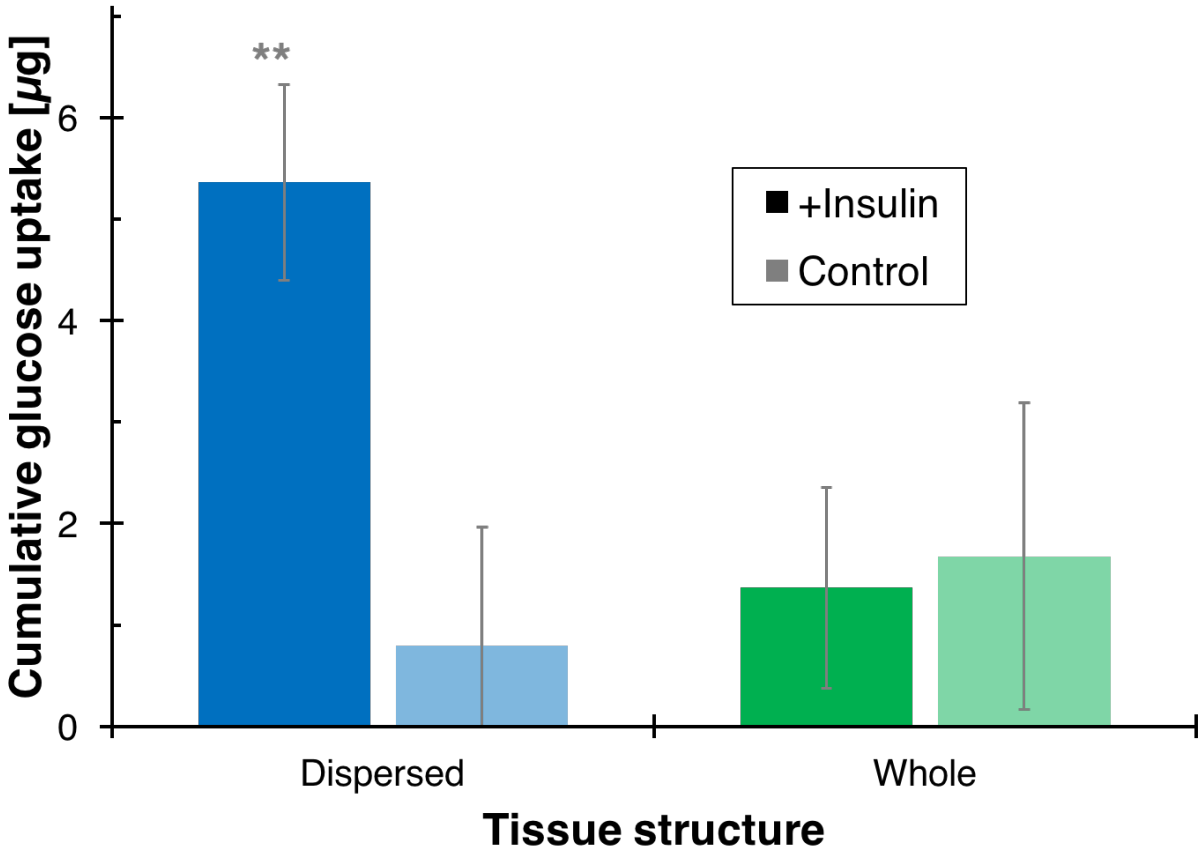

Figure 3-6. Effect of tissue structure on glucose uptake

Tissue structure (*i.e.* intact or dispersed spheroid) significantly affects cumulative insulin-stimulated glucose uptake for a microfluidic model of fat. Dispersed condition consists of cells from three 64k adipospheroids dissociated by collagenase and mechanical aspiration. Data plotted as average ± standard deviation for n=7-8 with outliers identified and excluded by Pierce's test. ** indicates statistically significant against all other conditions by two-way ANOVA and Tukey post hoc test with $p<0.01$.

Scale	Blood volume[α]	Lung					Fat	
		Dimensions[β]			Volume	% BV	Mass[γ]	Cell number[δ]
		Length	Width	Height				
Human[ε]	6 L	---	---	---	---	---	23 kg	$2x10^{13}$
$x10^{-4}$	600 μL	1 cm	70 cm	25 μm	175 μL	35	2.3 g	$2x10^{9}$
$x10^{-6}$	6 μL	9 mm	8 mm	35 μm	2.5 μL	42	23 mg	$2x10^{7}$
$x10^{-7}$	600 nL	5 mm	1 mm	35 μm	175 nL	30	2.3 mg	$2x10^{6}$

Table 3-1. Key design values for lung and fat at different miniaturization factors

To determine an appropriate absolute system size, we examine critical parameters for prototypical 2-dimensional (lung) and 3-dimensional (fat) organs across three miniaturization factors. Considering the challenges presented by small blood volumes, large surface areas, and total cell numbers, we conclude that $x10^{-6}$ is the most convenient scaling factor for constructing a microfluidic human on a chip.

α – According to QPSRs, blood volume scales with M^1 (9).
β - Lung dimensions are chosen to match physiologic shear values given cardiac output at the chosen scale. Shear is calculated according to the Equation 3-2 (37).
γ – Organ mass is scaled according to M^1.
δ – Assuming a cell mass of 1 ng/cell (42).
ε – Human values derived from several sources (38–41).

Chapter 4:

Building an Experimental Model of the Human Body with Non-Physiological Parameters

New advances in engineering and biomedical technology have enabled recent efforts to capture essential aspects of human physiology in microscale, in vitro systems. The application of these advances to experimentally model complex processes in an integrated platform – commonly called a “human on a chip” (HOC) – requires that relevant compartments and parameters be sized correctly relative to each other and the entire system. Empirical observation, theoretical treatments of resource distribution systems, and natural experiments can all be used to inform ration design of such a system, but technical and fundamental challenges (e.g. small system blood volumes and context-dependent cell metabolism, respectively) pose substantial, unaddressed obstacles. Here, we develop a holistic, nature-inspired approach to these problems, demonstrating that O_2 deprivation is a viable strategy for inducing in vivo-like cellular metabolic rates in vitro and that the effects on increased blood volumes on drug concentration can be mitigated. Combining these principles, observations, and strategies, we derive a basic set of design criteria for a practically-realizable, physiologically-faithful, five-organ x10-6 microfluidic model of the human body.

4.1 Introduction

Advances in micro-scale engineering, cell sourcing, and culture techniques are presenting new opportunities to recapitulate key structural and functional characteristics of the human body in controlled, *in vitro*, experimental systems. Already, organ-level devices (commonly called “organs-on-a-chip” or OOCs) are quite prolific (1–3). Efforts at devising systems-level platforms (“humans-on-a-chip” or HOCs) hold even greater promise (4–7). Ideally, these small HOCs would predict the effects of potential drugs or toxins will have on the human body (8–10), significantly reducing costs associated with animal and human clinical trials in the drug discovery pipeline and clarifying mechanisms of human health and disease. However, unresolved issues in both the design and fabrication of such systems present scientists and engineers with a complex, interconnected set of problems.

Nutrient distribution networks (specifically those for oxygen) generally control the relationship between organism size and metabolism (11–13). As a result, many important physical parameters scale with organism mass (M) raised to the power of a multiple of ¼, called quarter-power scaling relationships (QPSRs) for short (*e.g.* metabolic rate: $M^{¾}$, heart rate: $M^{-¼}$, and blood volume: M^{1}). These QPSRs (6, 14, 15), along with simple heuristics (16, 17), residence time and PB-PKPD models (4, 5, 8, 18–20), empirical allometry (21, 22), and functional approaches (21–23) have also been used in the design of HOCs. Although these approaches do inform values for organ compartment size and other physiological parameters, they also present intractable problems. Some issues that arise, such as context-dependent changes in cellular BMR

(24–27), are fundamental and may only be remedied by careful and deliberate design. Others, such as difficult to fabricate, low total blood volumes for a $x10^{-6}$ HOC (2, 7, 17, 20, 21), are technical and may be overcome with suitable advances in science and engineering.

We propose that these challenges themselves only merit concern so far as they affect the end output of the HOC. That is, the *structure* of a $x10^{-6}$ HOC may assume strange and unexpected forms so long as the *function* – the system-level behavior of the HOC – is accurate and relatable to the human body. Therefore, discrete parts of an HOC need not be confined by conventional notions of what constitutes "normal" or "physiologic" even if those values are prescribed by well-supported research such as QPSRs. To that end, we focus on designing and $x10^{-6}$ HOC capable of mimicking key *functions* of a macro human: (1) cellular and macro basal metabolic rates and (2) basic pharmacokinetics. We further demonstrate how Nature herself may stray from structures of typical physiology (*e.g.* a hemoglobin-free vertebrate), yet produce species capable of adapting and surviving. As modification of any one system parameter necessarily affects all others, both natural and artificial design alterations demand a holistic approach. Applying these general principles, we propose specific design parameters for an HOC that is practical in terms of fluid to cell ratios and is a $x10^{-6}$ miniaturization of the human body with regards to total cell mass, yet remains a faithful model of macroscopic human physiology with regards to cellular BMR, basic pharmacokinetics, and inter-organ scaling.

4.2 Control of cellular BMR

As predicted by QPSRs, cellular metabolic rate scales with animal mass (24, 25, 27). However, cells cultured *in vitro* tend to operate at the same, elevated metabolic rate regardless of their origins (Figure 4-1, A) (24, 26). Without accounting for this phenomenon, cells in an HOC would have a high BMR, more akin to cells in mouse (Figure 4-1, B) than in a human (Figure 4-1, C). As a result, the total BMR of the modeled organism diverges from that observed in nature; the magnitude of the error increases with organism size as $\propto M^{1/4}$ (Figure 4-1, D). For example, failure to consider the context-dependent behavior of cells in attempting to design a $x10^{-6}$ model of a human would result in an HOC wherein the cellular BMR is high and thus approximates that of a mouse and the system BMR is also high and approximates that of a $x10^{-6}$ elephant! Because of this non-linearity in scaling, rational design – and control – of the metabolic infrastructure of an HOC is crucial. We propose that designers must force cells in an HOC to function as they would in the body – that is, designers must suppress cellular BMR in accordance with Figure 4-1, A. Accordingly, we dub this principle "metabolically-supported" scaling. An interesting consequence of this strategy is that, by virtue of holding cell BMR constant, it abolishes the $M^{3/4}$ dependence of system BMR, instead replacing it with a M^{1} dependence and causing the relationship between human and HOC BMR to lie on a fundamentally different trajectory than human-animal (Figure 4-2).

Although others have demonstrated metabolic control by regulating glucose (28), ions (29), or ECM cues (30), we propose to suppress cellular BMR by regulating oxygen

(23). Not only does this approach more closely approximate conditions in the body than the hyperoxic conditions of incubator cell culture, but *in situ* microfluidic O_2 sensing and control is an established and active area of research (31–33). We attempt, with three different experimental techniques, to demonstrate this effect. Although we are unsuccessful here, we note that others have observed a ~2.5 fold decrease in cellular oxygen consumption when cells are subjected to *in vivo*-like oxygen tension (34).

4.2.1 Extracellular flux analysis

To demonstrate that O_2 deprivation is a viable method for controlling cellular metabolic rate, we examine the behavior of five human cell types in a Seahorse XFe Extracellular Flux Analyzer: IMR-90, a lung fibroblast cell line; HepG2-C3A, a liver carcinoma cell line; NHBE, primary normal bronchial epithelial cells; NHA, primary astrocytes; and HCMEC, primary brain endothelial cells. The XFe Analyzer creates a microchamber around the cells and monitors O_2 and pH levels over time (Figure 4-2, A). Accordingly, our hypothesis was that as cells depleted environmental O_2, we would be able to observe a corresponding decrease in BMR

HEK-293, HS-5, HepG2-C3A, and IMR-90 (ATCC) cells were grown in DMEM supplemented with 10% FBS and 1% antibiotic-antimycotic. NHBE cells (Lonza) were cultured using BEGM BulletKit media (Lonza), NHA cells (Lonza) were cultured in ABM BulletKit media (Lonza), and HCMEC cells (Cedarlane Labs) were cultured in EBM-2 BulletKit media (Lonza). The night before the experiment, cells were trypsinized, counted, resuspended, and plated in a 96-well assay microplate. A second, identical microplate was seeded for cell quantification. The same assay media was used for all

cell types and consisted of Seahorse Base Medium (Seahorse Bioscience), supplemented with 4.5 g/L D-glucose, 110 mg/L sodium pyruvate, and 54 mg/L L-glutamine. Before use, the pH was adjusted to 7.4 ± 0.05. The morning of the experiment, the assay plate was washed three times with assay media and placed in a CO_2-free incubator. After 1 hour, the assay plate was washed twice more and the experiment begun. The XFe Analyzer forms a 2.12 μL microchamber around the cells and monitors pH and O_2 levels over the course of an hour.

The rates of change of these measurements are then computed using an algorithm to account for the gas permeability of the plate and diffusion into and out of the chamber (35). We calculate BMR using the known stoichiometry between O_2 consumption, H^+ production, and ATP production (36). BMR is normalized according to the number of cells per well as determined by CellTiter-Glo (Promega) on the quantification plate. Since oxygen depletion in the microchamber is driven solely by the cells, only one condition reached *in vivo* organ O_2 levels (37) over the course of the hour-long experiment (Figure 4-3, B). Therefore, we conclude that cellular activity alone is not sufficient to drive the necessary microchamber oxygen depletion over the course of the hour-long experiment and search out an alternative method to test our hypothesis.

4.2.2 Glucose and lactate measurements

Since the cells alone were incapable of driving sufficient oxygen depletion, we used an atmosphere control system to impose different oxygen tensions on cellsand sought to determine cell BMR by measuring glucose uptake. Using the same setup as

in §4.2.3, we exposed HEK-293, IMR-90, HS-5, and HepG2-C3A cells to 2, 7, and 20 percent oxygen for a total of 24 hours. As suggested by a previous report (34), the 2 and 7 percent O_2 conditions were gradually drawn down from atmospheric oxygen over the course of four hours. At the end of the experiment, media samples were collected and glucose levels were measured as described in §2.4.1. Subsequently, a CellTiterGlo (Promega) kit was used to assay ATP levels of the cells.

With some conditions characterized by large error bars, the glucose measurements showed that cellular uptake increased with decreasing oxygen tension (Figure 4-4, A). This data, however, is confounded by two issues. First, cells may use glucose to produce energy either by aerobic respiration or via glycolysis/fermentation (36, 38). As cells shift to glycolytic/fermentation pathways, increased glucose uptake could still result in an overall decrease in cellular BMR. We attempted to tease out this effect by assaying for lactate in our samples, however a lactate detection kit (Sigma) provided inconsistent results, with internal controls giving different values. Second, glucose uptake does not necessary correspond to glucose *usage*. For example, liver cells, including the HepG2 line used here, also uptake glucose to synthesize glycogen, storing nutrients for later use (38–40). ATP levels showed a more expected trend, with ATP content per cell decreasing significantly with decreasing oxygen availability (Figure 4-4, B). At the very least, this indicates that cell reduce their energy reserves under low oxygen tension conditions and agrees with previous results (34).

4.2.3 Metabolic reduction indicator

Finally, we used the same oxygen control system and used AlamarBlue, a metabolic indicator, to look for evidence of oxygen conformance. HEK-293, IMR-90, HS-5, and HepG2-C3A cells were seeded at 25k cells/well in 96 well plates and allowed to adhere overnight. The plates were then placed in an atmosphere control chamber (BioSphyrix OxyCycler, New York) within an incubator and set to 2, 8, or 20 percent oxygen with 5 percent CO_2. Each condition was allowed to equilibrate in the controlled atmosphere for 4 hours at which point AlamarBlue (LifeTech), an indicator of metabolic activity, was added. Two hours later, the fluorescence of each plate (proportional to the amount of reduced AlamarBlue) was measured on a fluorescent plate reader (BioTek) at 560/590 nm (ex/em). Surprisingly, the results indicated that AlamarBlue metabolism actually increased in low oxygen conditions (Figure 4-5, A) – the opposite of what we had expected.

Initially, we hypothesized that AlamarBlue may be subject to re-oxidation. A more oxygen-rich environment would then lead to less reduced (fluorescent) AlamarBlue in solution. We tested this suspicion by fully reducing AlamarBlue solution in an autoclave according to manufacturer instructions, incubating the solution at oxygen tensions of 2, 7, and 20 percent, and measuring the fluorescence after two hours. The data showed no measurable change in fluorescence (Figure 4-5, B), indicating that oxygen tension does not influence the AlamarBlue signal itself.

However, if we scrutinize the mechanism by which AlamarBlue is reduced and becomes fluorescent, an important consideration emerges. AlamarBlue indicates cell

metabolic activity by serving as an electron acceptor during aerobic respiration. It has a strongly positive oxidation reduction potential value compared to other relevant biomolecules (*e.g.* cytochrome c) meaning that it is more likely to serve as an oxidizing agent. Nevertheless, this value is still nearly three times less than that of oxygen. As a result, changing the oxygen availability across different conditions will necessarily change how well AlamarBlue is able to compete to accept electrons – the two parameters are thus convoluted and changing O_2 levels must be controlled for.

To account for the affect of changing oxygen tension on AlamarBlue reduction, we use Equation 4-1 to account for the reduction potential of both molecular oxygen and AlamarBlue in the face of changing oxygen level:

$$BMR = AB_{Red} * \frac{\Delta P_{AB} + X * \Delta P_{O2}}{\Delta P_{AB}}$$

Equation 4-1

where AB_{Red} is the fluorescent measurement from the assay, ΔP_{AB} is the difference in reduction potential between AlamarBlue and cytochrome c, the ultimate reducing agent of oxygen in aerobic respiration, X is the fractional reduction of oxygen tension compared to a 20 percent O_2 atmosphere, typical for a laboratory cell culture incubator, and ΔP_{O2} is the difference in reduction potential between O_2 and cytochrome C. Using values standard values to calculate ΔP (41), we can generate a corrected BMR. Although this metric is unitless, we may nevertheless compare relative BMR's (Figure 4-6). With this new dataset, we see that all four cell types do indeed respond to lower oxygen levels by decreasing cellular BMR, validating our approach. Two caveats must apply to this analysis, however. First, the BMR values compared here are *aerobic*

only; we make no effort to measure energy derived from fermentation. As respiration is an order of magnitude more efficient, any error introduced by this approach is likely to be sufficiently small. Second, while these BMR's are purely *relative* measurements, one may theoretically use a series of calibration experiments to arrive at a set of *absolute* measurements for cellular metabolic rates by this method.

4.3 An example of extra-physiologic survival – the icefish

The design modifications proposed in §4.2 beg the question of whether such extreme departures from expected physiologic parameter values are acceptable. Would an organism with drastically altered blood O_2 carrying capacity or completely lacking Hb be viable at all? Fortunately Nature herself has provided a unique example of such extra-physiologic adaptation and survival. The family *Channichthyidae* (sometimes called "icefish") comprises hemoglobin-negative (Hb-) fish living in the Antarctic waters of the Southern Ocean. First documented in the 1840's, initial attempts to examine the fish were thwarted by an uncooperative cat who absconded with the specimen before it could be further studied (42). Subsequent investigations highlighted family members', including *Chaenocephalus aceratus*'s (Figure 4-7, A) startling lack of blood pigment and hemoglobin (Figure 4-7, B) (43–46). Just as technical and fundamental limitations force HOC designers to contort system parameters in strange or unexpected ways, so too has Nature forced *C. aceratus* to counter its own maladaptation in order to survive.

To demonstrate, and perhaps learn from, this extra-physiologic survival, we examine the fish in more detail. As a control, we use a cousin of *C. aceratus*, *N. coriiceps* (also called *neglecta*), from the common suborder *Nototheniodei* (47). *N.*

coriiceps shares a similar environment and metabolic rate (measured by oxygen consumption) as *C. aceratus* (48–50), but unlike the icefish, produces Hb at normal levels. Starting from a healthy *N. coriiceps*, we remove Hb and then apply the adaptations that allow *C. aceratus* to thrive: increasing cardiac output by a factor of nearly two and allowing for increased cutaneous respiration (44, 45, 48–52). The result is a test-fish with several surprising extra-physiologic features, but nevertheless capable of survival (Table 4-1). In particular, the ability of *C. aceratus* to absorb oxygen through its skin evokes polydimethylsiloxane (PDMS) – a common polymer in microfluidic and biomedical research applications that has similar properties of gas permeability (Appendix A).

In addition to larger-than-expected cardiac output, *C. aceratus* also has a blood volume of ~90 mL/kg, nearly 2x greater than the ~50 mL/kg expected for a fish its size (46, 53–56). Another member of *Channichthyidae*, *C. hamatus*, has a blood volume over two-fold its predicted value (54). These Hb- fish substantially exceed expected blood volumes yet thrive (Appendix B), reinforcing the idea that extra-normal physiology can be an acceptable mechanism to survive in the face of limitations. Related to that increased blood volume, *C. aceratus* also exhibits increased capillary density. Recent results demonstrated that 3 different metrics of vascularization were all ~2x greater in *C. aceratus* than in *N. coriiceps* (Figure 4-8, A&B) (57). Therefore, even though blood flow rates are double in *C. aceratus*, so too is organ blood volume, indicating that tissue residence times – a key parameter in PBPK/PD models – should also remain unchanged between it and *N. coriiceps*.

This increased vascularity also helps compensate for dilution of soluble factors (*e.g.* O_2, drugs, or hormones) due to increased blood volume. At steady state the perfusion-limited diffusion of molecules from blood into tissue is described by Equation 4-2:

$$D \cdot \nabla^2 C = R$$

Equation 4-2

where *C* is the concentration, *D* is the diffusion coefficient, and *R* is the uptake of solute by cells, governed in this case by Michaelis-Menten kinetics (16, 58). Although a decrease in blood concentration leads to a decrease in potential gradient to drive diffusion, a corresponding decrease in intervessel distance (IVD) suggests that solute penetration may be similar, shown here specifically for O_2 (Figure 4-8, C). This icefish adaptation is another example of Nature finding a holistic, multi-faceted solution to physiologically challenging conditions. Of course, applying designs such as these to an HOC may still introduce problems with drugs or molecules that act in a concentration-dependent mechanism on the blood vessels themselves as well as other unforeseen consequences. Conversely, these data also suggest that depletion of soluble factors (*e.g.* oxygen) could be achieved over shorter distances, an important design consideration for engineering organ compartments such as the liver (16, 59). Nevertheless, this preliminary analysis demonstrates that blood O_2 carrying capacity and the presence of Hb may be tuned to counter maladaptations – or possibly induce more appropriate cellular metabolic behavior. The icefish further suggests that increased blood volumes may be accommodated without drastically altering organism pharmacokinetics or stromal solute concentration gradients.

4.4 A distribution-informed approach to HOC blood volume

Designing a x10^{-6} HOC according to QPSRs alone would result in a system blood volume of ~6 μL, too small for even cutting-edge microfluidics and an acknowledged problem in the field (7, 17, 20, 21, 23). Although a 10x (or greater) increase would yield an HOC with a more manageable circulating volume, it would also dilute soluble factors and violate QPSRs. Therefore, we adopt a pharmacokinetic approach to investigate whether and to what extent the blood volume of an HOC can be increased while maintaining physiological relevance.

When a drug is administered, only a portion circulates dissolved in the blood. Accordingly, pharmacologists define volume of distribution, V_D (Equation 3-1), to describe how much drug is available in the plasma compared to the initial dose (60, 61). Conceptually, V_D closely resembles a partition coefficient describing the equilibrium distribution of a drug between the body and the blood. Using a slightly different approach, we consider the distribution of a drug between body water – including blood – and tissue. Therefore, this treatment is most applicable to small, perfusion-limited drugs without substantial serum protein binding. This ratio, *D*, is defined by Equation 4-3:

$$D = \frac{C_T}{C_W}$$

Equation 4-3

where *D* is the distribution coefficient, C_T is the concentration of drug in body tissue, and C_W is the concentration of drug in body water. Introducing terms for the total amount of drug in the system (*Dose*), blood volume (V_B), concentration of drug in blood (C_B), tissue volume (V_T), and non-blood water (V_O), we rearrange to obtain Equation 4-4:

$$C_B = \frac{Dose}{(V_O+V_B)+D^*V_T}$$

Equation 4-4

If we apply an arbitrary *Z*-fold increase to the blood volume compartment and normalize the result to the *Z*=1 condition, C_{B0}, Equation 4-5 follows:

$$C_B/C_{B0} = \frac{(V_o+V_B)+D^*V_T}{(V_o+Z^*V_B)+D^*V_T}$$

Equation 4-5

In general, C_B falls as 1/*Z*. However, the partitioning properties of the drug and the fact that V_B is a small fraction of the total system serve to substantially temper the effect of increasing *Z* on blood concentration. For example, this treatment suggests that a highly hydrophilic drug, epinephrine, can tolerate ~10x increase in blood volume with only a ~2x change in blood concentration. More hydrophobic drugs, such as amiodarone, are predicted to show almost no change in blood level at higher values of *Z*, and would require ~10^6 increase in blood volume to approach that same two-fold dilution.

To test these predictions, we construct a simple model of the body mimicking the two-compartment set up of our theoretical treatment. The water compartment – including variable blood volume – is represented by phosphate buffered saline and tissue is represented by an organic liquid (here, 1-octanol). The concentration of three small-molecule drugs – epinephrine, propranolol, and amiodarone – was measured and normalized to the *Z*=1 condition. The data (mean ± S.D.), along with curves resenting the values predicted by Equation 4-5 are plotted in Figure 4-9. All three cases show reasonable agreement between predicted and experimental values. For scenarios where even these small dilutions are unacceptable – or in instances where the

preceding treatment does not apply – other pharmacokinetic-based approaches may be useful, especially if PDMS or another gas-permeable material is used to decouple O_2 delivery from blood flow rate (Appendix C).

4.5 HOC design

4.5.1 Organ compartment design strategy

As §3.4 demonstrated, it is important to consider both size and function of each individual organ compartment of an HOC. Therefore, we use organ structure to determine a critical constrained dimension (surface area or volume) and set the organ compartment size accordingly. The specific approach, dubbed metabolic functional scaling and elucidated Moraes et al. (23), classifies organs according to principle function: 2-dimensional (F-2D) or membranous tissue (*e.g.* lung) is scaled by surface area while functionally 3-dimensional (F-3D) or lobular tissue (*e.g.* adipose) is scaled by volume (23). Rather than relying on the principles of Euclidean geometry – which can lead to strange inconsistencies (62) – we scale the critical dimension according the expected change in *function*. Since we propose suppressing cell BMR, eliminating the $M^{1/4}$ change in cellular BMR and therefore inducing a M^1 relationship between organism size and function, both volume- *and* surface area-based functions should now scale with M^1. This is an especially critical insight for F-2D organs since surface area scales as $V^{2/3} \sim M^{2/3}$ under the principles of simple Euclidean geometry. In this way, MSFS is both functionally constrained and metabolically supported.

This approach, therefore, provides an underlying explanation for the failure of purely QPSR- and metabolism-based scaling approaches to capture certain

fundamental aspects of biology (62). It also avoids inconsistencies that appear when empirical laws are extrapolated outside the range of the original dataset – a key problem for applying empirical, allometric organ-organism size relationships to HOC design (21, 22). Design parameters for F-2D organs are achieved by scaling according to surface area and compartment size is selected to match fluidic shear values found in vivo for each tissue. F-3D organs are simply scaled according to mass. For more complicated organs such as the liver that may be classified as both F-2D and F-3D, we use a two compartment approach: one section with high surface area and another with high mass that together approach the appropriate values (Table 4-2). Spheroids and other tissue aggregation strategies may be particularly useful in these cases (Appendix D).

The endothelium presents another special case. Since several sources estimate the endothelial surface area of the body at 1,000 m^2 or greater (63–65), including the whole of the endothelium in this HOC would be an impossible undertaking. Since the endothelium mainly acts in concert with its associated organ rather than as a distinct entity, we include only endothelial tissue from organs already represented in this model (lung and liver). These tissues serve to recapitulate EC function within the organs included in this design and also provide a readout for general endothelial “health” across the HOC.

In addition to the organs *explicitly* included in this HOC design, we must also account for the body volume not represented by any of the designated organ compartments. Including a blank “other organs” zone to represent *implied* (but absent)

organs ensures that our total system mass will be commensurate with that of a macro version and other groups have included “missing organ formulators” and “other tissues” compartments to similar ends (18, 19, 21, 23). Importantly, since we justify a substantially increased blood volume based in part on a volume distribution-based treatment that considers the entire body volume, it is critical that that volume be faithfully replicated in our model system.

4.5.2 Overall design parameters

The insights provided by our examinations of metabolic scaling, *C. aceratus’s* unique physiology, and volume of distribution indicate that we need not be confined by preconceived notions of what is or is not “physiologic” in designing an HOC. Instead, it is the ultimate response – the function – of the HOC and not the underlying structure that is paramount. Specifically:

1. Without additional controls, on-chip cellular BMR will exceed *in vivo* levels and cause a fundamental mismatch between the model system and reality. We propose limiting oxygen delivery as one effective mechanism for controlling cellular BMR.
2. Lack of Hb or an Hb substitute does not doom a vertebrate organism (or an HOC) *ex ante*. In fact, by introducing systemic redundancies and extra-normal physiologic values Nature has, and engineers may, successfully addressed such anomalies.
3. Blood volume increases are necessary to address technical limitations of current tissue engineering and microfabrication techniques. A distribution-based

treatment of supra-physiologic blood volumes and the example of the icefish indicate that designers have some latitude in determining HOC blood volume, especially for perfusion-limited drugs.

Finally, we formalize a complete set of design parameters for a lung, liver, endothelium, fat, and heart $x10^{-6}$ HOC (Table 4-3) that follows the design principles laid out here. We further compare relevant design criteria of this more practical $x10^{-6}$ HOC to *C. aceratus*, a standard human, and a mouse (Figure 4-10). Values for this five-parameter comparison across blood oxygen content (Blood O_2), intervessel distance (IVD), skin gas exchange, cardiac output, and blood volume were drawn from many sources and normalized against values predicted by QPSRs (16, 22, 38, 44, 53, 54, 56, 57, 66–76). For details, see Appendix E. Another set of charts predicting behavior based on theses parameters is calculated and show in (Figure 4-11), demonstrating the superiority of our holistic design strategy over an unmodified approach.

Inspired by the example of *C. aceratus* and motivated to suppress cellular BMR to physiologic levels (and to avoid the challenges inherent in developing a synthetic substitute), we have deliberately excluded Hb from this HOC design in order to restrict oxygen availability and limit cellular BMR. However, Hb also plays a key role in transporting carbon dioxide away from metabolically active tissues – carrying up to 30 percent of the CO_2 transported in blood (38). In this HOC design, we justify ignoring these effects because CO_2 transport can occur by other means. At 35 °C, PDMS is nearly five times more permeable to carbon dioxide than oxygen (77). Similarly, the solubility of CO_2 and NO (nitrous oxide, an important signaling molecule) in water are

both orders of magnitude greater than O_2 (78–80). Beyond oxygen transport, Hb plays important roles in other aspects of physiology including NO catalysis (38). Depending on the specific application, each function may need to be explicitly accounted for in HOC design.

4.5.3 Validation of HOC design strategy

For this (or any) HOC system to be accepted as a microphysiological model of the body, some method of validating the underlying design strategy is necessary. Although such a system may not be directly tested against humans we may apply the same design criteria outlined here to build rats-, mice-, etc.-on-a-chip. Parallel studies comparing the response of the microphysioological model system to the genuine animal will provide information on areas where HOCs may be particularly well- (or ill-) suited to serve as a complimentary research tool. In and of themselves, these experiments may also yield new mechanistic insights into previously unexplored aspects of common biomedical research models.

A second validation approach for this design strategy would be to challenge the ability of the HOC system to maintain homeostasis in the face of systemic perturbations. Rather than focusing on the response of the system on a specific stimulus, this approach focuses on more general aspect of the body that should better port across systems, targets, and toxins. For example, any HOC included fat and pancreas compartments should be able to regulate the glucose level of the circulating medium. Once the system is ready, it should be able to correct an applied glucose bolus (or an artificial glucose dearth) by sequestering (mobilizing) glucose as appropriate. Once

validate, such a system would be useful for studying *any* toxins or diseases that affect the process.

4.6 Conclusions

Quarter power scaling relationships are both empirically and theoretically supported and provide guidance for sizing physiologic parameters in the face of changing system size. Their application to the development of microphysiological models of the body or “humans-on-a-chip,” however, introduces both fundamental and technical challenges which currently frustrate efforts at design and construction of a relevant, feasible system. We posit that HOC designers may avoid these issues by selecting parameters outside the realm of what is considered physiologic so long as the ultimate function of the system is preserved. We use a natural experiment, the icefish, to conceptually justify this approach and demonstrate how extra-physiologic parameters may interact to give a normal physiologic response – essentially using two wrongs to make a right. Since cell behavior is context dependent, suppressing cellular BMR on-chip to mimic in vivo levels is crucial to designing a physiologically relevant HOC. We observe a substantial O_2-dependent decreases in cell metabolism across four different cell types to demonstrate the feasibility of this approach. Further study of an HOC system through a distribution-informed treatment of blood concentration of small-molecule drugs indicates that we may indeed increase HOC blood volumes with only minor consequences. In cases where even that is unacceptable, we provide frameworks to estimate the magnitude of and/or mitigate the error. Integrating these lessons in the design of a liver-lung-heart-fat-blood system, we propose a complete set of design

parameters for a $x10^{-6}$ miniaturized HOC system. This work forms a basis of a Nature-inspired approach to govern design of in vitro model systems.

4.7 Works cited

1. Huh D, et al. (2010) Reconstituting Organ-Level Lung Functions on a Chip. *Science* 328(5986):1662–1668.

2. Moraes C, Mehta G, Lesher-Perez SC, Takayama S (2012) Organs-on-a-Chip: A Focus on Compartmentalized Microdevices. *Ann Biomed Eng* 40(6):1211–1227.

3. Bhatia SN, Ingber DE (2014) Microfluidic organs-on-chips. *Nat Biotechnol* 32(8):760–772.

4. Sung JH, et al. (2013) Microfabricated mammalian organ systems and their integration into models of whole animals and humans. *Lab Chip* 13(7):1201.

5. Sung JH, Kam C, Shuler ML (2010) A microfluidic device for a pharmacokinetic–pharmacodynamic (PK–PD) model on a chip. *Lab Chip* 10(4):446.

6. Vozzi F, Heinrich J-M, Bader A, Ahluwalia AD (2008) Connected culture of murine hepatocytes and human umbilical vein endothelial cells in a multicompartmental bioreactor. *Tissue Eng Part A* 15(6):1291–1299.

7. Maschmeyer I, et al. (2015) A four-organ-chip for interconnected long-term co-culture of human intestine, liver, skin and kidney equivalents. *Lab Chip* 15(12):2688–2699.

8. Esch MB, et al. (2014) How multi-organ microdevices can help foster drug development. *Adv Drug Deliv Rev* 69-70:158–169.

9. Tissue chip for drug screening (2012) Available at: ncats.nih.gov/tissue-chip.html.

10. Polini A, et al. (2014) Organs-on-a-chip: a new tool for drug discovery. *Expert Opin Drug Discov* 9(4):335–352.

11. Kleiber M (1947) Body size and metabolic rate. *Physiol Rev* 27(4):511–541.

12. West GB, Brown JH, Enquist BJ (1997) A General Model for the Origin of Allometric Scaling Laws in Biology. *Science* 276(5309):122–126.

13. Banavar JR, et al. (2010) A general basis for quarter-power scaling in animals. *Proc Natl Acad Sci* 107(36):15816–15820.

14. Iori E, et al. (2012) Glucose and Fatty Acid Metabolism in a 3 Tissue In-Vitro Model Challenged with Normo- and Hyperglycaemia. *PLoS ONE* 7(4):e34704.

15. Mazzei D, Guzzardi MA, Giusti S, Ahluwalia A (2010) A low shear stress modular bioreactor for connected cell culture under high flow rates. *Biotechnol Bioeng*:127–137.

16. Mattei G, Giusti S, Ahluwalia A (2014) Design Criteria for Generating Physiologically Relevant In Vitro Models in Bioreactors. *Processes* 2(3):548–569.

17. Marx U, et al. (2012) “Human on a chip”developments: a translational cutting-edge alternative to systemic safety assessment and efficiency evaluation of substances in laboratory animals and man? *Altern Lab Anim-ATLA* 40(5):235.

18. Viravaidya K, Sin A, Shuler ML (2004) Development of a Microscale Cell Culture Analog To Probe Naphthalene Toxicity. *Biotechnol Prog* 20(1):316–323.

19. Esch MB, Mahler GJ, Stokol T, Shuler ML (2014) Body-on-a-chip simulation with gastrointestinal tract and liver tissues suggests that ingested nanoparticles have the potential to cause liver injury. *Lab Chip* 14(16):3081.

20. Abaci H, Shuler M (2015) Human on a chip Design Strategies and Principles for Physiologically Based Pharmocokinetics/Pharmacodynamics Modeling. *Integr Biol*. doi:10.1039/C4IB00292J.

21. Wikswo JP, et al. (2013) Engineering Challenges for Instrumenting and Controlling Integrated Organ-on-Chip Systems. *IEEE Trans Biomed Eng* 60(3):682–690.

22. Wikswo JP, et al. (2013) Scaling and systems biology for integrating multiple organs-on-a-chip. *Lab Chip* 13(18):3496.

23. Moraes C, et al. (2013) On being the right size: scaling effects in designing a human on a chip. *Integr Biol* 5(9):1149.

24. West GB, Woodruff WH, Brown JH (2002) Allometric scaling of metabolic rate from molecules and mitochondria to cells and mammals. *Proc Natl Acad Sci U S A* 99(Suppl 1):2473–2478.

25. Porter RK, Brand MD (1995) Cellular oxygen consumption depends on body mass. *Am J Physiol-Regul Integr Comp Physiol* 269(1):R226–R228.

26. Brown MF, Gratton TP, Stuart JA (2007) Metabolic rate does not scale with body mass in cultured mammalian cells. *AJP Regul Integr Comp Physiol* 292(6):R2115–R2121.

27. Heusner AA (1991) Size and power in mammals. *J Exp Biol* 160(1):25–54.

28. Wang W, Upshaw L, Strong DM, Robertson RP, Reems J (2005) Increased oxygen consumption rates in response to high glucose detected by a novel oxygen biosensor system in non-human primate and human islets. *J Endocrinol* 185(3):445–455.

29. Wataha JC, Hanks CT, Craig RG (1994) In vitro effect of metal ions on cellular metabolism and the correlation between these effects and the uptake of the ions. *J Biomed Mater Res* 28(4):427–433.

30. Huang G, Greenspan DS (2012) ECM roles in the function of metabolic tissues. *Trends Endocrinol Metab* 23(1):16–22.

31. Mehta G, et al. (2007) Quantitative measurement and control of oxygen levels in microfluidic poly(dimethylsiloxane) bioreactors during cell culture. *Biomed Microdevices* 9(2):123–134.

32. Lo JF, Sinkala E, Eddington DT (2010) Oxygen gradients for open well cellular cultures via microfluidic substrates. *Lab Chip* 10(18):2394.

33. Oppegard SC, Nam K-H, Carr JR, Skaalure SC, Eddington DT (2009) Modulating Temporal and Spatial Oxygenation over Adherent Cellular Cultures. *PLoS ONE* 4(9):e6891.

34. Schumacker PT, Chandel N, Agusti AG (1993) Oxygen conformance of cellular respiration in hepatocytes. *Am J Physiol-Lung Cell Mol Physiol* 265(4):L395–L402.

35. Gerencser AA, et al. (2009) Quantitative Microplate-Based Respirometry with Correction for Oxygen Diffusion. *Anal Chem* 81(16):6868–6878.

36. Donald Voet, Judith G. Voet (2004) *Biochemistry* (John Wiley & Sons, USA). 3rd Ed.

37. Carreau A, Hafny-Rahbi BE, Matejuk A, Grillon C, Kieda C (2011) Why is the partial oxygen pressure of human tissues a crucial parameter? Small molecules and hypoxia. *J Cell Mol Med* 15(6):1239–1253.

38. Widmaier EP, Raff H, Strang KT (2006) *Vander's Human Physiology* (McGraw-Hill, New York). 10th Edition.

39. Sung-Jin Kim, et al. (1998) Butanol Extract of 1:1 Mixture of Phellodentdron Cortex and Aralia Cortex Stimulates PI3-Kinase and ERK2 with Increase of Glycogen Levels in HepG2 Cells. *Phytother Res* 12:255–260.

40. Ha DT, et al. (2010) Selected compounds derived from Moutan Cortex stimulated glucose uptake and glycogen synthesis via AMPK activation in human HepG2 cells. *J Ethnopharmacol* 131(2):417–424.

41. Invitrogen alamarBlue Technical Datasheet.

42. Gon O, Heemstra PC (1990) *Fishes of the Southern Ocean* (J.L.B Smith Institute of Icdhthyology, South Africa). First Edition.

43. Regan CT (1913) II.—The Antarctic Fishes of the Scottish National Antarctic Expedition. *Trans R Soc Edinb* 49(02):229–292.

44. Ruud JT (1954) Vertebrates wtihout erythrocytes and blood pigment. *Nature* 173(4410):848–850.

45. Hemmingsen EA (1991) Respiratory and Cardiovascular Adaptations in Hemoglobin-Free Fish: Resolved and Unresolved Problems. *Biology of Antarctic Fish* (Springer-Verlag, New York), pp 191–203.

46. Sidell BD, O'Brien KM (2006) When bad things happen to good fish: the loss of hemoglobin and myoglobin expression in Antarctic icefishes. *J Exp Biol* 209(10):1791–1802.

47. FishBase (2005) Notothenia coriiceps. Available at: http://www.fishbase.se/Photos/PicturesSummary.php?ID=4702&what=species.

48. Ralph R, Everson I (1968) The respiratory metabolism of some antarctic fish. *Comp Biochem Physiol* 27:299–307.

49. Holeton GF (1970) Oxygen uptake and circulation by a hemoglobinless antarctic fish (*Chaenocephalus aceratus* Lonnberg) compared with three red-blooded antartic fish. *Comp Biochem Physiol* 34(2):457–471.

50. Hemmingsen EA, Douglas EL (1970) Respiratory characteristics of the hemoglobin-free fish *Chaenocephalus aceratus*. *Comp Biochem Physiol* 33(4):733–744.

51. Egginton S (1996) Blood rheology of Antarctic fishes: viscosity adaptations at very low temperatures. *J Fish Biol* 48(3):513–521.

52. Hemmingsen EA, Douglas EL, Johansen K, Millard RW (1972) Aortic blood flow and cardiac output in the hemoglobin-free fish *Chaenocephalus aceratus*. *Comp Biochem Physiol A Physiol* 43(4):1045–1051.

53. Hemmingsen EA, Douglas EL (1970) Respiratory characteristics of the hemoglobin-free fish *Chaenocephalus aceratus*. *Comp Biochem Physiol* 33(4):733–744.

54. Acierno R, MacDonald JA, Agnisola C, Tota B (1995) Blood volume in the hemoglobinless Antarctic teleost Chionodraco hamatus (Lönnberg). *J Exp Zool* 272(5):407–409.

55. Eastman JT (1993) *Antarctic Fish Biology: Evolution in a Unique Environment* (Academic Press Limited, New York).

56. Twelves EL (1972) Blood volumes of two antarctic fishes. *Antarct Surv Bull* (31):85–92.

57. Wujcik JM, Wang G, Eastman JT, Sidell BD (2007) Morphometry of retinal vasculature in Antarctic fishes is dependent upon the level of hemoglobin in circulation. *J Exp Biol* 210(5):815–824.

58. Bianconi E, et al. (2013) An estimation of the number of cells in the human body. *Ann Hum Biol* 40(6):463–471.

59. Allen JW, Bhatia SN (2003) Formation of steady-state oxygen gradients in vitro:Application to liver zonation. *Biotechnol Bioeng* 82(3):253–262.

60. Leon Shargel, Andrew B.C. Yu (1993) *Applied Biopharmaceutics and Pharmacokinetics* (Appleton & Lange, Norwalk, CT). Third Edition.

61. Malcom Rowland, Thomas N. Tozer (1995) *Clinical Pharmacokinetics: Concepts and Applications* (Williams & Wilkins, Baltimore). Third Edition.

62. Ucciferri N, Sbrana T, Ahluwalia A (2014) Allometric Scaling and Cell Ratios in Multi-Organ in vitro Models of Human Metabolism. *Front Bioeng Biotechnol* 2. doi:10.3389/fbioe.2014.00074.

63. Wolinsky H (1980) A proposal linking clearance of circulating lipoproteins to tissue metabolic activity as a basis for understanding atherogenesis. *Circ Res* 47(3):301–311.

64. Jaffe EA (1987) Cell biology of endothelial cells. *Hum Pathol* 18(3):234–239.

65. Augustin HG, Kozian DH, Johnson RC (1994) Differentiation of endothelial cells: analysis of the constitutive and activated endothelial cell phenotypes. *BioEssays* 16(2):901–906.

66. Petschow R, Petschow D, Bartels R, Baumann R, Bartels H (1978) Regulation of oxygen affinity in blood of fetal, newborn and adult mouse. *Respir Physiol* 35(3):271–282.

67. Williams LR, Leggett RW (1989) Reference values for resting blood flow to organs of man. *Clin Phys Physiol Meas* 10(3):187.

68. Hemmingsen EA, Douglas EL, Johansen K, Millard RW (1972) Aortic blood flow and cardiac output in the hemoglobin-free fish *Chaenocephalus aceratus*. *Comp Biochem Physiol A Physiol* 43(4):1045–1051.

69. Egginton S (1997) Control of tissue blood flow at very low temperatures. *J Therm Biol* 22(6):403–407.

70. Tournoux F, et al. (2011) Validation of Noninvasive Measurements of Cardiac Output in Mice Using Echocardiography. *J Am Soc Echocardiogr* 24(4):465–470.

71. Stücker M, et al. (2002) The cutaneous uptake of atmospheric oxygen contributes significantly to the oxygen supply of human dermis and epidermis. *J Physiol* 538(3):985–994.

72. Brandrup J, Immergut EH, Grulke EA (1998) *Polymer Handbook* (John Wiley & Sons, New York). Fourth Edition.

73. Folarin AA, Konerding MA, Timonen J, Nagl S, Pedley RB (2010) Three-dimensional analysis of tumour vascular corrosion casts using stereoimaging and micro-computed tomography. *Microvasc Res* 80(1):89–98.

74. Malkusch W, Konerding MA, Klapthor B, Bruch J (1995) A simple and accurate method for 3-D measurements in microcorrosion casts illustrated with tumour vascularization. *Anal Cell Pathol* 9(1):69–81.

75. Peters RH (1983) *The Ecological Implications of Body Size* (Cambridge University Press, New York).

76. Schmidt-Nielsen K (1984) *Scaling: Why is Animal Size so Important?* (Cambridge University Press, New York).

77. Merkel TC, Bondar VI, Nagai K, Freeman BD, Pinnau I (2000) Gas sorption, diffusion, and permeation in poly (dimethylsiloxane). *J Polym Sci Part B Polym Phys* 38(3):415–434.

78. Weiss RF (1970) The solubility of nitrogen, oxygen and argon in water and seawater. *Deep Sea Research and Oceanographic Abstracts* (Elsevier), pp 721–735.

79. Weiss RF (1974) Carbon dioxide in water and seawater: the solubility of a non-ideal gas. *Mar Chem* 2:203–215.

80. Weiss RF, Price BA (1980) Nitrous oxide solubility in water and seawater. *Mar Chem* 8:347–359.

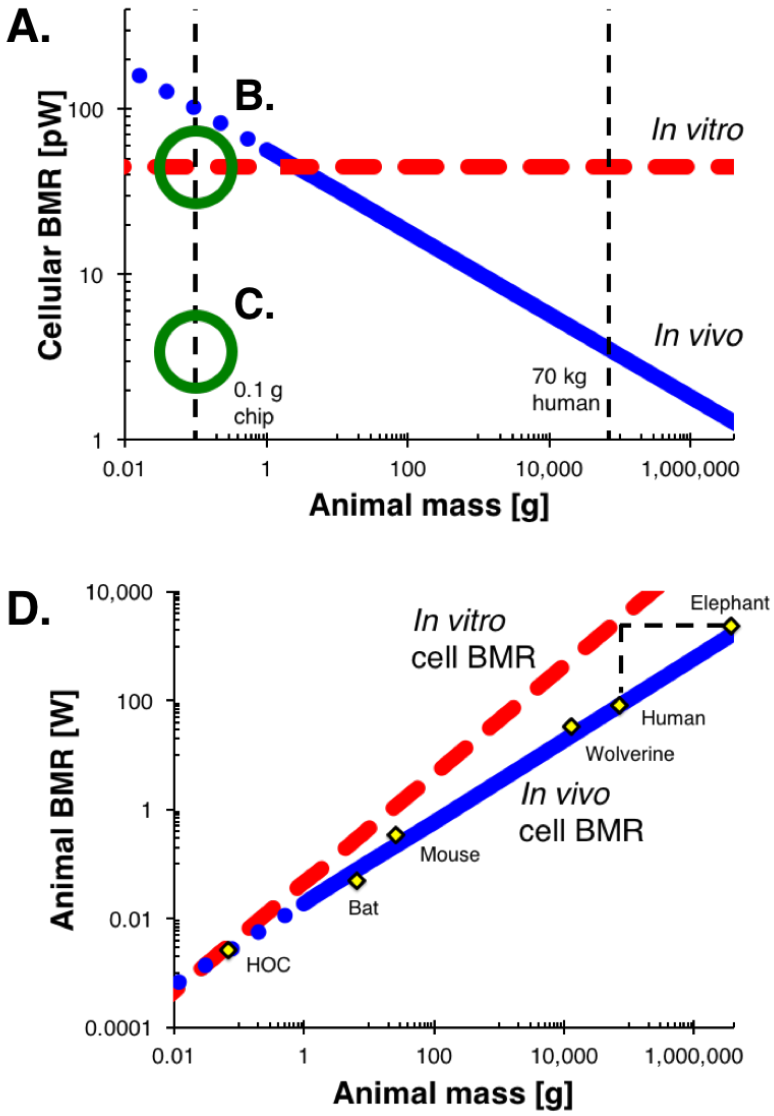

Figure 4-1. Consequences of context-dependent cell BMR

(A) Cellular BMR scales as $\propto M^{-¼}$ *in vivo* but mammalian cells cultured *in vitro* have a stable BMR ($\propto M^{0}$) regardless of the mass of the source organism. (B) *In vitro* cell culture of human cells leads to a cellular BMR ~1 order of magnitude larger than that of a normal human (24, 26). (C) A high fidelity, physiologically relevant HOC will be designed with mechanisms to ensure cellular BMR matches typical *in vivo* values for the organism to be modeled. (D) Failure to account for the context-dependent behavior of cells can substantially alter the modeled organism-level BMR, especially for larger animals (24, 27).

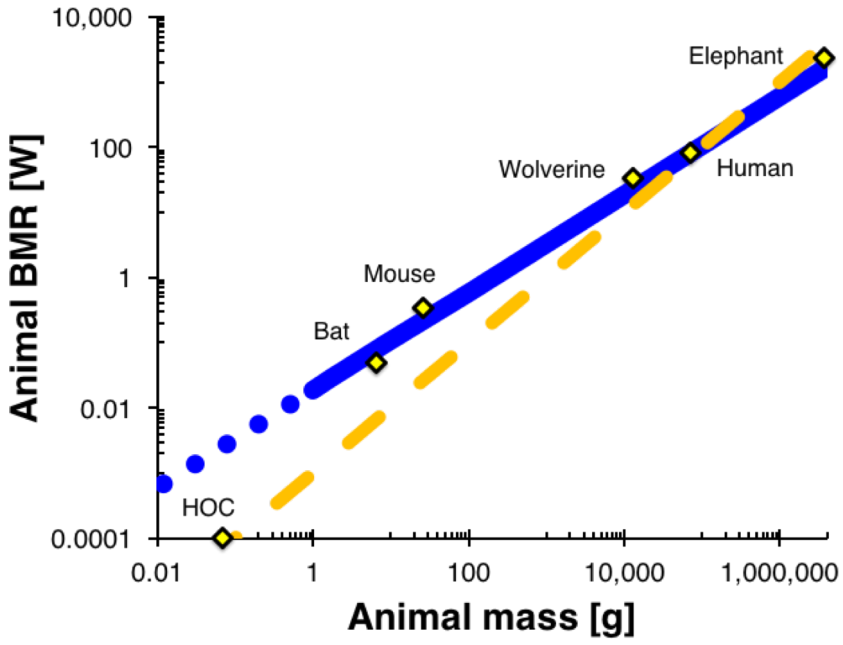

Figure 4-2. Metabolically supported scaling

Metabolically-supported scaling posits that designers must control cellular BMR in order to achieve a generalizable, *in vivo*-like response. A consequence of eliminating the $M^{-¼}$ dependence of cellular BMR is that system BMR scales as M^{1}.

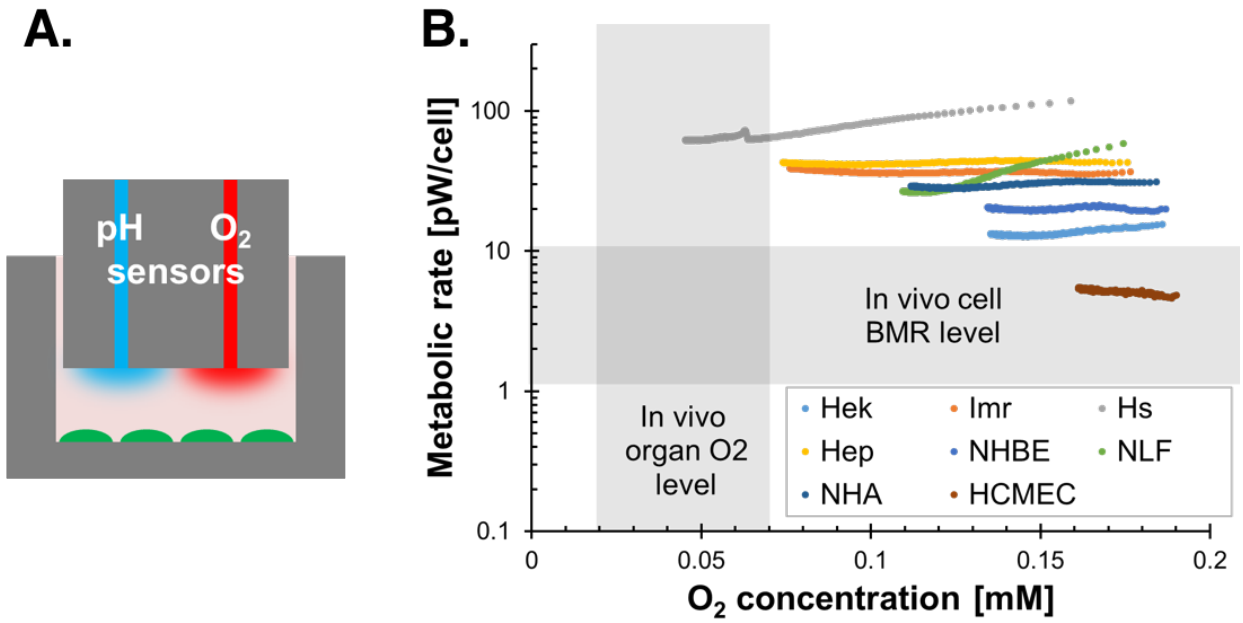

Figure 4-3. Seahorse XFe cellular BMR measurement

To assess the effect of oxygen tension on cellular BMR, we used a Seahorse XFe extracellular flux analyzer. (A) The instrument contains a 96-probe array with integrated pH and O2 sensors that forms a transient microchamber around the cells. (B) Holding that microchamber allows cells to deplete oxygen from their surroundings and we can calculate BMR from the rates of change in pH and O_2 measurements. Unfortunately, cellular metabolic activity alone was insufficient to achieve *in vivo* like oxygen tension in all but one instance. Data plotted as average of n=7 distinct experimental wells per cell type.

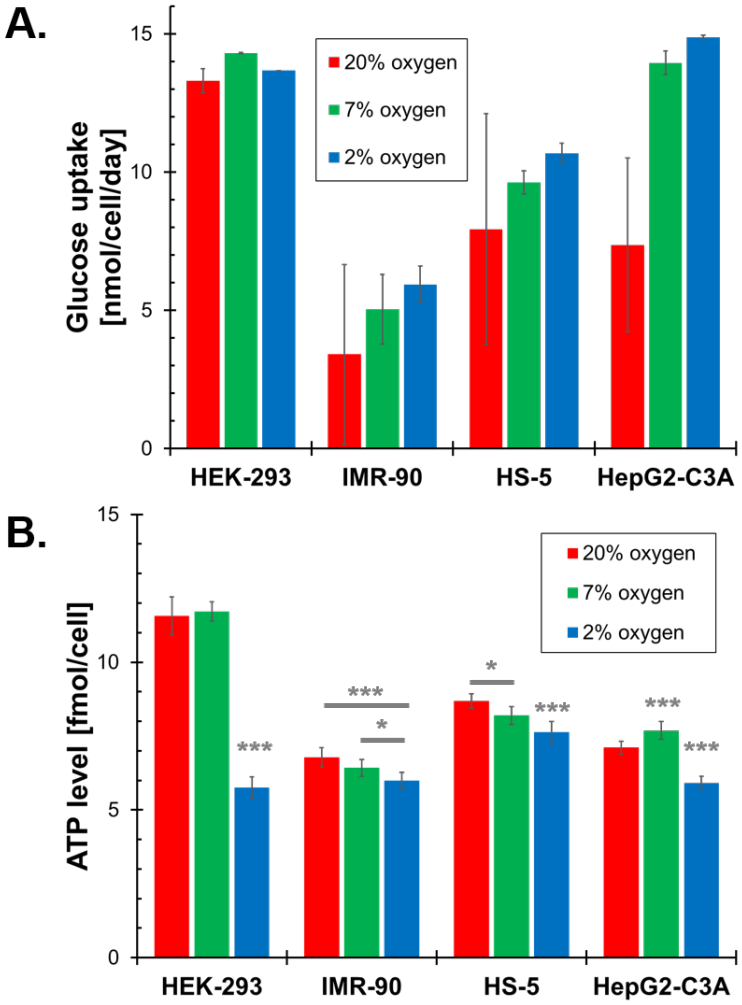

Figure 4-4. Glucose-based cellular BMR measurement

(A) Cellular uptake data showed a somewhat increasing relationship between glucose uptake and oxygen tension for most cell types tested. These data may be refined by incorporating a lactate measurement to differentiate between metabolic pathways. Moreover, glucose uptake does not necessarily indicate glucose usage for ATP production. Data reported as average ± standard deviation, n=12. (B) Per cell ATP levels decrease with decreasing oxygen tension for all cell types tested. Data reported as average ± standard deviation, n=8; * indicates $p<0.05$, *** indicates $p<0.001$ by one way ANOVA with Tukey post-hoc test.

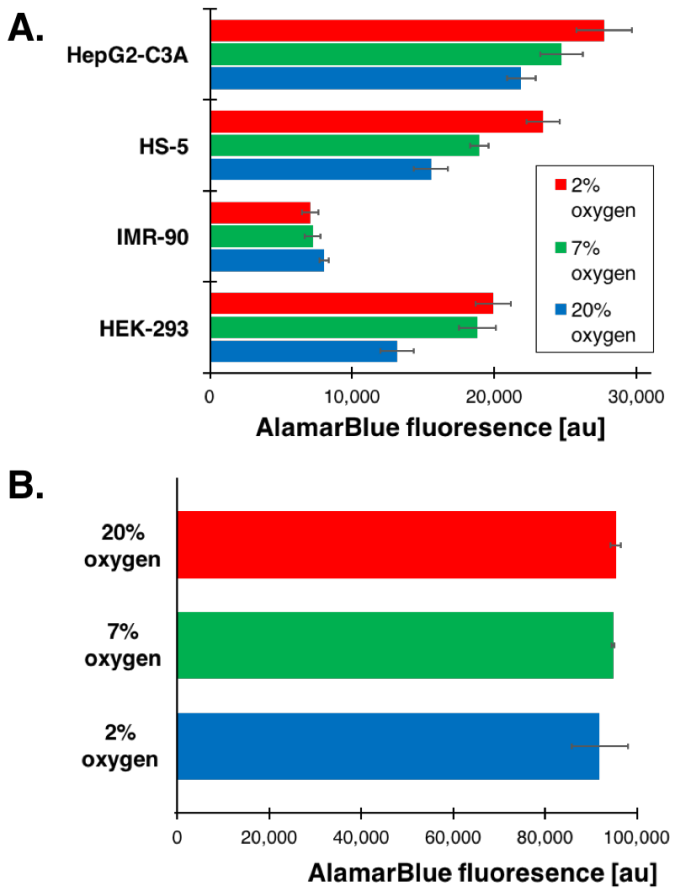

Figure 4-5. AlamarBlue cellular BMR measurement

(A) AlamarBlue metabolic indicator was used to measure cellular BMR in different oxygen tension environments. Surprisingly, BMR seemed to decrease with increasing oxygen – a trend we attribute the mechanism by which AlamarBlue is reduced by metabolically active cells (and thus becomes fluorescent). (B) A test to see whether oxygen tension affected the re-oxidation of reduced AlamarBlue showed no effect. Data plotted as average ± standard deviation for n=7.

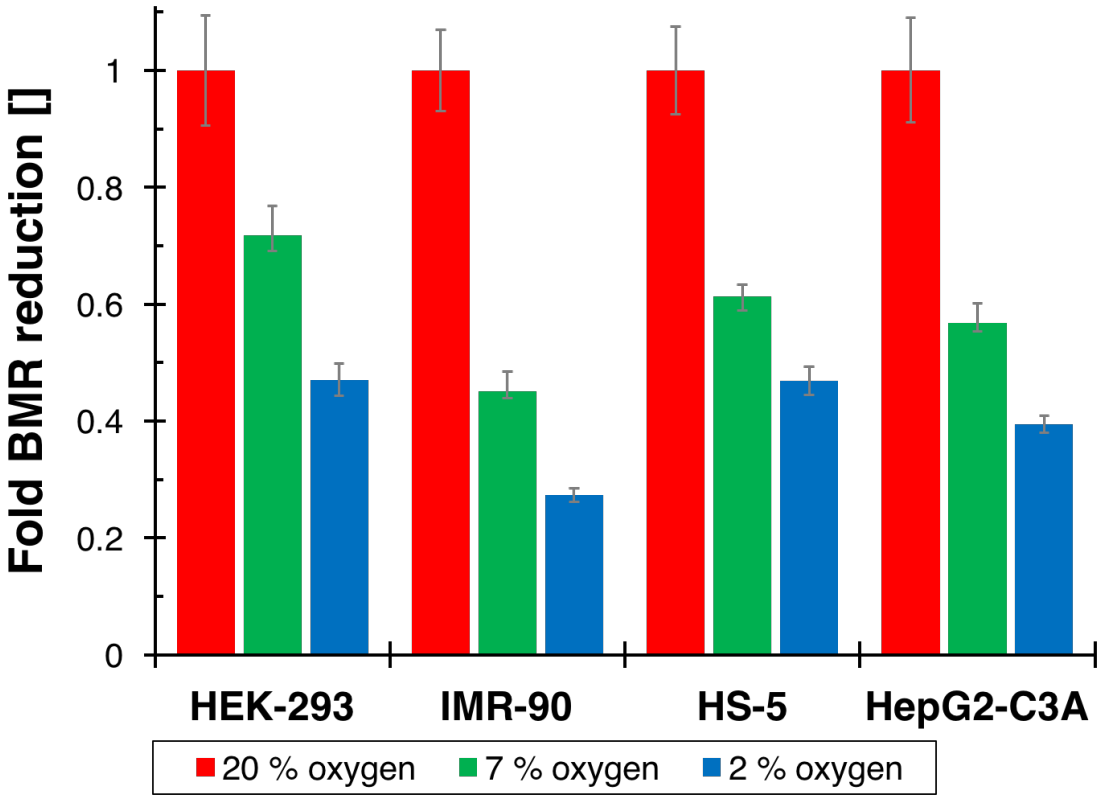

Figure 4-6. AlamarBlue shows oxygen-induced suppression of cellular BMR

Using Equation 4-1 to correct for the affect of oxygen tension on AlamarBlue metabolism, we show that decreasing oxygen tension consistently surpasses cellular BMR across four different human cells lines. Data reported as average ± standard deviation, n=8.

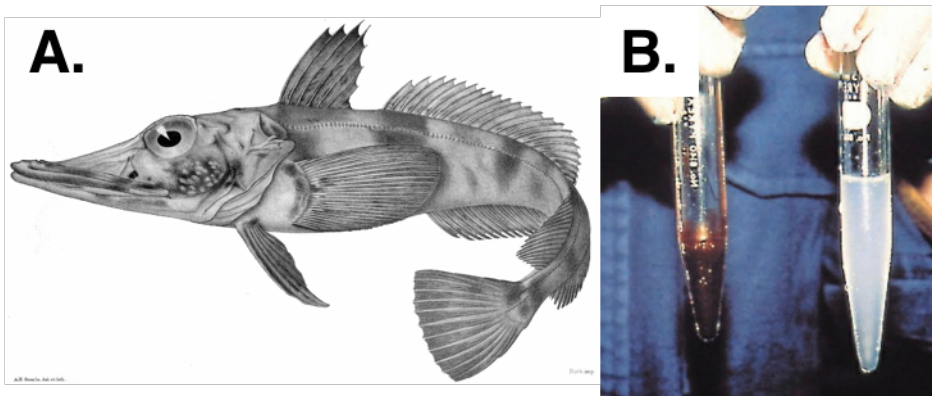

Figure 4-7. *C. aceratus*, the icefish

(A) Artist's rendering of *C. aceratus*, a hemoglobin-free fish living in the Southern Ocean near Antarctica. Adapted from (43). (B) Freshly drawn blood from *C. aceratus* (right) is milky white while blood from Hb+ *N. coriiceps* is a familiar shade of red (left). Adapted from (46).

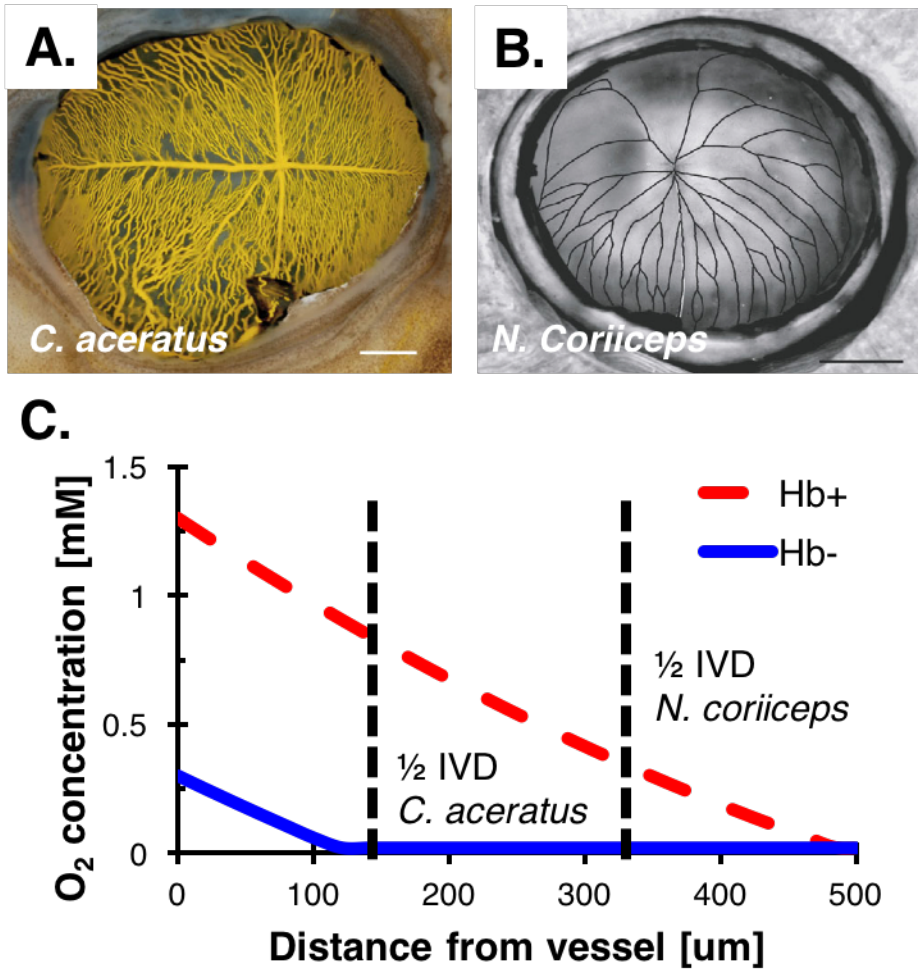

Figure 4-8. Oxygen delivery in *Notothenioidei*

Retinal micrographs of (A) C. aceratus and (B) N. coriiceps demonstrate the difference in capillary density and intervessel distance (IVD) between the two fish. Reprinted from (57). (C) These decreased intervessel distances help compensate for low blood O2 levels in C. aceratus. A similar effect should act on other solute (e.g. growth factors or drugs) diluted by larger blood volumes as well. Equation 4-2 solved numerically using data from (16, 44, 57, 58).

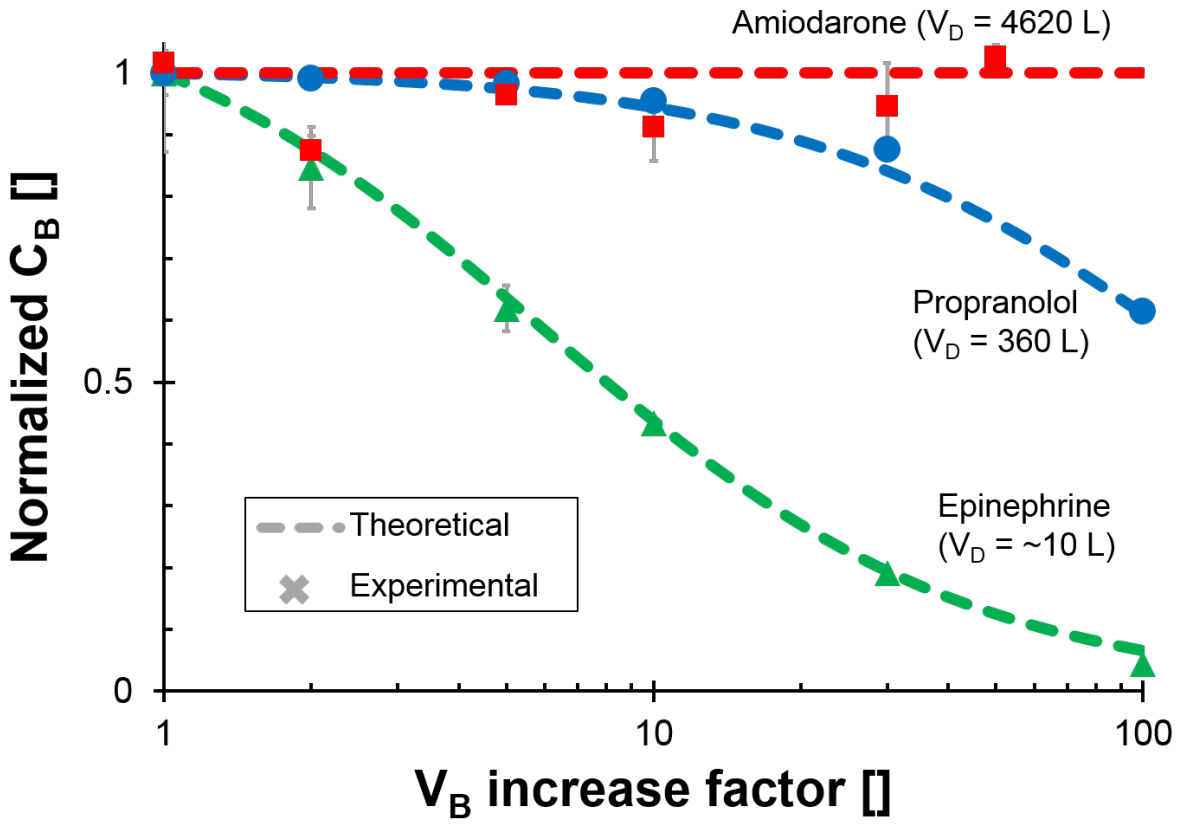

Figure 4-9. Effect of blood volume increase on blood concentration of a drug

Increased blood volumes minimally effect blood concentration depending on drug properties for perfusion-limited drugs according to Equation 4-5. Hydrophobic drugs (*e.g.* amiodarone) partition mostly to tissue and blood concentration is largely unaffected by changes in blood volume. More hydrophilic drugs (*e.g.* epinephrine) partition largely to the blood and are more affected by large changes in blood volume.

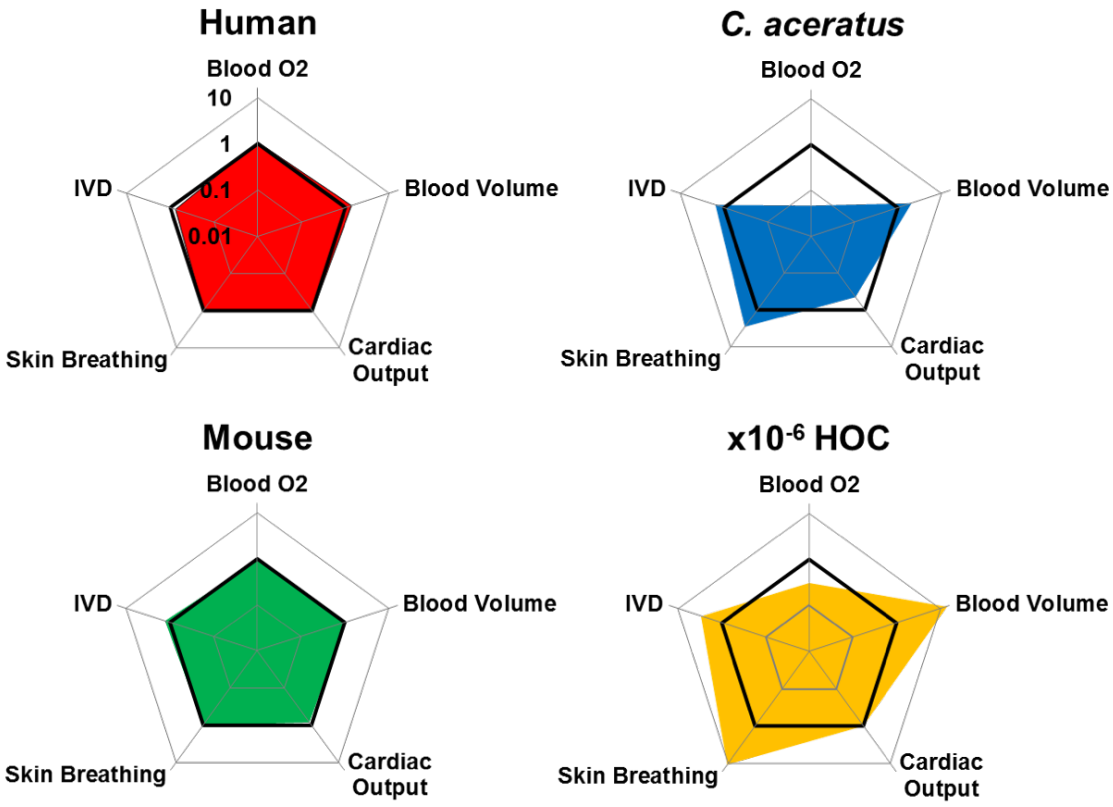

Figure 4-10. HOC design parameter comparison

Radar charts comparing design parameter values for a human, a mouse, the Hb- icefish *C. Aceratus*, and a $x10^{-6}$ miniaturized HOC. Values plotted on a log scale and normalized to QPSR estimates for all graphs. Note that observed values for the mouse and human match QPSR estimates (bold lines) closely while the general shape of the charts for *C. Aceratus* and the HOC have similar shapes. A $x10^{-6}$ human designed only according to QPSR would lie exactly along the bolded line representing a normalized value of 1. Computed using data from (16, 22, 38, 44, 53, 54, 56, 57, 66–76).

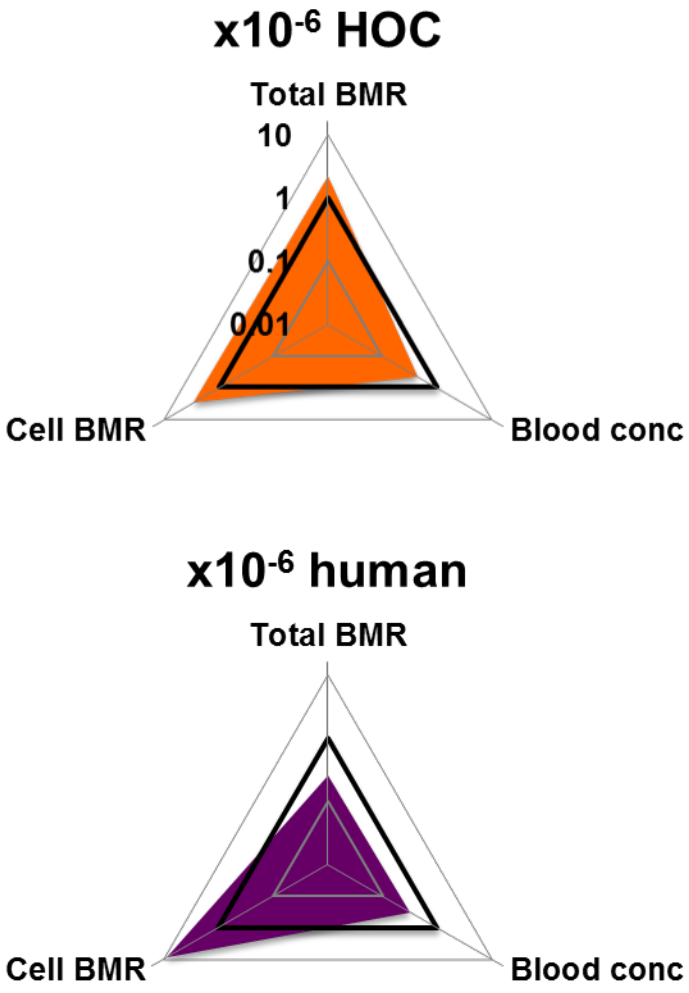

Figure 4-11. Modified HOC design strategy more effective than conventional scaling

Applying the modifications proposed here to build a x10^{-6} HOC is predicted lead to a more accurate model of the human body. Despite straying from conventional parameters, our design strategy yields an HOC that more closely matches human levels of cellular BMR, total BMR and blood concentration of a low volume distribution drug (*e.g.* epinephrine).

Condition imposed on *N. coriiceps*	O_2 solubility in blood [mg / mL]*	Cardiac output (Q) [mL / hour]	Cutaneous respiration [mg O_2 / hour]	Max O_2 delivery [mg / hour]	Fish health
Normal	0.085[a]	3,900[b]	---	330	☺
-Hb	0.0095[a]	3,900	---	37	☹
-Hb, ↑Q	0.0095	7,140[c]	---	68	😐
-Hb, ↑Q, +C. Resp.	0.0095	7,140	10[d]	78	☺
		N. coriiceps resting VO_2 = 42 mg O_2 / hour[e]			
		C. aceratus resting VO_2 = 32 mg O2 / hour[f]			

Table 4-1. Hypothetical icefish experiment

Physiological values for a hypothetical 1 kg test-fish as hemoglobin (Hb) is removed and icefish characteristics – increased cardiac output (Q) and cutaneous respiration (C. Resp) – are introduced.

*Measured at 0 ºC and 101.3 kPa

[a] denotes value from (44), [b] value from (69), [c] value from (68), [d] value adjusted from (45), [e] value from (48, 49), and [f] value averaged from (48, 49, 53). Values reported in literature on a per mass basis are presented here for a test-fish of 1 kg.

HOC organ compartment class	Tissue size	Blood volume
F-2D	Surface area constrained, $\propto M^1$ scaling from macro human	Dimensions selected to maintain physiologic shear given fractional cardiac output
F-3D	Volume constrained, $\propto M^1$ scaling from macro human	Calculated so that organ blood volume matches target fractional organ mass of whole body
F-2.5D	Use 3D tissue constructs and/or divide into F-2D and F-3D domains with each domain scaled according to F-2D or F-3D design rules	

Table 4-2. HOC organ compartment design strategy

Design strategy for different HOC organ compartment classes defined by metabolically-supported function scaling (MSFS) theory.

Organ		Class	x10^{-6} HOC							
			SA [mm^2]	Tissue mass [mg]	Blood volume [uL]	% BV	% CO	Compartment dimension		
								Length [mm]	Width [mm]	Height [mm]
Lung	*Endothelium*	*F-2D*	*30*	*0.12*	*1.1*	---	---	---	---	---
	Non-EC	*F-2D*	*40*	*0.16*	*1.4*	---	---	---	---	---
	Total	F-2D	70	0.28	2.5	4	100	9.02	7.76	0.035
Liver	*Endothelium*	*F-2D*	*80*	*0.32*	*2*	---	---	14.87	5.38	0.025
	Non-EC	*F-3D*	*34*	*1.75*	*1.03*	---	---	1.57	1.57	1
	Total	F-2/3D	114	2.07	3.03	5	25	---	---	---
Heart		F-3D	---	0.33	0.28	0.5	4	1.06	1.06	0.5
Fat		F-3D	---	12.5	10.7	18	5	4.96	4.96	1
Blood		---	---	---	60	---	---	---	---	---
"Other tissues"		F-3D	---	48.8	43.5	73	66	6.6	6.6	1
Blood oxygen content [BL_{O2}; mM]						~2				
Cutaneous respiration [mol / m / sec / mmHg]						≤3.8x10^{-11}				
Cardiac output [mL/sec]						3.4x10^{-3}				
Intervessel distance [IVD; µm]						250				

Table 4-3. Table of HOC design parameters

A comprehensive table of design parameters for a five-organ x10^{-6} HOC. We propose increasing blood volume levels beyond those called for by conventional QPSR to account for engineering limitations in organ design. Chamber dimensions are selected to match *in vivo* shear levels (F-2D) or match *in vivo* mass (F-3D).

Chapter 5:

Conclusions and Future Directions

As bio- and micro- engineering technologies mature, researchers will continue to press these advances and develop increasingly complex models of human health (*e.g.* a “human on a chip” or HOC). Certainly, a drastically improved experimental model would prove a potent guide to transform life science research and, at its best, usher in a new age of exploration in basic science and medicine – a welcome change from the current paradigm of reduced efficiency and diminishing returns. Therein lies the rub: how can we begin to formulate these generalizable experimental systems? What examples can we use? What rules must we follow?

What rules may we break?

This dissertation constructed an experimentally- and theoretically-supported framework to answer those questions in hopes that a coherent, top-down design strategy will form the basis for this next generation of experimental models. To that end, Chapter 1 presented the context and motivation for this work.

In Chapter 2, we develop a well-controlled, cell-dense model of adipose tissue, which we characterize with morphological measurements, tissue staining, and biomarker analyses. Together, these data indicate that our adipospheroids are not only indeed fat, but point to important functional differences between spheroids of different

sizes and – importantly – conventional 2D cultures. We confirm those functional differences with an insulin-mediated glucose uptake assay.

In Chapter 3, we leverage the unique properties of our adipospheroid microtissues to investigate experimentally what parameters may merit consideration in designing an HOC. Our data indicate that metabolism/oxygen, drug/tissue distribution behavior, and size/structure must all be carefully accounted for in any approach. Chapter 4 applies those lessons as we set out to devise specific design parameters for a physiologically relevant, $x10^{-6}$ HOC. In particular, we find that control of cellular BMR and organ compartment design according to function are important principles, an approach we dub metabolically supported functional scaling. Additionally, we use a distribution-based approach to address technical challenges such as the dilution of soluble factors in the circulating media of an HOC.

These efforts represent concrete steps toward a workable, relevant HOC. However, many obstacles remain. The dearth of experimental studies on generalized HOCs is an appropriate place to start: focusing on metabolic and homeostatic indicators rather than crude dose response relationships (*i.e.* moving beyond the “drug kills cell” model) may not be as appealing in the short run, but will pay dividends over time. Developing a self-regulating system or smaller, self-regulating circuits (for example, by introducing a pancreas compartment to the experimental setup of §3.4) would serve as a far more generalizable platforms and allow researchers to study more nuanced phenomena. Life is a delicate, interconnected, and complex – the key advantage of an

HOC is to represent that complexity as accurately as possible, but still with some degree of control.

By that same token, designers must continue, like diligent cartographers described by Miranda and Wikswo, to search for what details must be included, which may be omitted, and how to best represent those whose complexity exceeds our modeling capabilities. Technical challenges (such as small circulating media or “blood” volumes) are substantial hurdles – especially for the development of a generalized experimental platform. Here, clever shortcuts and careful workarounds are essential to reduce error to within an order of magnitude or (but preferably and) estimate any residual mismatch. These efforts serve an intellectual purpose as well: new technology or engineering advances that absolves us of today’s challenges will carry with them their own set of difficulties and require the same suite of creative, rational approaches examined by this dissertation. Often times, as we saw with the icefish, compromising one parameter can rescue another. If well thought out and carefully controlled, two wrongs may indeed make a right.

Throughout this document, the question of how to measure whether a model is an accurate mimic of the Natural has lurked just below the surface. In some ways, that question sits at this dissertation’s very heart. Whether evaluating a simple, lobular microtissue or designing a multi-organ model of the human body, these are fundamental issues that may escape scientists who are too often tempted (and too often forced) to consider increasingly minute details. Clearly, both the minutia and a broader, rigorous

context are important. The great goal, and the great challenge of this effort and others like it, is to simultaneously keep focus on both.

Appendices

Appendix A: Calculation of *C. aceratus* skin permeability

The following steps were used to calculate the permeability of *C. aceratus's* skin to molecular oxygen. The equation

$$N * A = {}^{P}/_{L}\,(C_0 - C_i)$$

Describes transport of gas across a barrier (1) where:

N = molar flow O_2 [mol O_2 / sec]
- = ~10 mg O_2 / hr for a 1 kg *C. aceratus* (2)
- = 0.00278 mg O_2 / sec
- = 8.68×10^{-8} mol O_2 / sec

A = fish surface area [m^2]
- = 1892 cm^2 for a 1 kg *C. aceratus* (3)
- = 0.1892 m^2

L = fish skin thickness [m]
- = ~0.7 mm averaged between sensory line and lateral line values for *C. aceratus* (4)
- = 7×10^{-4} m

C_o = ocean ppO_2 [mmHg]
- = 150 mmHg

C_i = *C. aceratus* blood ppO_2 [mmHg]
- = 120 mmHg from (5)

P = permeability of *C. aceratus* skin to oxygen

$$P = \frac{NL}{A(C_O - C_i)}$$

= 1.07×10^{-11} mol O_2 * m / m^2 / sec / mmHg

Compare to 3.79×10^{-11} mol O_2 * m / m^2 / sec / mmHg for PDMS (6)

Appendix B: Other details concerning icefish blood volume

Icefish blood volume as a function of body size

In addition to larger-than-expected cardiac output (mediated by a larger heart mass-body mass ratio) (7), *C. aceratus* also has a blood volume of ~90 mL/kg, nearly 2x greater than the ~50 mL/kg predicted for a fish its size (2, 8–11). Another member of *Channichthyidae*, *C. hamatus*, has a blood volume over two-fold its predicted value (8). These Hb- fish significantly exceed the blood volume expected from conventional QPSRs yet manage to function and flourish. Importantly, this observation reinforces the idea that extra-normal parameters can be an acceptable mechanism to thrive in the face of surprising physiology.

Organism	Mass [g]	Blood volume [mL]	
		Expected[a]	Observed
N. coriiceps	900	55	57[b]
C. aceratus	1,400	85	126[c]
C. hamatus	360	21	46[c]
Human	$70x10^3$	$4.3x10^3$	$5.9x10^{3}$ [d]
$x10^{-6}$ Human	0.07	0.006	---
$x10^{-6}$ HOC	0.07	0.006	0.06

Expected and actual blood volumes in several *Nototheniodae*. In addition to the two fish considered in the bulk of this study, another species of icefish, *C. hamatus,* has been included to illustrate a second example of elevated blood volumes in *Channichthyidae.* Scaled values for macro and $x10^{-6}$ miniaturized humans are also included.

[a] denotes values calculated from Refs. (12, 13)
[b] value from Ref (11)
[c] value from Ref. (8)
[d] value from Ref. (14)

Energy cost associate with increased blood volume

The increased blood volume shown in certain hemoglobin-less (Hb-) Channichthyidae species means that C. aceratus's heart must exert more energy to circulate that volume, especially at the high cardiac output required to maintain tissue oxygen levels. Researchers have estimated that C. aceratus allocates over one-fifth of its energy to driving circulation and that such a cost tradeoff offsets any gains in energy conservation made as a result of lower blood viscosity due to the loss of hemoglobin (15, 16). While this increased energy demand for circulation (driven mostly by a larger stroke volume rather than a faster heart beat) is certainly a concern for C. aceratus (5, 16, 17), it could easily be addressed in an in vitro system with the use of external assist devices, such as pumps (18–20), to make up for the energy deficit imparted by elevated blood volumes.

Increased vascular density and vessel bore diameter

Observations of increased vascular density in *C. aceratus* (21), made in retinal tissue, stand in contrast to other studies of icefish muscle that found decreased capillary density (17, 22). These muscle studies, however, also noted larger muscle fiber size in Hb- *Channichthyidae* compared to their Hb+ cousins. One group observed that such an increase in size would also decrease the rate of current leak from the muscle, conserving a substantial amount of energy and thereby decreasing the metabolic demand of the tissue (22). Therefore, measurements made in the retina, where no special adaptations (other than increased capillary density, of course) have been

observed and oxygen demand is largely activity-level agnostic, may be a more faithful representation of the overall character of the fish. Furthermore, the large vessel diameters observed in *C. aceratus* may be explained by constitutive overexpression of NO, a potent vasodilator (10, 21). Since Hb-derivatives are involved in the major pathway for NO elimination (23), their absence explains this overexpression and dictates that capillary diameter may not deviate as sharply from values predicted by scaling theory as initial reports indicate (12, 13, 21, 24). In an HOC, NO elimination in the absence of Hb may be achieved by incorporating PDMS, which is highly permeable to gases (6), as well as taking advantage of the greater solubility of NO in liquid (25).

Appendix C: Other pharmacokinetic approaches to compensate for high HOC blood volumes for perfusion/transport limited substances

Classical pharmacokinetic/pharmacodynamics models address inter-organ interactions by using rate constants to account for mass transfer between different compartments that may effectively capture clinical behavior but have little physiological significance. Physiologically-based (PBPK/PD) models explicitly define blood flow as the medium by which analytes move between compartments (26). Although PBPK/PD models (also referred to as “flow models”) require extensive information about flow rates, compartment volumes, and reaction rates, they also require less data fitting, are better able to accommodate pathological conditions, and are more easily extrapolated to describe PK/PD behavior across species (27).

In §4.4 of the main text, we explored one way in which specific drug properties could be used to improve the efficacy of our HOC with super-physiologic blood volume (or estimate the error introduced by such an approach). Here, we further examine PBPK/PD approaches to mitigate any residual mismatch between HOC drug concentration levels and those that may occur in the body. We sketch out approaches to maintain steady state tissue concentration in the face of 1^{st}-order and Michaelis-Menten reaction kinetics, as well as techniques to hold half-life and area under the curve constant from human to HOC. It should be noted that each of these approaches comes with its own set of caveats. For example, area under the curve (AUC) can be a useful metric for assessing total exposure, but can also mislead when different exposure profiles have the same AUC value but fall below or exceed certain critical thresholds such as minimum effective concentration or minimum toxic concentration.

PBPK/PD treatment to maintain $C_{T\text{-}SS}$ with 1st-order kinetics

PBPK/PD approaches typically idealize individual organ compartments as continuous-stirred tank reactors (CSTRs) where mixing times are negligible and the concentration of a solute in the compartment is equal to the concentration of the outflow (28–30). Assuming 1st-order reaction kinetics where the rate of reaction depends linearly on the concentration of the solute of interest within the compartment, as has been described previously (30), we begin with the mass (or molar) balance for a particular solute in the tissue compartment:

$$dX_T/_{dt} = Q_T * C_O - {Q_T}/_{K_T}\, {X_T}/_{V_T} - k * N_{Cells}\, {X_T}/_{V_T}$$

which describes the mass balance of a CSTR-idealized organ compartment where:

C_O = concentration of solute in the blood
X_T = amount of solute in the organ/itssue compartment
V_T = volume of the tissue compartment
k = per cell 1th-order reaction rate constant (+ indicates consumption)
Q_T = tissue compartment flow rate
N_{Cells} = number of cells in tissue compartment
KT = partition coefficient between the tissue and blood

Assuming steady state ($dX_T/dt \rightarrow 0$) and replacing X_T/V_T with $C_{T\text{-}SS}$, the steady-state concentration in the tissue compartment, we obtain:

$$Q_T * C_O = C_{T-SS}\left(\frac{Q_T}{K_T} + k * N_{Cells}\right)$$

Solving for $C_{T\text{-}SS}$ yields the following:

$$C_{T-SS} = \frac{Q_T * C_O}{{Q_T}/_{K_T} + k * N_{Cells}}$$

We now reduce the blood concentration, C_O, by a blood volume increase induced dilution factor, J (which can be estimated from the distribution-based treatment outlined

in §4.4, for example, in the face of a 10x blood volume increase, J=2.28 for epinephrine, J=1.06 for propranolol, and *J*=1 for amiodarone), and introduce a new tissue flow rate, P_T:

$$C_{T-SS} = \frac{P_T \, {C_O}/{J}}{{P_T}/{K_T} + k * N_{Cells}}$$

where: *J* = dilution factor induced by blood volume increase, depends on both drug properties (*D*) and magnitude of blood volume increase (*Z*)

Since we wish to maintain $C_{T\text{-}SS}$ across both scenarios, we set the two preceding equations equal to each other and solve for P_T, yielding:

$$P_T = \frac{J * Q_T * N_{Cells} * k}{N_{Cells} * k - (J-1) \, {Q_T}/{K_T}}$$

Therefore, if fractional flow rates to each organ and other relevant parameters are maintained, a new system flow rate (cardiac output) can be selected to maintain steady-state tissue level of a *specific* drug. This approach may be especially useful if another method (*e.g.* incorporation of gas permeable materials such as PDMS) is used to decouple oxygen delivery from blood flow.

PBPK/PD treatment to maintain $C_{T\text{-}SS}$ with Michaelis-Menten kinetics

A more complicated, but perhaps more realistic, treatment involves assuming Michaelis-Menten reaction kinetics in the organ compartment. We note that MM kinetics have previously been used to numerically model oxygen consumption within a

bioreactor (31) as well as toxicity of an anti-cancer drug in a 3-organ HOC (29). Starting with the mass balance:

$$dX_T/_{dt} = Q_T C_O - Q_T/_{K_T}\, X_T/_{V_T} - \frac{V_{Max}\, X_T/_{V_T}}{K_M + X_T/_{V_T}} N_{Cells}$$

which describes the mass balance of a CSTR-idealized organ compartment where:

C_O = concentration of solute in the blood
X_T = amount of solute in the tissue/organ compartment
V_T = volume of the tissue compartment
V_{Max} = maximum per cell reaction rate
K_M = the Michaelis constant
Q_T = tissue compartment flow rate
N_{Cells} = number of cells in compartment
K_T = partition coefficient between the tissue and blood

Assuming steady state ($dX_T/dt \rightarrow 0$) and replacing X_T/V_T with $C_{T\text{-}SS}$, the steady-state concentration in the tissue compartment, we obtain:

$$Q_T C_O = C_{T-SS}\, Q_T/_{K_T} + N_{Cells} \frac{V_{Max} C_{T-SS}}{K_M + C_{T-SS}}$$

Expanding and collecting terms gives:

$$0 = C_{T-SS}^2 \left(Q_T/_{K_T}\right) + C_{T-SS}^1 \left(K_M\, Q_T/_{K_T} - V_{Max} - Q_T C_O\right) + C_{T-SS}^0 (K_M Q_T C_O)$$

Using the quadratic formula to solve for $C_{T\text{-}SS}$ yields:

$$C_{T-SS} = \frac{Q_T C_O + V_{Max} - K_M \frac{Q_T}{K_T} \pm \sqrt{\left(K_M \frac{Q_T}{K_T} - V_{Max} - Q_T C_O\right)^2 - 4 \frac{Q_T}{K_T} (K_M Q_T C_O)}}{2\, Q_T/_{K_T}}$$

At this point the analytical treatment becomes quite cumbersome. The interested reader may obtain a solution for an adjusted flow rate, P_T, as above, or may instead choose to solve the problem numerically as done previously (29, 31).

PBPK/PD treatment to maintain half-life

Drug half-life is another important parameter that concerns pharmacologists (32). Half-life can be described by the following equation:

$$Half\ Life = \frac{0.693 K_P}{Q/V}$$

where Q = flow rate

V = compartment volume

K_P = equilibrium partition coefficient

Therefore, half-life is unaffected by changes in blood volume.

PBPK/PD treatment to maintain area under the curve (AUC)

Area-under-the-curve (AUC) is a common metric for assessing patient dose (33–35). For example if the clearance of a drug and its metabolites can be assumed to be perfusion limited – that is the rate of clearance from the bloodstream is much greater than the rate of delivery to clearing organ – decreasing the cardiac output will increase the AUC (or vice versa) according to (36):

$$AUC = \frac{X}{F_{CL} * Q}$$

where X = the amount of drug administered in mg or moles

F_{Cl} = clearance fraction of drug

Q = cardiac output

Thus, even in the face of increased dosing as proposed above, engineering modifications can be used to maintain other important pharmacokinetic parameters such as AUC. Using an open-source PBPK modeling package, PKQuest, we can examine how dose and cardiac output may be manipulated to preserve AUC (37–39). Critically, uncoupling these and other parameters – as we have begun to attempt here – will offer technologists multiple axes along which to tune exposure profiles and represents one potential solution to overcoming the substantial engineering challenges of developing a micro-scale model of the human body.

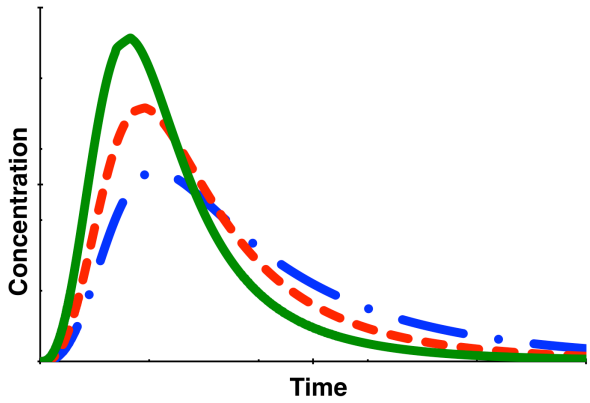

Three arterial concentration curves with different cardiac output-dose parameters but identical AUC's demonstrating how engineering controls can be used to maintain a target exposure profile in the face of challenges associated with miniaturization. Computed using PKQuest software from Refs (37, 38) and data from Ref (39).

Appendix D: Surface area-mass considerations for 3D constructs in an HOC system

3D tissue constructs can lead to improved phenotype and function *in vitro* for a variety of cell types, including liver cells (40). Using 3D aggregates also introduces a more complicated relationship between mass and surface area. For this reason, spheroid size and number must be carefully considered during design. Below is a graph representing the relationship between HOC organ mass and surface area for spheroids of various sizes. Since spheroids of diameter 250 μm have been shown to exhibit highest levels of liver specific function (unpublished data), the dashed, purple curve is used to inform our design process.

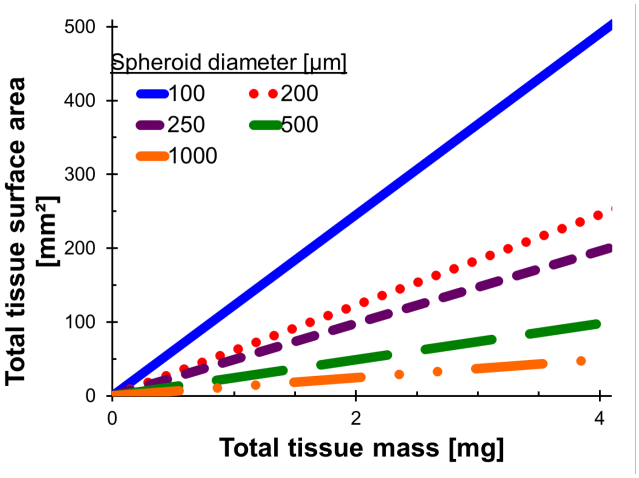

Cell-dense 3-dimensional tissue constructs (spheroids) can control the relationship between tissue surface area and volume. Depending on spheroid diameter, different surface area-volume curves may be obtained.

Appendix E: Derivation of design radar charts

Table of observed values (with sources)

	Blood O2 [mol O_2 / m^3]	Blood volume [mL]	Cardiac output [mL / sec]	Cutaneous respiration [mol / m / sec / mmHg]	Intervessel distance [µm]
C. Aceratus	0.3 (41)	125 (8)	2 (16)	$1x10^{-11}$ (2)	293 (21)
N. Coriiceps	2.7 (41)	55 (11)	1 (42)	$3.5x10^{-12}$ (43)	646 (21)
Human	7 (23)	5900 (14)	112 (14)	$3.5x10^{-12}$ (43)	200 (44)
$x10^{-6}$ HOC	~2 (α)	0.06 (β)	$3.4x10^{-3}$ (γ)	$3.8x10^{-11}$ (6)	250 (δ)
Mouse	5.95 (45)	2 (19)	0.27 (46)	$3.5x10^{-12}$ (43)	180 (47)

α – Design consideration to induce *in vivo* like cellular BMR (see main text §4.2)
β – Design consideration arrived at by applying QPSR isometric scaling of blood volume to miniaturize human by six orders of magnitude. The resulting value (6 µL) is adjusted upwards by a factor of 10 to achieve a more workable volume.
γ – Design consideration arrived at by applying QPSR ¾-power scaling of cardiac output to a $x10^{-6}$ miniaturized human
δ – Design consideration to accommodate liver spheroids of 250 µm diameter

Table of scaling values (calculated from scaling laws)

	Mass [kg]	Blood O2 [mol O_2 / m^3] (ε)	Blood volume [mL] (ζ)	Cardiac output [mL / sec] (η)	Cutaneous respiration [mol / m / sec / mmHg] (θ)	Intervessel distance [µm] (ι)
C. Aceratus	1	6.5	60.9	4.44	$3.5x10^{-12}$	186
N. Coriiceps	1	6.5	60.9	4.44	$3.5x10^{-12}$	186
Human	70	6.5	4263	107.4	$3.5x10^{-12}$	265
x10-6 HOC	$7x10^{-5}$	6.5	$6x10^{-3}$	$3.4x10^{-3}$	$3.5x10^{-12}$	87
Mouse	0.03	6.5	1.83	0.32	$3.5x10^{-12}$	139

ε – Assumed to be mass invariant ($\propto M^0$) for Hb+ vertebrates.
ζ – Calculated according to the equation $Y = 60.9*M^1$. Exponent selected according to scaling law and coefficient taken as average of 4 values reported in (13).
η – Calculated according to the equation $Y = 4.44*M^{0.75}$. Exponent selected according to scaling law and coefficient taken as average of 2 values reported in (13).
θ – No scaling value known. Permeability of human skin used for all values (43).
ι – Calculated according to the equation $Y = 186*M^{0.083}$. Exponent selected according to scaling law and, since no literature value could be found, coefficient selected to give reasonable match to mouse and human values (12).

Creation of radar charts

To create radar graphs of Figure 4-10 of the main text for human, mouse, icefish, and $x10^{-6}$ HOC observed values were normalized against scaling values and plotted along five log_{10} axes in Microsoft Excel.

C. aceratus radar chart normalized against *N. coriiceps*

Since *C. aceratus* is poikilothermic, metabolic values for the fish are likely substantially affected by ambient temperature. Although several correction factors have been proposed to compare cold-water fish to animals with warmer body temperatures (48, 49), no reliable method exists to adjust all relevant parameters considered here. One way to circumvent this problem is to normalize *C. aceratus* to another fish from the same environment that can be assumed to follow conventional scaling laws that describe most of the rest of the natural world. For completeness, this chart for *C. aceratus* normalized against *N. coriiceps* is included here.

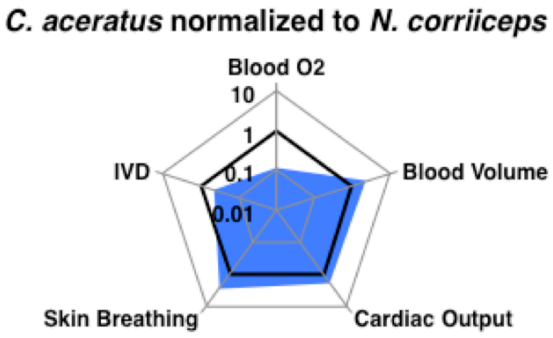

Radar chart of *C. aceratus* normalized to its cousin, *N. coriiceps* instead of conventional parameters predicted by quarter power scaling relationships.

Appendices works cited

1. Bird RB, Stewart WE, Lightfoot EN (2007) *Transport Phenomena* (John Wiley & Sons, New York). Second Edition.

2. Hemmingsen EA, Douglas EL (1970) Respiratory characteristics of the hemoglobin-free fish *Chaenocephalus aceratus*. *Comp Biochem Physiol* 33(4):733–744.

3. Holeton GF (1976) Respiratory morphometrics of white and red blooded Antarctic fish. *Comp Biochem Physiol* 54A:215–220.

4. Walvig F (1960) The integument of the icefish Chaenocephalus Aceratus (Lonnberg). *Nor J Zool* 9:31–36.

5. Holeton GF (1970) Oxygen uptake and circulation by a hemoglobinless antarctic fish (*Chaenocephalus aceratus* Lonnberg) compared with three red-blooded antartic fish. *Comp Biochem Physiol* 34(2):457–471.

6. Brandrup J, Immergut EH, Grulke EA (1998) *Polymer Handbook* (John Wiley & Sons, New York). Fourth Edition.

7. Tota B, Acierno R, Agnisola C (1991) Mechanical performance of the isolated and perfused heart of the haemoglobinless Antarctic icefish Chionodraco hamatus (Lonnberg): effects of loading conditions and temperature. *Philos Trans R Soc Lond B Biol Sci* 332(1264):191–198.

8. Acierno R, MacDonald JA, Agnisola C, Tota B (1995) Blood volume in the hemoglobinless Antarctic teleost Chionodraco hamatus (Lönnberg). *J Exp Zool* 272(5):407–409.

9. Eastman JT (1993) *Antarctic Fish Biology: Evolution in a Unique Environment* (Academic Press Limited, New York).

10. Sidell BD, O'Brien KM (2006) When bad things happen to good fish: the loss of hemoglobin and myoglobin expression in Antarctic icefishes. *J Exp Biol* 209(10):1791–1802.

11. Twelves EL (1972) Blood volumes of two antarctic fishes. *Antarct Surv Bull* (31):85–92.

12. West GB, Brown JH, Enquist BJ (1997) A General Model for the Origin of Allometric Scaling Laws in Biology. *Science* 276(5309):122–126.

13. Peters RH (1983) *The Ecological Implications of Body Size* (Cambridge University Press, New York).

14. Williams LR, Leggett RW (1989) Reference values for resting blood flow to organs of man. *Clin Phys Physiol Meas* 10(3):187.

15. Hemmingsen EA (1991) Respiratory and Cardiovascular Adaptations in Hemoglobin-Free Fish: Resolved and Unresolved Problems. *Biology of Antarctic Fish* (Springer-Verlag, New York), pp 191–203.

16. Hemmingsen EA, Douglas EL, Johansen K, Millard RW (1972) Aortic blood flow and cardiac output in the hemoglobin-free fish *Chaenocephalus aceratus*. *Comp Biochem Physiol A Physiol* 43(4):1045–1051.

17. Fitch NA, Johnston IA, Wood RE (1984) Skeletal muscle capillary supply in a fish that lacks respiratory pigments. *Respir Physiol* 57:201–211.

18. Moraes C, et al. (2013) On being the right size: scaling effects in designing a human on a chip. *Integr Biol* 5(9):1149.

19. Wikswo JP, et al. (2013) Engineering Challenges for Instrumenting and Controlling Integrated Organ-on-Chip Systems. *IEEE Trans Biomed Eng* 60(3):682–690.

20. Wikswo JP, et al. (2013) Scaling and systems biology for integrating multiple organs-on-a-chip. *Lab Chip* 13(18):3496.

21. Wujcik JM, Wang G, Eastman JT, Sidell BD (2007) Morphometry of retinal vasculature in Antarctic fishes is dependent upon the level of hemoglobin in circulation. *J Exp Biol* 210(5):815–824.

22. O'Brien KM (2003) Muscle fine structure may maintain the function of oxidative fibres in haemoglobinless Antarctic fishes. *J Exp Biol* 206(2):411–421.

23. Widmaier EP, Raff H, Strang KT (2006) *Vander's Human Physiology* (McGraw-Hill, New York). 10th Edition.

24. Banavar JR, et al. (2010) A general basis for quarter-power scaling in animals. *Proc Natl Acad Sci* 107(36):15816–15820.

25. Weiss RF, Price BA (1980) Nitrous oxide solubility in water and seawater. *Mar Chem* 8:347–359.

26. Jones H, Rowland-Yeo K (2013) Basic Concepts in Physiologically Based Pharmacokinetic Modeling in Drug Discovery and Development. *CPT Pharmacomet Syst Pharmacol* 2(8):e63.

27. Leon Shargel, Andrew B.C. Yu (1993) *Applied Biopharmaceutics and Pharmacokinetics* (Appleton & Lange, Norwalk, CT). Third Edition.

28. Schmidt LD (1998) *The Engineering of Chemical Reactions* (Oxford University Press, New York).

29. Sung JH, Kam C, Shuler ML (2010) A microfluidic device for a pharmacokinetic–pharmacodynamic (PK–PD) model on a chip. *Lab Chip* 10(4):446.

30. Abaci H, Shuler M (2015) Human on a chip Design Strategies and Principles for Physiologically Based Pharmocokinetics/Pharmacodynamics Modeling. *Integr Biol*. doi:10.1039/C4IB00292J.

31. Mattei G, Giusti S, Ahluwalia A (2014) Design Criteria for Generating Physiologically Relevant In Vitro Models in Bioreactors. *Processes* 2(3):548–569.

32. Malcom Rowland, Thomas N. Tozer (1995) *Clinical Pharmacokinetics: Concepts and Applications* (Williams & Wilkins, Baltimore). Third Edition.

33. US Environmental Protection Agency (2006) Approaches for the application of physiologically based pharmacokinetic (PBPK) models and supporting data in risk assessment.

34. Clewell 3rd HJ, Andersen ME, Barton HA (2002) A consistent approach for the application of pharmacokinetic modeling in cancer and noncancer risk assessment. *Environ Health Perspect* 110(1):85.

35. Voisin EM, Ruthsatz M, Collins JM, Hoyle PC (1990) Extrapolation of animal toxicity to humans: interspecies comparisons in drug development. *Regul Toxicol Pharmacol* 12(2):107–116.

36. Upton RN, Ludbrook GL, Grant C, Martinez AM (1999) Cardiac output is a determinant of the initial concentrations of propofol after short-infusion administration. *Anesth Analg* 89(3):545.

37. Levitt DG (2002) PKQuest: a general physiologically based pharmacokinetic model. Introduction and application to propranolol. *BMC Pharmacol Toxicol* 2(1):5.

38. Levitt DG (2009) PKQuest_Java: free, interactive physiologically based pharmacokinetic software package and tutorial. *BMC Res Notes* 2(1):158.

39. Arancibia A, Guttmann J, Gonzalez G, Gonzalez C (1980) Absorption and disposition kinetics of amoxicillin in normal human subjects. *Antimicrob Agents Chemother* 17(2):199–202.

40. Torisawa Y, et al. (2007) A multicellular spheroid array to realize spheroid formation, culture, and viability assay on a chip. *Biomaterials* 28(3):559–566.

41. Ruud JT (1954) Vertebrates wtihout erythrocytes and blood pigment. *Nature* 173(4410):848–850.

42. Egginton S (1996) Blood rheology of Antarctic fishes: viscosity adaptations at very low temperatures. *J Fish Biol* 48(3):513–521.

43. Stücker M, et al. (2002) The cutaneous uptake of atmospheric oxygen contributes significantly to the oxygen supply of human dermis and epidermis. *J Physiol* 538(3):985–994.

44. Folarin AA, Konerding MA, Timonen J, Nagl S, Pedley RB (2010) Three-dimensional analysis of tumour vascular corrosion casts using stereoimaging and micro-computed tomography. *Microvasc Res* 80(1):89–98.

45. Petschow R, Petschow D, Bartels R, Baumann R, Bartels H (1978) Regulation of oxygen affinity in blood of fetal, newborn and adult mouse. *Respir Physiol* 35(3):271–282.

46. Tournoux F, et al. (2011) Validation of Noninvasive Measurements of Cardiac Output in Mice Using Echocardiography. *J Am Soc Echocardiogr* 24(4):465–470.

47. Malkusch W, Konerding MA, Klapthor B, Bruch J (1995) A simple and accurate method for 3-D measurements in microcorrosion casts illustrated with tumour vascularization. *Anal Cell Pathol* 9(1):69–81.

48. Ege R, Krogh A (1914) On the relation between the temperature and the respiratory exchange in fishes. *Int Rev Gesamten Hydrobiol Hydrogr* 7(1):48–55.

49. Clarke A, Johnston NM (1999) Scaling of metabolic rate wtih body mass and temperature in telost fish. *J Anim Ecol* 68:893–905.